Bio-oils as compatibilizers for nanoclays in linear low density polyethylene

Aalborg University
Department of Mechanical
and Manufacturing
Engineering
Master thesis
Group: 2.105A
12. August 2016

Department of Mechanical & Manufacturing Engineering
Fibigerstræde 16
DK - 9220 Aalborg øst
Tlf. 99 40 93 09
Fax 99 40 71 10
lft@m-tech.aau.dk
http://www.m-tech.aau.dk

Title: Bio-oils as compatibilizers for nanoclays in linear low density polyethylene

Project period: MT4, Spring 2016
Semester 4th
ETCS: 30
Supervisors:
J. de Clavile Christiansen
Catalina-Gabriela Sanporean
Projectgroup: MT1e15
Participant:

Bjarke Hangstrup Høgsaa

Number of copies: 3 and Digital version
Number of pages: 70
Number of appendix: 42
Completed: 12-08-2016

Synopsis:

The main objective was to investigate bio-oils, from different origins, which can be used as intercalants/surfactants for two types of unmodified nanoclay; halloysite nanotubes (HNT) and montmorillonite (MMT). The modified nanoclays were utilized, as filler materials, in linear low density polyethylene (LLDPE). The results from the experiments showed signs of intercalation/exfoliation of the investigated modified nanoclays. The mechanical and thermal properties of the obtained nanocomposites was investigated to assess the bio-oils potential as a intercalants /surfactants for LLDPE/clay nanocomposites. The dispersion was investigated to assess the compatibility between the matrix and modified filler material. The results of organic modification of the nanoclays were deemed a success with increased basal spacing and intercalated/exfoliated structure. The compatibility with the chosen matrix linear low density polyethylene (LLDPE) with modified nanoclays yielded a aggregated structure and poor dispersion. The obtained mechanical and thermal properties were slightly improved with a 2 wt % clay loading, when compared to the pure polymer matrix material. However the potential of the two surfactants is promising and further studies of the investigated material systems and other systems with other polymer matrices have to be conducted.

Resumé(Danish summary)

Kandidatspecialet undersøgte anvendelsen af bio-olier fra biologisk genanvendelige materialer som kompatiabilisator for nanokompositer, bestående af linear low density polyethylene (LLDPE) og to typer af nano-ler, montmorillonite (MMT) og halloysite nanorør (HNT). De udvalgte bio-olier var en bio-rest (bio-residue) og en bio-olie, som er produceret ud fra aspe træ og glycerol, wood-based bio-oil (WB). Bio-resten er fra universitet i North Carolina og er baseret på svinegylle. Den anden bio-olie er produceret ved Institutet for Energiteknik ved Aalborg Universitet. De to olier var valgt qua deres forskellige kemiske sammensætninger for at vurdere deres interaktion med de udvalgte lertyper og polymer matrixen som kompatiabilisator. Specialet er opdelt i tre dele: Undersøgelse af de anvendte materialer, modificeringen af nano-ler, nanokompositterne og deres egenskaber. Følgende karakteriseringsteknikker til at undersøge effekterne af materialerne, og interaktionerne imellem materialerne, blev anvendt: Røntgen diffraktion (XRD), oscillatorisk rheometri (OR), fourier transform infrarød spektroskopi (ATR-FTIR), termisk analyse(TGA), gaskromatografi –massespektrometri(GC-MS), optisk analyse(OP) og trækprøvning(UTT).

Resultaterne viste at modifiksering af de forskellige nano-ler var en succes med interkaleret/exfolieret struktur. De producerede nanokompositer havde lidt forbedre termiske og mekaniske egenskaber i sammenligning med den rene polymer. Men sammenlignet med resultere fra andre studier var egenskaberne af ringere karakter. Men potentialet for bio-olierne er lovende og yderligere studier af deres funktion som kompatiabilisator er anbefalet. De udvalgte ler-typer og polymer matrixen blev udvalgt, grundet deres manglende kompatiblitet. Dette blev gjort for at se om bio-oilerne ville have en positiv effekt på egenskaberne og kompatiblitet imellem bestanddelene. Det blev bevist at der var postive effekter, ved at bruge bio-oiler, dog er disse begrænset i forhold til rene stoffer som kompatiabilisator som set i andre studier. Dette skyldes at bio-olierne er komplekse miksture med mange forskellige bestandele. Derved er det kun en lille bestanddel af bio-olien der kan øge komptibliteten. For at forbedre dette vil det være fordelagtigt at lave yderligere studier, hvor der bliver testet mere i forhold til ratio og med mere kompertible typer af polymer. Forsøg med at øge blandingstiden for at øge dispergerings graden of nano-leret var forsøgt, men dette skal undersøges yderligere.

Contents

Introduction 1

Polymeric materials have been reported for decades to obtain improved properties with the addition with a filer material. A conventional filler material can be in the form of particles, fibers or platelets [Pavlidou and Papaspyrides, 2008]. Small addition of 1-5 weight % of the filler material is sufficient to improve the properties (e.g thermal and mechanical) significantly of the resulting composite. A new kind of composite, nanocomposites, have attracted attention in the last decades, due to their improved properties. This new class of composites have filler material with at least one dimension in nanometer range [Pavlidou and Papaspyrides, 2008]. To obtain nanocomposites, several types of fillers can be used, where one type is nanoclay or silicate clay. There are several different types of nanoclay (e.g. montmorillonite, kaolinite and halloysite nanotubes) with different dimensions and structures. According to Pavlidou and Papaspyrides [2008] any physical mixture of a polymer and a silicate clay is not sufficient to form a nanocomposite. The structure and chemical composition of the silicate clay determines if the filler is compatible with a selected polymer matrix material; therefore is appropriate processing conditions important to obtain nanocomposites. The process of dispersing the layered silicate into a polymer matrix can be complex, due to the silicate's preferred stacking of the clay platelets into tactoids. An other obstacle is the incompatibility between the hydrophobic polymer and the hydrophyllic silicate. To overcome these obstacles the layered nanoclay needs to be organically modified to polymer compatible clay (organoclay), which has a better interaction with polymer matrix. The modification treatment of nanoclay is known as; compatibilization, or intercalation. Where an intercalant is an organic chemical capable of entering the spacing between the clay platelets or cover the surface of the platelets [Uddin, 2008]. The compatibilization can be necessary for a good dispersion and interphase between the filler and polymer matrix. The properties of a nanocomposite are dependent on the dispersion and interphase between filler and polymer matrix. A strong compatibility and good dispersion between these constituents are essential to achieve improved properties (e.g. mechanical and thermal) of the nanocomposite.

In this thesis, it was chosen to investigate nanocomposites with linear low density polyethylene (LLDPE) and selected nanoclays (montmorillonite (MMT) and halloysite nanotubes (HNT). The choice of this material system was the poor compatibility between the hydrophobic LLDPE and the hydrophyllic nanoclays. A compatibilizer can intercalate the interlayer distance in the clay galleries by separating the clay platelets. A secondary function of the compatibilizer is to establish a bridge/connection between the hydrophobic polymer and the hydrophyllic filler. Therefore it was chosen to investigate if the selected compatibilizer could improve the interphase between the fillers and polymer in of each investigated material system. A conventional and frequently used compatibilizer for polyolefin nanocomposites is maleic anhydride grafted polyolefins [Durmuş et al., 2007]. However other compounds have been investigated as possible new compatibilizers for LLDPE/clay nanocomposites. Several studies have investigated LLDPE/MMT nanocomposite with and without different compatibilizers and organoclays [As' habi et al., 2013; Durmuş et al., 2007; Durmus et al., 2007, 2008; Hotta and Paul, 2004; Irani et al., 2013; Jin et al., 2009; Khederlou et al., 2014; Marchante et al., 2013; Qiu et al., 2006; Ryu and Chang, 2005; Truss and Yeow, 2006]. The results of these studies have shown the promising potential of these new types of compatibilizers, with improved mechanical and thermal properties of the nanocomposites. In comparison the search for studies with LLDPE/HNT material systems only had few articles: Jia et al. [2009]; Pedrazzoli [2013]; Pedrazzoli et al. [2015]. This could indicate that montmorillonite have been investigated more extensively. The structure and chemical composition of the two different types of nanoclay could help determine the possible interactions and mechanisms with a chosen compatibilizer. This approach was conducted by Carli et al. [2011] with a commercially modified montmorillonite, Cloisite 30B, and halloysite nanotubes, which were melt-blended with PHBV(Poly(3-hydroxybutyrate-co-3-hydroxyvalerate)). This polymer is biodegradable, nontoxic, bio-compatible thermoplastic linear aliphatic polyester, produced naturally by bacteria. The organically modified montmorillonite Cloisite 30B was chosen to be more compatible with the polymer matrix [Carli et al., 2011]. A similar approach is conducted in this thesis. However the idea in this thesis was to investigate if two types of bio-oils could be used as compatibilizers in LLDPE/MMT and LLDPE/HNT nanocomposites, where the montmorillonite was unmodified.

The choice of using bio-oils as compatibilizers is based on the author's previous work Høgsaa [2015], where one of the selected bio-oils, which was based on swine manure. This bio-oil showed potential as an intercalant for organic modification of sodium montmorillonite clay to an organoclay. The results of this previous work, which is essential for this thesis, is presented in the following section.

1.1 Previous work

In the previous study, Investigation of materials from bio-renewable resources [Høgsaa, 2015], was a bio-oil from the Agricultural and Technical State University of North Carolina (NC A&T) investigated. The bio-oil, or bio-residue (BR), was produced from swine manure with thermochemical conversion process. The bio-oil was investigated to assess if it could be used as a surfactant/intercalant in modification process of sodium montmorillonite. The bio-residue (BR) was added 10% sodium montmorillonite to asses if it could modify the sodium montmorillonite to a organoclay. The following results were obtained:

- **The basal spacing increased with the addition of MMT.**
  The increase in the interlayer d-spacing of the organically modified montmorillonite (BRMMT_{dried}) indicated an intercalated state. This was verified with X-ray diffraction (XRD) and Attenuated total reflectance fourier transform infrared spectroscopy (ATR-FTIR). The basal d-spacing increased with approximately 35%, compared to the measured d-spacing of the pure montmorillonite (MMT). This was supported by the measurement conducted in the ATR-FTIR, where the peak of 1080 cm^{-1} was clearly present. This indicated that the sodium montmorillonite was modified into an organoclay.
- **The viscosity of the bio-residue increased with the addition of MMT.**
  A transition from a liquid-like to a semi-solid behavior of the treated bio-residue with montmorillonite, indicated interaction between the montmorillonite (MMT) and bio-residue.
- **The thermal stability of the bio-residue decreased with the addition of MMT.**

  The decrease in thermal stability could be attributed to release of bounded water within the MMT or the degradation of long fatty acids in the bio-residue (BR).

The results indicated that the modification process of the sodium montmorillonite was a success, however there were uncertainties regarding which organic compounds of the bio-residue (BR), and mechanism, facilitated the intercalation process. The process yielded an increased intercalation degree after a solution-blending modification process, which could be due to a possible dipole-dipole intercalation mechanism. However a deeper understanding is needed to assess which polymer material would be suitable for the modified nanoclay, and obtaining a nanocomposite with improved properties.

The former project is included in appendix A.

Based on the findings in the former project, it was chosen to investigate if the bio-residue (BR) could be used as compatibilizer for the LLDPE/HNT and LLDPE/MMT material systems. Another bio-oil, with a different chemical composition, was chosen to possibly determine the interactions between the compatibilizer, the clay and the polymer in each material system. This bio-oil was provided by the Energy department - Aalborg University (AAU). The bio-oil was processed under similar conditions as the bio-residue (BR). The new bio-oil is based on liquefied aspen wood and glycerol and denoted as wood-based bio-oil (WB). In order to gain understanding of interactions and behaviors of the constituents in the LLDPE/nanoclay composites, it is important to have a proper knowledge of the all the constituents in each material system. In the following sections are presentations of the general structure and chemical composition of each constituent presented.

1.2 Nanocomposite constituents

In the following sections, a presentation of the materials utilized in the thesis, where the structure, chemical and physical properties of the materials and their interactions are described.

1.2.1 Bio-oils

The utilized bio-oils are from different bio-renewable resources, where one is based on plant material and the other on waste material. Even though the bio-oils have different origins, they both will be used as organic surfactants for modification process of the untreated nanoclays.

Bio-residue (BR)

The bio-residue is from NC A&T and the raw material is based on swine manure. The raw material is processed with thermal liquefaction with specific heat and pressure settings, under nitrogen atmosphere, to yield several products [Fini, 2013]. Bio-residue (BR) is one of these products. This was investigated in the earlier project Høgsaa [2015].

The bio-residue (BR) is not a conventional bio-oil, but a post production product of the bio-oil obtained by filtration and fractionation, as seen in figure 1.1 of the conversion process. The bio-residue is described as a dark black/brownish, sticky substance with no odors at room temperature, but has a small scent of sulfur at elevated temperatures [Høgsaa, 2015].

Properties of the oil

The chemical composition of the bio-residue (BR) was never investigated before the project Høgsaa [2015], to the author's knowledge, and therefore the obtained results were compared to two other products, the bio-oil and the bio-binder, described in Fini [2013]. The chemical composition was determined using a visual comparison of the spectra, described in the literature study of the former project. This indicated a similar spectra of the bio-residue, when compared to the bio-oil and bio-binder. In table 1.1, the results of the measured peaks, for BR_{raw} and BR_{dried} are listed and compared with the ranges of functional groups described by Hosseinnezhad

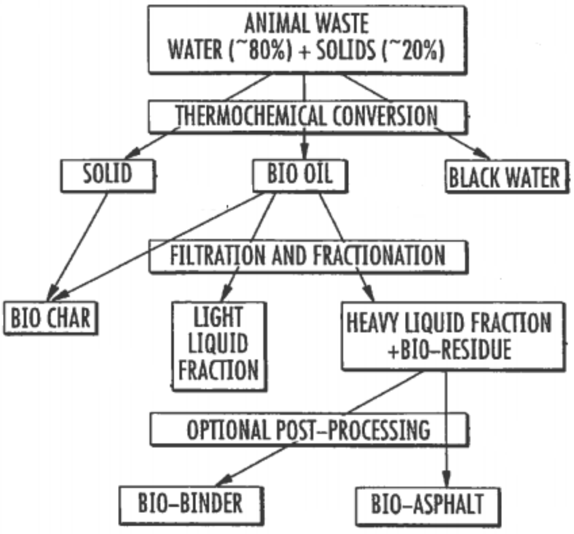

Figure 1.1. Direct conversion process from swine manure into bio-residue (BR) [Fini, 2013].

et al. [2015] for bio-oil. The BR$_{raw}$ and BR$_{dried}$ are the raw bio-residue and a dried version until mass stability, obtained in the earlier project.

Table 1.1. Functional groups of bio-oil with ranges, described by Hosseinnezhad et al. [2015] compared to the results of the raw bio-residue(BR$_{raw}$) and the dried version(BR$_{dried}$)[Høgsaa, 2015].

Functional group	Range	BR$_{raw}$	BR$_{dried}$
O-H stretching	3200-3400	-	-
O-H stretching	2800-3000	2923.27 2853.25	2922.65 2852.71
Aromatic carbonyl/carboxyl C=0 stretching	1700-1710	1709.05	1704.05
Aromatic C=C ring stretching	1514-1560	-	1515.33
Aliphatic C-H deformation	1454	1456.08	1455.91
Aliphatic CH3 deformation	1370	1363.05	1376.79
Aromatic CO- and phenolic -OH stretching	1250-1270	1218.66	1271.39

The peaks of the different functional groups of bio-binder and bio-oil are present in the different processed bio-residues, as seen in the table 1.1. This indicates that the materials could have the similar chemical composition. The compounds found in the bio-oil and bio-binder were investigated by a couple of studies ([Fini et al., 2011], [Oldham et al., 2015]) and they concluded that the materials had amines, alcohols, olefins, nitrogen- and oxygen-containing organic molecules (e.g. carbonyl, aldehyde, amine, and nitrosyl functionalists). There were also olefinic carbons, amide functional groups, sulfur-containing organics, long fatty acids and other organics present in the bio-oil and bio-binder. According to Fini et al. [2011], the reason for the more complex mixture of functionalized organics in the bio-binder is due to the increased concentration of nitrogen, oxygen, and sulfur in the bio-binder compared to conventional binders, as seen in table 1.2 of the elemental analysis. The bio-binder is the post processing step of the bio-residue [Fini, 2013], therefore the chemical composition of the bio-binder is interesting, to gain an understanding of. The preliminary chemical composition of the bio-residue is based on FTIR-analysis, NMR, GC-MS, Elemental analysis, conducted by Fini et al. [2011] and Oldham et al. [2015].

Table 1.2. Chemical composition of the bio-binder and conventional bituminous binder (ADD-1) Fini et al. [2011].

Component (percent by weight)	Bio-binder	AAD-1
C	72.58	81.60
H	9.76	10.80
N	4.47	0.77
O	13.19	0.90

The FTIR analysis, conducted by Høgsaa [2015] was deemed inconclusive, because the peaks of the functional groups are not a direct indication of the full chemical composition of the bio-residue. Other tests like GC-MS are required to gain a better indication of the chemical composition.

Bio-oil from wood (WB)

The wood based bio-oil is produced at the Energy department - Aalborg University (AAU) and the raw material is based on liquefied aspen wood and glycerol [Pedersen et al., 2016]. The raw material is processed with continuous hydrothermal co-liquefaction at 400 °C and 300 bars, under depleted atmosphere, to yield bio-oil. The provided bio-oil is a mixture of several batches of processed bio-oil and therefore the properties are not specific to one batch of the oils, but a generalization of the processed type.

Properties of the oil

The chemical composition is described in Pedersen et al. [2016] and the compounds are listed in table 1.3. The wood-based -bio-oil (WB) is termed as bio crude in the original article.

The bio crude is a complex mixture of chemical compounds for which the majority of compounds are oxygenated cyclic structures having carbon atoms in the range of C_6-C_{21}. There are also unsaturated hydrocarbons compounds with higher number of carbon atoms, including fused ring structures, but in minor quantities compared to the other groups. The bio-oil has cyclic C_5 or aromatic C_6 backbones compounds, substituted with various functional groups (ketonic, aldehyde, phenolic) [Pedersen et al., 2016]. Compared to the bio-residue (BR), the wood-based bio-oil (WB) has more aromatic compounds and no nitrogen compounds (amines and amides). Long fatty acids are not present in the wood-based bio-oil (WB). These measurements, are supported by the elemental analysis were the nitrogen content of the bio-binder is 4.47 wt% [Fini et al., 2011] and the wood-based bio-oil (WB) is 0.5 wt% [Pedersen et al., 2016]. However the nitrogen should not be present in the wood-based bio-oil(WB), based on the original feed stock materials. The oxygen levels are 13.19 wt% and 15.8 wt% for the bio-binder and the wood-based bio-oil (WB) respectively. These high levels of oxygen is the reason for the high amount of polar compounds in both bio-oils.

Table 1.3. List of identified compounds in the dried version of wood-based bio-oil (WB) by GC-MS.

RT (min)	Identified compound	Chemical formula	C_n
2.06	Cyclopentanone	C_5H_8O	5
2.59	3,5,5-Trimethyl-2-hexene	C_9H_{18}	9
2.94	2-Methyl-cyclopentanone	$C_6H_{10}O$	6
3.37	Ethylbenzene	C_8H_1O	8
3.56	p-Xylene	C_8H_1O	8
3.87	2,5-Dimethyl-cyclopentanone	$C_9H_{16}O$	9
4.04	3,4-Dimethyl-3-penten-2-one	$C_7H_{12}O$	7
4.38	2-Methyl-2-cyclopenten-1-one	C_6H_8O	6
5.04	1-Cyclohexylethanol	$C_8H_{16}O$	7
5.19	1,2-Dimethyl-cyclohexene	C_8H_{14}	8
5.56	3-Methyl-2-cyclopenten-1-one	C_6H_8O	6
6.93	2,3-Dimethyl-2-cyclopenten-1-one	$C_7H_{12}O$	7
7.37	2,3,4-Trimethyl-2-cyclopenten-1-one	$C_8H_{12}O$	8
7.65	p-Cresol	C_7H_8O	7
8.12	2,3-Dimethyl-phenol	$C_8H_{10}O$	8
8.50	2-Ethyldienecyclohexanone	$C_8H_{14}O$	8
8.81	3,5-Dimethyl-phenol	$C_8H_{10}O$	8
9.15	2,4,6-Trimethyl-3-cyclohexen-1-carboxaldehyde	$C_{10}H_{16}O$	10
9.35	4-Methyl-1-(1-methylethyl)-cyclohexene	$C_{10}H_{18}$	10
9.44	4-Methyl-1-(1-methylethyl)-cyclohexene	$C_{10}H_{18}$	10
9.62	2,4,6-Trimethyl-3-cyclohexen-1-carboxaldehyde	$C_{10}H_{16}O$	10
9.82	4-Ethyl-3,4-dimethyl-2,5-cyclohexadien-1-one	$C_{10}H_{14}O$	10
10.14	2,4,6-Trimethyl-3-cyclohexen-1-carboxaldehyde	$C_{10}H_{16}O$	10
10.71	2,6-Dimethoxytoluene	$C_9H_{12}O_2$	9
11.07	2,3-Dihydroxy-3-methyl-1H-inden-1-one	$C_{11}H_{12}O_3$	10
11.33	Duroquinone	$C_{10}H_{12}O_2$	11
11.71	2,6-Dimethyl-1,4-benzenediol	$C_8H_{10}O_2$	8
12.13	4-Ethylcatechol	$C_8H_{10}O_2$	8
12.42	2,5-Dimethyl-1,4-benzenediol	$C_8H_{10}O_2$	8
12.76	5-Methoxy-2,3-dimethyl-phenol	$C_9H_{12}O_2$	9
12.90	4-Ethylguaiacol	$C_9H_{12}O_2$	9
13.68	2,3,5-Trimethyl-1,4-benzenediol	$C_9H_{12}O_2$	9
13.97	3-Tert-butyl-4-hydroxyanisole	$C_{11}H_{16}O_2$	11
14.19	4-Butoxybenzyl alcohol	$C_{10}H_{16}O$	10
14.81	2,3,5,6-Tetramethyl-1,4-benzenediol	$C_{10}H_{14}O_2$	10
15.30	2,6-Dimethoxy-4-(2-propenyl)-phenol	$C_{11}H_{14}O_3$	11
16.32	6-Tert-butyl-2,4-dimethylphenol	$C_{12}H_{18}O$	12
16.44	Benzaldehyde, 3-hydroxy-4-methoxy-2-(2-propenyl)-	$C_{11}H_{12}O_3$	12
16.63	4-(2,4,4-Trimethyl-cyclohexa-1,5-dienyl)-but-3-en-2-one	$C_{13}H_{18}O$	13
18.82	Methyl dehydroabietate	$C_{21}H_{30}O_2$	21
19.79	10,18-Bisnorabieta-5,7,9(10),11,13-pentene	$C_{18}H_{22}$	18
20.82	Retene	$C_{18}H_{18}$	18

1.2.2 Nanoclay

In this study two types of silicate nano-clay, halloysite nanotubes (HNT) and montmorillonite (MMT), were investigated. These are investigated with regard to the the structure, particle sizes and morphology. Both clay types belongs to the phyllosilicate or sheet silicate family.

Montmorillonite (MMT)

Montmorillonite is a clay mineral, which has been investigated, due to its ability to improve the properties of nanocomposites; especially mechanical, thermal and barrier properties of matrix materials, at low additions as 2-5 % [K.Fukushima et al., 2008].

The average particle size of montmorillonite, or layered silicate, can vary from 10.000 to 100.000 nm. Each of these particles are agglomerates of smaller particles with dimensions varying from 1.000 to 10.000 nm. The thickness of each individual layer is around 1 nm. The lateral dimensions can vary from around 300 nm to several micrometers, depending on the type of layered silicate [Maneshi et al., 2006]. Each particle consists of small clusters or stacks of clay platelets, denoted tactoids. The close packed platelets are held together, due to the charges present within each platelet. Each platelet of montmorillonite consist of an inner octahedral layer, which is dominated by aluminum oxides, with some magnesium atoms. This central layer is fused between two silicate tetrahedral layers, or silicon oxides sheets, in a 2:1 layered structure with oxygen molecules [Paul and Robeson, 2008]. The resulting structure is illustrated in figure 1.2.

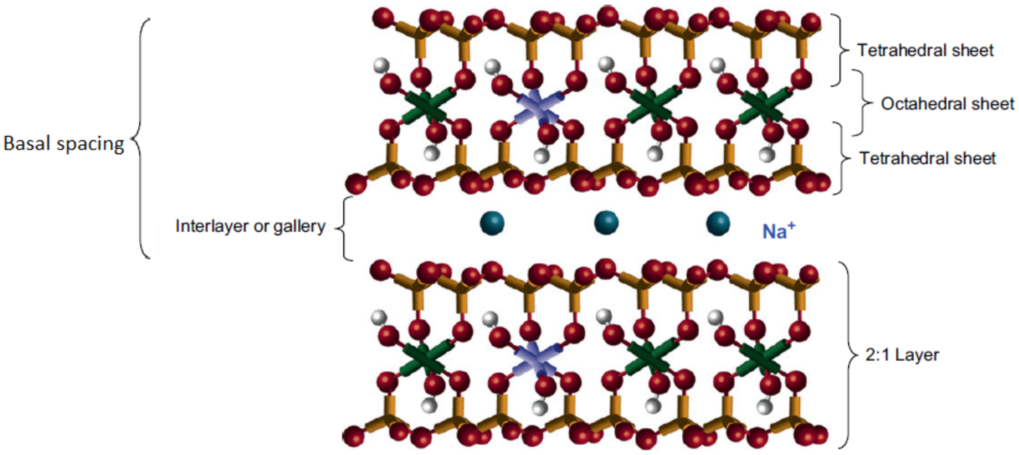

Figure 1.2. Molecular structure of sodium montmorillonite. Modified schematic from [Uddin, 2008].

The platelets in a tactoid are held together with different kinds of forces (e.g Van der Waals forces, electrostatic forces and hydrogen bonding). The clay platelets are negatively charged due to substitution of Si in the tetrahedral and Al atoms in the octahedaral layer with lower valances atoms like Mg, Ca, K, Na. The negative charges are counter balanced by positive counter ions (e.g. sodium ions), absorbed between the galleries. The montmorillonite clay can be modified due to positive interlayer charges, known as cation exchange. This cation exchange has the capabilities of replacing ions between the individual clay platelets [Klitkou, 2012]. When submerged into an aqueous solution, e.g. water, montmorillonite has the ability to swell, due to the hydration of the sodium ions, which causes the space between the platelets to expand. However montmorillonite is difficult to disperse in hydrophobic polymers, because montmorillonite is hydrophylic, thus modification of the clay is required. The intercalated structure is achieved because of the organic cations will act as pillars, which permanently increases the interlayer spacing between the inorganic layers of montmorillonite [Önal and Sarıkaya, 2008]. The electrostatic forces between the platelets can determine the intercalated/exfoliated structure.

The modification will increase the compatibility and thereby the dispersion of the clay in a hydrophobic polymer material. The dispersion of clay in matrix materials can be obtained in three different stages: Immiscible, where the clay particle consists of large agglomerates in the matrix material; Intercalated structure consisting of isolated stacks with an intercalant in the gallery of the clays; Exfoliated structure with individual clay platelets dispersed uniformly in polymer matrix [Klitkou, 2012]. The three stages are illustrated in figure 1.3.

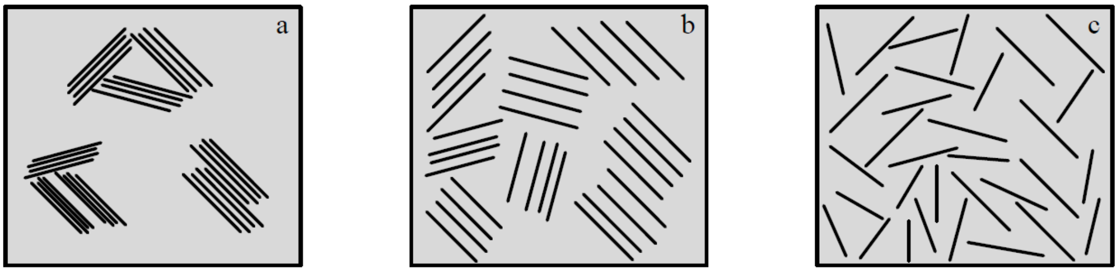

Figure 1.3. Possible dispersion states for clay-containing polymeric nanocomposites [Klitkou, 2012]

Ammonium cations can be used for compatibilization, because they can replace the sodium cations (Na+) in the interlayer spacing of the montmorillonite. The ammonium cations have hydrocarbon tails. These are amphiphilic, which means the molecule consists of two parts; a hydrophyllic and hydrophobic. The hydrophyllic part will be attracted to the natural hydrophyllic surface of the clay, and hydrophobic part is attracted to hydrophobic surface of the polymer matrix. These types of molecules can be used as bridges, or surfactant, between the polymer and the clay [Paul and Robeson, 2008]. There is another possible interaction between the nanofiller and the matrix material for intercalation, which is achieved with a dipole-dipole attraction. The attraction is possible, because the polar groups (e.g. -OH or -COOH) of the surfactant forms hydrogen bonds with the oxygen groups of montmorillonite [Potarniche et al., 2013].

Halloysite nanotubes (HNT)

The chemical structure of the halloysite nanotubes (HNT) is similar to kaolinite, except the structure is rolled into a hollow tube instead of a flat sheet.

Halloysite has a molecular formula of $Al_2Si_2O_5OH_4nH_2O$ with 1:1 layer, where the layers are separated by a monolayer of water molecules. The hydrated form of halloysite (when $n = 2$) is named Halloysite-(10 Å), in which one layer of water molecules is present between the multilayers and where the 10 Å designation indicates the d001-value of the layers [Yuan et al., 2015]. The dehydrated structure of halloysite (when $n = 0$) is named Halloysite-(7 Å), and may be obtained through the loss of the interlayer water molecules under mild heating and/or a vacuum environment [Yuan et al., 2015]. The typical length of the nanotubes is in the range of 100-15.000 nm, an inner diameter of the tubes is of 5-30 nm, and a outer diameter is of 30-70 nm [Pedrazzoli et al., 2015]. The surfaces of the nanotubes, are rolled so the external surface is comprised of siloxane (-Si-O-Si-) and the internal surface of aluminol (-Al-OH), as seen in figure 1.4 [Yuan et al., 2015].

Halloysite nanotubes is an effective and powerful nanofiller in nanocomposites, because it is naturally dispersed, due to the tubular structure. According to Gorrasi [2015], the tubular shape and less abundant OH groups on the surface, is the reason why halloysite nanotubes (HNT) can be easily dispersed in polymers without any need for exfoliation, as required for a good dispersion of platted clay, unlike kaolin and montmorillonite. Other clay fillers (e.g

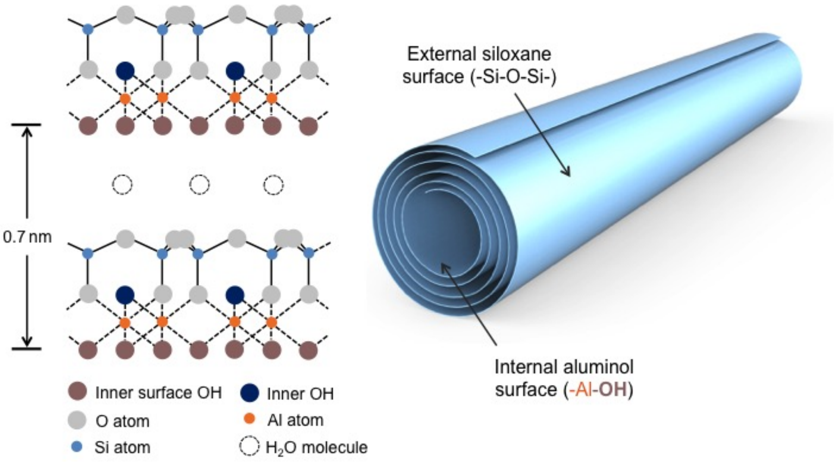

Figure 1.4. Molecular structure of Halloysite nanotubes(HNT).

montmorillonite, bentonite) have to undergo intercalation/exfoliation pre-treatments to produce modified nanoclays. Two crucial factors for determining the performance of nanocomposites, containing halloysite nanotubes, is a good dispersion and a desirable interfacial compatibility between the clay and the matrix material. Halloysite is easily dispersed in aqueous solutions, however due to the negatively charged external surface of HNT and the hydrophobic surface of some polymers, it can be difficult to achieve a good dispersion. This misalignment between the materials produces micron-sized aggregates or agglomerates [Yuan et al., 2015]. The structure of the halloysite nanotubes (HNT) affects which groups can react and be modified. The only reactive groups on the halloysite nanotubes (HNT) are predominantly aluminols, which are located on the inner side or at the ends of the tubes. In addition, a few silanols located at the edges of the halloysite nanotubes (HNT) and surface defects should also be considered [Liu et al., 2007]. Some studies have shown that the halloysite nanotubes (HNT) can be made compatible with polymers with surface modifications, by introducing functional groups onto the surface of the clay. This can be achieved by two different processes. Physical modifications, where a modifier is coated onto the clay surface by van der Waals forces, hydrogen bonding, and electrostatic attraction. The other process is chemical modifications by covalent attraction between the modifier and the clay surface, especially when halloysite nanotubes have multiple surfaces; the external surface, the interlayer surface, and the internal lumen surface [Yuan et al., 2015]. According to Pedrazzoli et al. [2015] halloysite nanotubes (HNT) can be dispersed relatively uniformly in thermoplastics by direct melt blending, if the polymers have a high amount of polar groups. However compatibilization is required between polyolefins and inorganics, due to the great polarity discrepancy and the chemical inertness of the polyolefins. This can be mended by chemical modification process, which expands the basal spacing of halloysite nanotubes (HNT) through intercalation of inorganic and organic compounds in their internal layers. This leads to a more homogeneous dispersion of halloysite nanotubes (HNT) within the corresponding polymer during melt blending.

The filler content for improved mechanical properties is reported to be between 5–10% wt [Yuan et al., 2015]. According to Yuan et al. [2008], very little is known of the chemical and physical properties of halloysite, compared to kaolinite, and there are few applications that utilizes this kind of clay structure.

1.2.3 Linear Low density polyethylene (LLDPE)

Polyethylene (PE) is a polyolefin, which is a class of polymers produced from simple olefins. Olefin or alkene is a monomer with a general chemical formula C_nH_{2n}. There are several types of polyethylene, which is used in the industry, where the classification is done by density and branching of the different grades. The properties of the grades depends on the extent and type of branching, the crystal structure, and the molecular weight. The processing of the raw monomer determines the structure of the obtained polymer.

The process for obtaining linear low density polyethylene (LLDPE) is co-polymerization, where a small amount of an other monomer is added to the feed stock of the low density polyethylene (LDPE). The process can be performed either in solution phase or in gas phase reactors, with initiation by transition metal catalysts, particularly Ziegler or Philips type of catalyst. Typically but-1-ene, hex-1-ene or oct-1-ene is utilized as the co-monomer, where oct-1-ene is processed in solution phase, and but-1-ene and hex-1-ene with ethylene in a gas phase reactor. The chemical reaction for obtained linear low density polyethylene (LLDPE) with but-1-ene pendant groups is seen in figure 1.5 [chemical industry online, 2016].

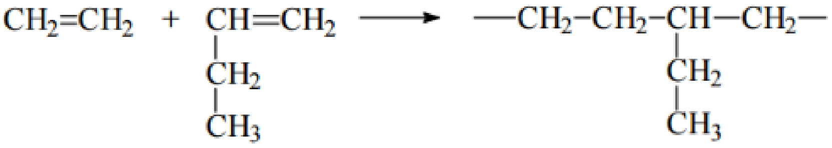

$$\mathrm{CH_2{=}CH_2} + \begin{array}{l}\mathrm{CH{=}CH_2}\\ |\\ \mathrm{CH_2}\\ |\\ \mathrm{CH_3}\end{array} \longrightarrow -\mathrm{CH_2{-}CH_2{-}}\begin{array}{l}\mathrm{CH{-}CH_2{-}}\\ |\\ \mathrm{CH_2}\\ |\\ \mathrm{CH_3}\end{array}$$

Figure 1.5. Chemical reaction for obtaining LLPDE with but-1-ene pendant groups.

The LLDPE processed with co-monomer but-1-ene produces a polymer with small pendant or short branching groups, as sen in figure 1.5.

Properties and applications

The structure of LLDPE is essentially linear, like high density polyethylene(HDPE), but because of the short chain branching it has a low density, like low density polyethylene (LDPE). The chemical structure of the linear low density polyethylene (LLDPE) makes the polymer highly hydrophobic, due the non existing polar groups in the backbone of the material [Jin et al., 2009]. The short branching structure hinders crystallization, and a higher level and size of co-monomer reduces the crystallization further [Peacock, 2000]. The chemical structure gives the material more resilience, tear strength and flexibility and therefore it is good for film production. An advantage of linear low density polyethylene (LLDPE) production is that the properties of the polymer can be altered with a different type or amount of co-monomers, without changing the production setup [chemical industry online, 2016]. According to Brydson [1999], linear low density polyethylene (LLDPE) is competing with low density polyethylene (LDPE) of similar melt flow index and density due to their high toughness at different temperatures, tensile strength, elongation at break and puncture resistance. At high levels of co-monomers in the material, the crystallinity is suppressed [Peacock, 2000].

According to Jin et al. [2009], it can be very difficult for hydrophobic polymers, such as linear low density polyethylene (LLDPE), to intercalate into clay layers because linear low density polyethylene (LLDPE) has no polar groups in the backbone of its chain.

1.3 How to assess compatibility and dispersion between the constituents

To asses compatibility and dispersion in nanocomposites, several different techniques have been developed. In previous studies, performed by Klitkou [2012], it was shown that the conventional TEM and XRD could be supported by FTIR and Oscillatory rheometry, in determining the morphology of the investigated nanocomposites and the interphase between constituents. Other studies, Xi et al. [2005] and Mallakpour and Dinari [2012] demonstrated that the thermal properties could be utilized to determine the placement and interaction of organic surfactants with regard to the decomposition temperature.

Effects on the crystal and chemical structure

The interlayer spacing or basal d spacing (d_{001}) of a nanoclay can be determined by XRD used to quantifying the different stages of dispersion, immiscible, intercalation and exfoliation. This is illustrated for pure organo clay in comparison with nanocomposite structure in figure 1.6.

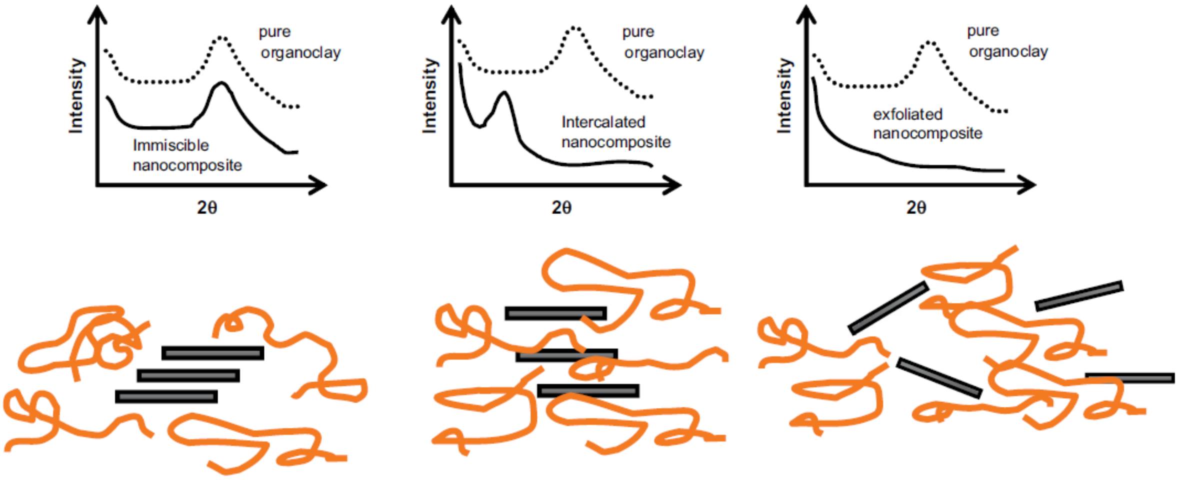

Figure 1.6. Illustration of different states of dispersion of modified nanoclays in polymers with regard to XRD [Paul and Robeson, 2008].

The different nano-clays have characteristic peaks, which with Bragg's law, the spacing between the platelets can be determined. The placement and size of the peaks can determine the state of intercalation/exfoliation, where no shift of the peak is interpreted as immiscible and no intercalant had penetrated the galleries of the clays. If the peak shifts to a lower angle, or larger d-spacing, this is generally interpreted as intercalation of matrix material (e.g. polymers or other species) into the galleries of nanoclay. If the peak is absent, it can be perceived as exfoliation, however this have to be supported by other characterization methods. If the peak shift to higher angles, it can be interpreted as loss of unbound surfactant or matrix material from the gallery, or degradation of the utilized surfactant [Paul and Robeson, 2008]. According to [Rawtani and Agrawal, 2012], dehydrated halloysite nanotubes (HNT) have the same crystal structure as disordered kaolinite structure, despite the different particle shape and morphology. The morphology of the nanotubes could cause overlapping and therefore it can be difficult to determine the exact crystal structure using XRD. This can be seen in figure 1.7, where the spectra of three different kinds of raw Halloysite nanotubes form different geographic origins are shown [Yuan et al., 2008].

The changes of the peaks for halloysite nanotubes should be compared for a raw sample and a

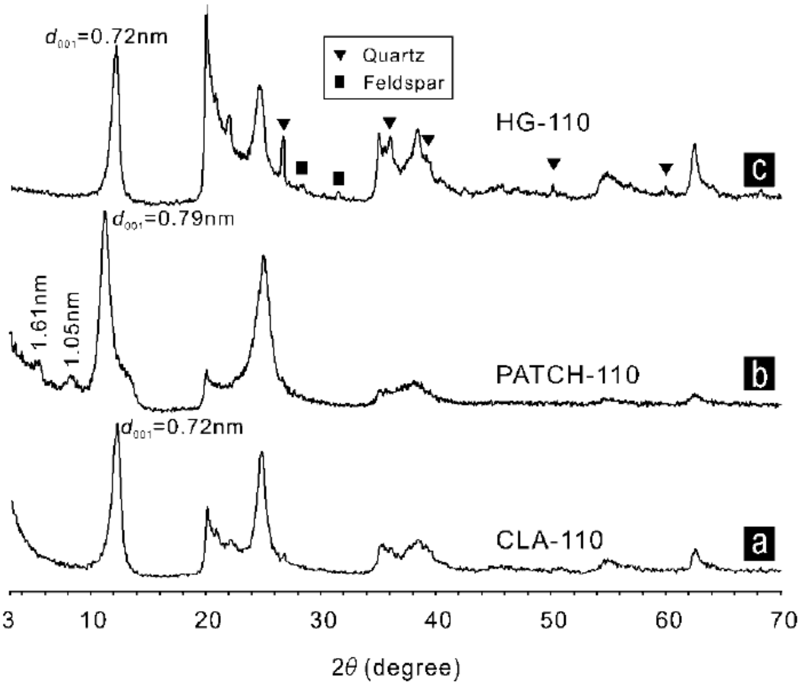

Figure 1.7. XRD patterns of three different kinds of raw Halloysite, CLA, PATCH and HG [Yuan et al., 2008].

modified version.

Another technique for investigation of clay dispersion and state of intercalation/exfoliation for some polymeric/clay nanocomposites, using the chemical composition, is FTIR. According to Cole [2008], montmorillonite has four distinct peaks in the region from 1150-1000 cm^{-1}, and corresponds to four Si-O stretching modes. The four peaks (1120, 1080, 1048, 1025) are affected with regard to the state of intercalation of the clay particles. The peak of 1080 cm^{-1} is reported to narrow in bandwidth and shift to higher angles with increasing intercalation/exfoliation. There is a relation between the four peaks, where the peaks 1080 and 1048 cm^{-1} gets more prominent, compared to the two other peaks 1120 and 1025 cm^{-1}, with increasing intercalation/exfoliation [Klitkou, 2012]. The spectra illustrated in figure A.9 are the results of the PP/OMMT nanocomposites, which were investigated. The four peaks are clearly present in both of the normalized spectra.

The effect on the thermal properties

The degree of intercalation/exfoliation can be determined with the thermal properties of the organo clay. This can be assessed with TGA, where the decomposition of an organoclay takes place in four steps: water desorption, dehydration, desurfactant and dehydroxylation [Xi et al., 2005]. The intercalant/surfactant of the organoclay, is affected by the molecular environment, in which it is present and this will affect the decomposition temperature. According to Xi et al. [2005], there are three different environments; surfactant cations intercalated into the clay interlayers through cation exchange and bound to surface sites via electrostatic interaction, surfactant (cations and/or molecules) are physically absorbed on the external surface of the clay and surfactant molecules are located within the clay interlayer. Pure montmorillonite clay does not undergo thermally induced changes in the temperature range of 130-650 °C,

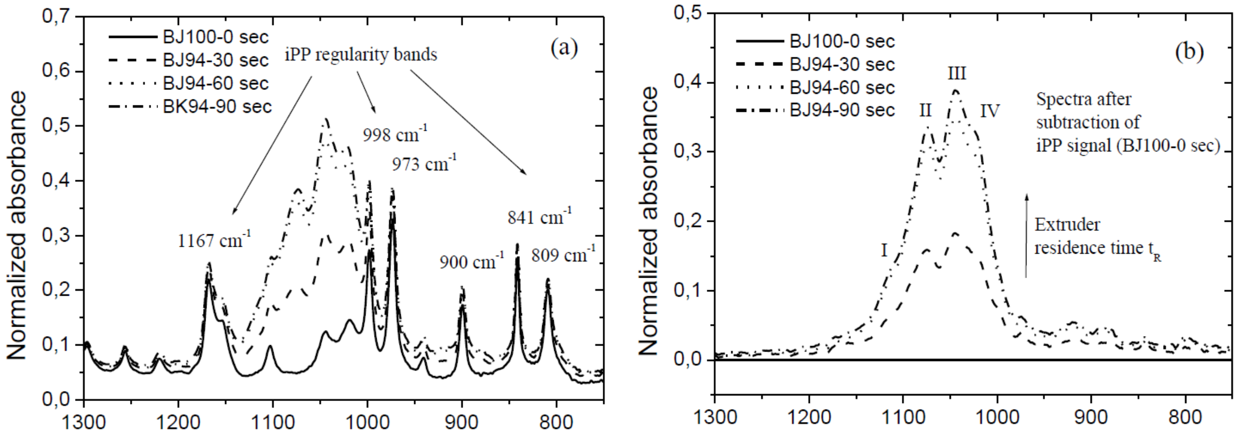

Figure 1.8. Normalized absorbance spectrum for the polypropylene nanocomposite, where (a) is the raw signal, and (b) is a subtracted signal [Klitkou, 2012].

and any mass loss in this temperature range can be attributed to the decomposition of the intercalant/surfactant within an organo clay [Mallakpour and Dinari, 2012].

The effect on rheological properties

The changes of the rheological properties can determine if a filler material is compatible with the polymer matrix [Klitkou, 2012]. In nanocomposites, if a plateau in the storage modulus (G') at low frequencies is located, it indicates a build-up of complexity viscosity($\eta*$). This build-up of complex viscosity is associated with filler dispersion and activation with the affected melt network. According to Klitkou [2012], the rheological measurements can be used as an indirect method to determine interaction between the polymer matrix and filler.

1.4 Projects focus and goal

This thesis has two main focuses, where the first is to investigate if two types of nanoclay could be compatiblized with different intercalants/surfactants to achieve an intercalated/exfoliated structure. The second focus of this project, is to investigate the mechanical and thermal properties of nanocomposites, which were obtained from the different organically modified clays with linear low density polyethylene (LLDPE).

An initial study of the two different nanoclays, montmorillonite (MMT) and halloysite nanotubes (HNT), and the two different surfactant/intercalants was conducted. The intercalants were the bio-residue (BR) from NC A&T, and a wood-based bio-oil (WB), which was supplied by the Energy department - Aalborg university (AAU). This bio-oil is based on aspen wood and glycerol .

The reason for investigating two surfactants is to assess which organic compounds in the bio-oils could interact with the nanoclays. The chemical composition of the two bio-oils are different, however both bio-oils have polar compounds. From the results from Høgsaa [2015], it is believed the interaction between the carboxyl groups (-COOH) of the long fatty acids, or the nitrogen rich compounds (e.g. amides and amines) of the bio-oil and the montmorillonite yielded the increase in the basal d-spacing of the modified montmorillonite. This is based on the findings of Rooj et al. [2012], where long fatty acids can facilitate intercalation in montmorillonite, where the polar carbxyl group (-COOH) was attracted to the backbone of the montmorillonite clay and the long non polar chain intercalated and expanded the interlayer spacing of the clay, as seen in figure 1.9.

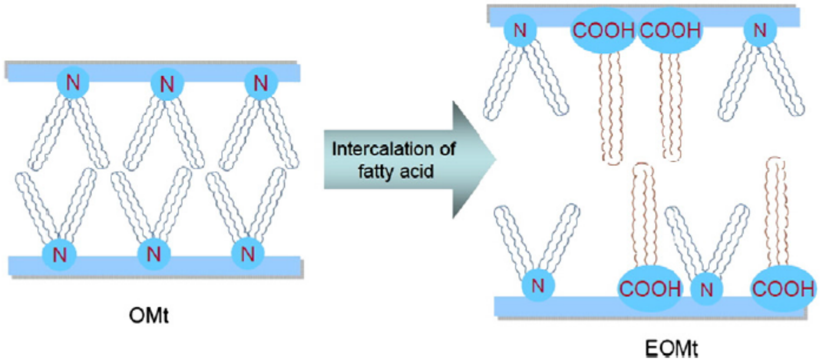

Figure 1.9. Representation of the intercalation process with long fatty acids [Rooj et al., 2012].

The wood-based bio-oil (WB) do not have long fatty acids or nitrogen present in its chemical composition [Pedersen et al., 2016]. However it was important that this surfactant had polar compounds e.g (hydroxyl(-OH) and ketone(=O)).These polar groups could possibly facilitate dipole-dipole interaction between the surfactant and the clay.

Montmorillonite clay can be compatibilizers with organic surfactants, because of its chemical structure. The choice for the halloysite nanotubes (HNT) clay was due to its chemical structure, where the sheets are rolled into nanotubes having siloxane (-Si-O-Si-) on the exterior and aluminol (-Al-OH) on the interior of the tube. The difference in the chemical structures of the two clays can be used to determine, which compound of the surfactant reacts with chemical structure of the clay. Additionally the halloysite nanotubes is supposed to be more easily dispersed compared to conventional nanoclay, due to its tubular structure, where the interactions forces between tubes are reduced.

The second focus is to investigate the mechanical and thermal properties of nanocomposites, which were obtained from the different organically modified clays with linear low density polyethylene. The properties are dependent on the compatibility between the filler and the polymer matrix, while the degree of dispersion of the filler is another indication of the compatibility. A study of the state of intercalation/exfoliation were conducted to gain a deeper understanding of intercalation mechanism, and compatibility, between the polymer matrix, fillers and the surfactant/intercalants. The polymer matrix was selected to be linear low density polyethylene (LLDPE), due to its chemical structure and properties. Linear low density polyethylene (LLDPE) is hydrophobic, while the clays are hydrophyllic. Thus compatibilization with an intercalant/surfactant containing compounds with polar and non-polar groups is necessary.

Problem statement 2

In this thesis, based on the project goals, it was chosen to investigate if different bio-oils can be used as surfactants for compatibilization of two different nano-clays. These modified nano-clays were investigated to determine the state of intercalation/exfoliation. The obtained organo clays were melt-blended with linear low density polyethylene (LLDPE), to evaluate if the modified nanoclays are compatible with hydrophobic polymer. The properties and dispersion of nanoclay are indications of how compatible the constituents are.

Literature studies of the different materials compiled from different sources(e.g articles and patents) and the findings of an earlier project Høgsaa [2015] showed that bio-residue (BR) can be used as an organic modifier to achieve intercalated or exfoliated structure of the montmorillonite. The other surfactant wood-based bio-oil (WB) and nanoclay halloysite nanotubes (HNT) were selected due to their different chemical structure and composition.

Based on this, the problem statements for this thesis are:

What are the chemical properties of the specified bio-oils and nanoclays?

and

Can the investigated bio-oils be used as modifiers for untreated Na-montmorillonite (MMT) and halloysite nanotubes (HNT) to achieve a intercalated/exfoliated structure?

and

Are the modified nanoclays compatible with linear low density polyethylene (LLDPE)?

The first focus area of this thesis is Investigated materials, where all materials used is investigated to achieve baseline information about selected properties e.g. chemical composition and thermal properties. This will be investigated with the following techniques; Gas chromatography/Mass spectrometry (GC-MS), X-ray diffraction (XRD), Attenuated total reflectance fourier transform infrared spectroscopy (ATR-FTIR) and Thermogravimetric analysis(TGA).

The second part of the thesis is Modification of the nanoclays. This chapter focuses on investigating the modification process and the interaction between the nanoclays; halloysite nanotubes (HNT) and montmorillonite (MMT), and the surfactants, bio-residue (BR) and wood-based bio-oil (WB). The structures of the modified nanoclays will be investigated with the following techniques; X-ray diffraction (XRD), Attenuated total Reflectance fourier transform infrared spectroscopy (ATR-FTIR) and Thermogravimetric analysis (TGA) to evaluate the effects of the modification, or pre-intercalation, process of the nanoclays with different surfactants.

In the third part of this thesis, denoted Nanocomposites and properties, the mechanical and thermal properties of nanocomposites were investigated. The nanocomposites were processed by melt-blending the linear low density polyethylene (LLDPE) with the raw and modified nanoclays. The nanocomposites will be investigated with the following techniques; X-ray diffraction (XRD), Attenuated total reflectance fourier transform infrared spectroscopy (ATR-FTIR), Oscillatory rheometry(OR), Thermogravimetric analysis(TGA), Optical analysis(OP) and Uni-axial tensile tests(UTT), to evaluate the properties and dispersion rate.

The outcome for this thesis is to assess if the chosen bio-oils, bio-residue (BR) and wood-based bio-oil (WB), can be used as surfactants/compatibilizers between the selected hydrophyllic nanoclays in the hydrophobic matrix material linear low density polyethylene (LLDPE).

Experimental part 3

3.1 Characterization methods

The following techniques were employed in order to characterize the raw, modified materials, and the nanocomposites investigated in this thesis.

Gas chromatography/ Mass spectrometry (GC-MS) were used to investigate if the utilized bio-oils have the desired molecular compositions with the amphiphilic compounds identified in the earlier project [Høgsaa, 2015] .

X-ray diffraction (XRD) was used to study the degree of possible intercalation or exfoliation of the modified nanoclays and the obtained nanocomposites by assessment of the d-spacing and peak intensities. The technique was further utilized to determine the crystal structure of the bio-oils.

Attenuated total reflectance fourier transform infrared spectroscopy (ATR-FTIR) was performed to obtain an infrared spectrum of the raw materials and the organically modified silicate to determine the possible chemical compositions. The state of intercalation/exfoliation of the nanocomposites and the modified clays was investigated.

Oscillatory rheometry is performed to determine the visco-elastic behavior and viscosity of the obtained nanocomposites, and indirectly the dispersion rate of the clay.

Thermogravimetric analysis (TGA) is used to assess the decomposition and thermal stability of materials to examine the physic-chemical processes occurring in the materials at different temperatures.

Uni-axial tensile test were utilized to investigate the mechanical response of the obtained nanocomposites with focus on maximum tensile stress at yield and break.

Optical analysis is utilized to investigated the effects of the extrusion process on the dispersion rate and particle size distribution.

3.1.1 Gas Chromatography/Mass Spectrometry (GC-MS)

Qualitative analysis of the bio-residue(BR) were carried out on a Thermo Scientific Trace 1300 ISQ GC–MS system, using a TG-SQC column (Length: 15 m, i.d.: 0.25 mm, film: 0.25 μm film). The obtained results were compared to the earlier results, reported in other publications, of the swine based bio-oils.

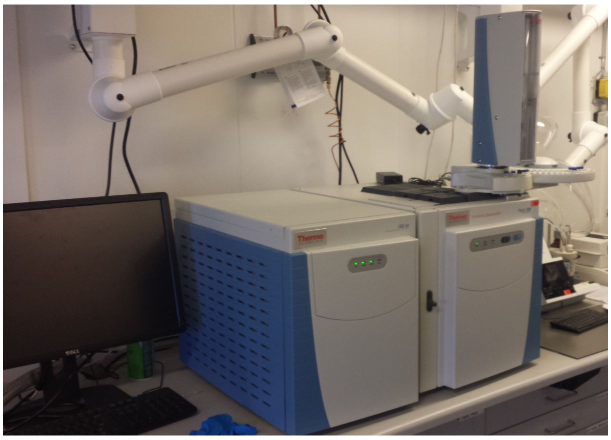

Figure 3.1. Thermo Scientific Trace 1300 ISQ GC–MS system.

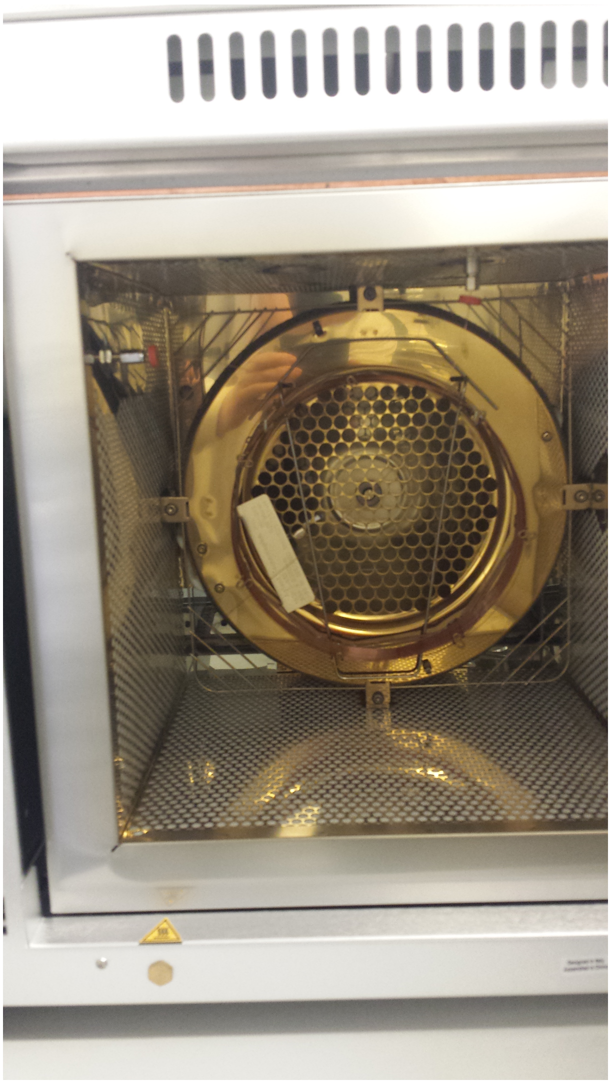

Figure 3.2. Colume of the Thermo Scientific Trace 1300 ISQ GC–MS system.

The samples were modified with TMS derivitization, where a small amount of each sample was inserted into a vial and a few drops of BSTFA (N,O-Bis(trimethylsilyl)trifluoroacetamide) were added to the vial. The reagent can be used to derivatize non-volatile compounds such as certain alcohols, phenols, or carboxylic acids by substituting a trimethylsilyl group for a hydrogen in the hydroxyl groups on the compounds. This lowers the polarity of the affected compound and reduces the boiling point and therefore is the compound more prone to volatilisation. The vial was heated in a water bath for 1 hour at 60 °C and then flushed with nitrogen gas to remove the excess reagents.

Prior to the analysis, the samples were diluted in solvent, in this case diethyl ether (DEE), and subjected to the following oven temperature profile: a ramp of at 8 °C/min until 300 °C. Injector and ion source temperatures were 300 °C, split ratio was 1:20, and flow rate of the carrier gas (helium) was 1.0 mL/min. The compounds were identified by mass spectra comparison with the obtained spectra in the NIST mass spectral data library. According to Pedersen et al. [2016], the identification process of all compounds by GC–MS is challenging due to the complexity of the mixture and to the fact only the volatile fraction is identifiable.

The theoretical aspects of this technique are elaborated in Appendix B.1.

3.1.2 X-ray diffraction (XRD)

X-ray diffraction patterns were investigated on a PANalytical Empyrean diffractometer, see figure 3.3 with CuKα radiation, running at 45 kV and 40 mA.

Figure 3.3. PANalytical - Empyrean diffractometer Panalytical [2015].

This setup was operated in the 2θ interval from 3 to 40°. Intercalation and exfoliation in the raw materials, modified nanoclays and nanocomposites were determined using Braggs law. The samples were prepared, as illustrated in figures 3.4 and 3.5. The bio-oils were tested with a sample holder with an amorphous plate, and nanoclays; modified, unmodified and nanocomposites were tested in traditional sample holders. The only change to the testing procedure was the nanocomposites. The injected molded sample were cut and placed in traditional sample holder with spacer discs to ensure the measuring surface height.

Figure 3.4. The prepared sample for XRD analysis.

Figure 3.5. A prepared nanocomposite sample with underlying spacer discs for XRD analysis.

Bragg's law, see equation 3.1 is used used to determine the basal d-spacing of the investigated nanoclays.

$$\mathrm{n}\lambda = 2\mathrm{d}\sin\theta \tag{3.1}$$

The theoretical aspects of this technique are elaborated in Appendix B.2.

3.1.3 Attenuated total reflectance fourier transform infrared spectroscopy (ATR-FTIR)

The attenuated total reflectance Fourier transform infrared spectroscopy (ATR-FTIR) measurements were performed on a Spectrum One spectrometer from Perkin Elmer. The tests were performed with the applied zinc selenide crystal in absorbance mode to acquire the spectra of the raw and modified materials in wave numbers ranging from 500 cm^{-1} to 4000 cm^{-1}. The penetration depth of the crystal is 1.66 μm [Perkin Elmer, 2004]. The samples were placed directly on the zinc selenide crystal and a force gauge was applied on samples to ensure appropriate contact. The crystal was cleaned with a cleaning agent, acetone or deionized water, after each measurement .

The theoretical aspects of this technique are elaborated in Appendix B.3.

3.1.4 Oscillatory rheometry (OR)

The rheological properties of the obtained nanocomposites were investigated with the Discovery hydrbrid H3 from TA instruments. The amplitude of 5% strain was determined with an initial amplitude sweep. This strain rate remains within the linear visco-elastic regime. The angular frequencies ranged from 600 rad/sec to 0.02 rad/sec in a CP25 parallel plate-plate configuration with a 25 mm diameter disc and a gap height of 0.105 mm. The initial tests were performed at 180°C and for the additional extruded samples at 170°C, to avoid degradation. The initial tests were performed with one sample per batch, while the extruded samples were tested with three repetitions per batch and the average value is determined.

The theoretical aspects of this technique are elaborated in Appendix B.5.

3.1.5 Thermogravimetric analysis (TGA)

Measurements were used for determining the thermal properties of the raw materials, modified nanoclays and the nanocomposites. The analysis was performed with two different setup, Netzsch STA 449 C Jupiter and Discovery TGA. The raw materials and the modified nanoclays were tested on a Netzsch STA 449 C Jupiter, which performs a simultaneous DSC and TGA analysis. These measurements were performed to obtain a baseline and assess the amount of intercalated surfactant of the modified nanoclays clays. All samples were tested in crucibles in argon atmosphere with a heating rate of 10 °C/min, from 40 °C to 1000 °C.

Discovery TGA were utilized to assess the thermal properties, thermal resistance and mass loss of the nanocomposites. Samples were performed in pans with nitrogen atmosphere with a heating rate of 10 °C/minute, from approximately 40 °C to 600 °C.

The theoretical aspects of this technique are elaborated in Appendix B.4.

3.1.6 Uni-axial tensile testing (UTT)

The mechanical properties were determined with an Instron 5844 tensile machine on injection molded samples of ISO 527 type 1BA specimens. Two samples were tested for each batch type in accordance with ISO standards. The tests were carried out at a cross head speed of 50 mm min^{-1} without extensometer and a gauge length of 50 mm. The following tensile properties were determined; Elastic modulus (Automatic), maximum tensile stress and strain stress at yield, maximum tensile stress and strain at break.

The theoretical aspects of this technique are elaborated in Appendix B.6.

3.1.7 Optical analysis (OP)

A microscopy with light at magnification of 10X were used for the optical analysis. A light source is directed vertically through the microscope objective and reflected back through the objective to the eyepiece or attached camera. Transmitted light is used for transparent and translucent materials. The thickness of the sample are kept small at 100 μm to ensure the light passes trough the samples. In this project the primary use for microscopy is to analysis the dispersion rate and hereby the size of possible agglomerates or particles in each batch type.

Film preparation

A process for obtained optical microscopy films was developed. An aluminum mold with an indention, with a diameter of 15 mm and a height of 100 micrometers, was manufactured. A hot plate, which is capable to reached 180 °C, was used. The mold was placed on the hot plate and heated for 2 minutes, afterward the granules were loaded onto the mold. The granules were melted for 2 minutes and then a copper spatula was used to scrap the excess of the mold.

The mold was removed from the hot plate and rapidly cooled down to room temperature with compressed air for 1 minute. The produced film is removed from the mold. Using this procedure, two films were obtained for each batch of nanocomposites. The setup is shown in figure 3.6.

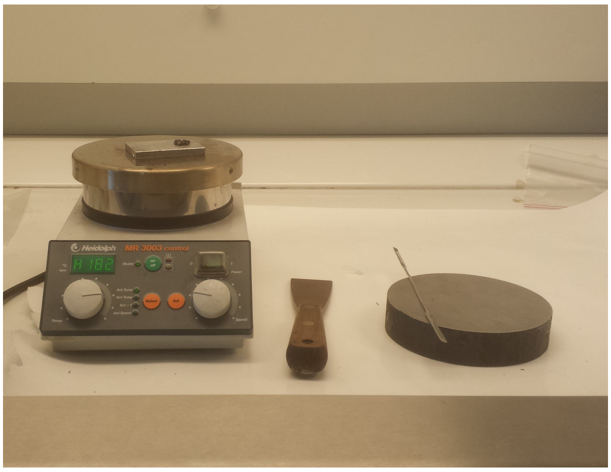

Figure 3.6. The setup for film preparation with selected equipment and loaded granulate.

Particle size analysis of the bio-oils

The bio-oils are examined with a Zetasizer Nano ZS from Malvern, see figure 3.7. This machine utilizes three different techniques; Dynamic Light Scattering, Laser Doppler Micro-electrophoresis, Static Light Scattering. The dynamic light scattering is used to determine the particle molecular size in the range of 0.3 nm - 10.0 microns. These measurements are to determine if particles are present in the bio-oils and an indication of the average value of the particle sizes.

Figure 3.7. Zetasizer Nano ZS from Malvern.

A solution consisting of a drop of bio-oil and 40 ml of ethanol were hand mixed/shaking until the bio-oils was dissolved. The solution was afterward ultrasonicated for 2 minutes. 2 ml of the solution was transferred to a cuvette and inserted into the sample stage of the machine. The reflective spectra of the diluent, ethanol, was removed in the analysis to ensure it is only the spectra of the bio-oil, which was analyzed.

3.1.8 Summary of characterization methods

The characterization techniques utilized in for the whole thesis, with indicated parts, are listed in table 3.1.

Table 3.1.

Part	GC-MS	XRD	ATR-FTIR	TGA	OR	OP	UTT
Investigated materials	X	X	X	X	-	-	-
Modification of nanoclays	-	X	X	X	-	-	-
Nanocomposites and their properties	-	X	X	X	X	X	X

3.2 Investigated materials

This part of the thesis is the technical specification and results of the initial characterization of the different materials, which are being investigated.

3.2.1 Technical specifications of the materials

Raw materials used in this thesis are two bio-oils, bio-residue (BR) and wood-based bio-oil (WB); two nanoclays, halloysite nanotubes (HNT) and montmorillonite (MMT); matrix material, linear low density (LLDPE). They are shown in figure 3.8.

Figure 3.8. Raw materials utilized in this thesis: bio-residue (BR), wood-based bio-oil (WB), halloysite nanotubes (HNT), montmorillonite (MMT), linear low density polyethylene (LLDPE).

Bio-residue (BR)

According to the data safety sheet the material is stable at room temperatures. The material will not polymerize and is not compatible with strong oxidizing agents. The decomposition products may include carbon monoxide, carbon dioxide and water vapor. The bio-oil had excess water content from the conversion process to bio-oil, and this was removed by drying.

Bio-oil from wood (WB)

The wood-based bio-oil do not have a specified data sheet and is a mixture of different batches, therefore there is no description for this product. From observations, it can be described as a thick, black substance with a strong odor. The wood-based (WB) had a small water content of approximately 4% [Pedersen et al., 2016], but it was deemed insignificant and could be processed with a small weight correction to ensure a 100% addition of oil for the modification process.

Montmorillonite (MMT)

The nanofiller used in this project is Cloisite Na^+, a natural montmorillonite enriched with Na^+ from Southern Clay Products, which is now a part of BYK Additives. Cloisite Na^+ has a typical dry particle size (d_{50}) of $< 25\mu$m, which contains 4-9% of moisture and has a specific density of 2.86 g/cm^3. The color of the powder is grayish/white. The material can be used to improve various physical properties, such as reinforcement, synergistic flame retardant and barrier properties [Additives and Instruments, 2015].

Halloysite nanotubes (HNT)

The color of the powder is white and has a mild odor of clay. The material is stable in a dry atmosphere. The specific density is 2.5 g/cm^3 [?]

Linear low density polyethylene(LLDPE)

The polymer is Flexirene MS produced by Polimeri Europa S.p.A. This polymer is a linear low density polyethylene with a meltflow index (MFI) of 26 g/10min, measured at 190°C. The density of the polymer is 0.921 g/cm^3 and has a melting point of 117 °C. The polymer was obtained using Ziegler–Natta catalysis polymerization method with butene as comonomer (C4-LLDPE). This type of LLDPE is suitable for injection molding applications. The reported tensile strength, at yield and break, is reported to be 9 and 10 MPa respectively. The elongation at break is less than 500 %. The suggested injection molding settings are between 160-210 °C for the barrel and 10-40 °C for the mold.

3.2.2 Results

Results of the baseline information about selected materials are covered in the following sections.

Attenuated total reflectance fourier transform infrared spectroscopy (ATR-FTIR)

FTIR analysis of the raw materials was used to gain a baseline information.

Spectra of the nanoclays can seen in figure 3.9. The bands in the 3100-3700 cm^{-1} region are attributed to O-H stretching vibration, while O-H bending vibration bands are located at 1600-1700 cm^{-1}. Si-O stretching band is observed at 1040 cm^{-1} as well as Si-O and Al-O bending bands at 400-600 cm^{-1}. Mg-O bending band was observed at 470 cm^{-1} [Rafiei and Ghomi, 2013]. HNT had similar peaks as MMT, however there are some difference. Two peaks are observed, instead of one, around 1000 and 3600 cm^{-1}. The two peaks at 3698 and 3626 cm^{-1}are attributed to the vibration of the aluminols of the HNTs [Liu et al., 2007]. The peak of 3626 cm^{-1} belongs is the inner OH groups, which is located in the plane between the alumina and silica sheets. This plane is not accessible for a intercalant/surfactant, and therefore this peak is always at this position [Khunova et al., 2013].v The peaks around 1000 cm^{-1} are associated with the Si-O stretching bands. A more pronounced peak is present around 900 cm^{-1}.

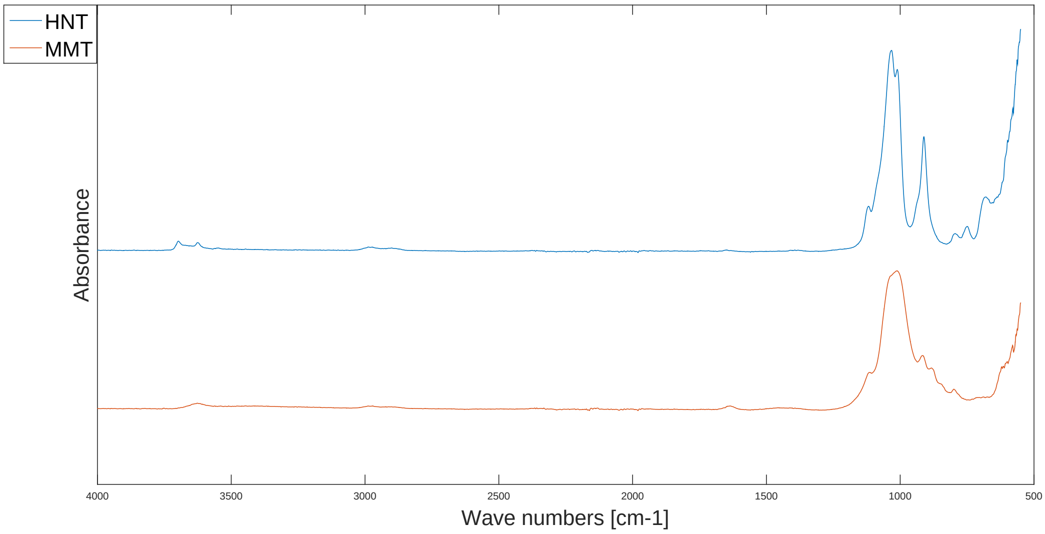

Figure 3.9. Absorbance spectra of the investigated HNT and MMT nanoclays.

The initial characterization of the received bio-residue (BR) yield interesting results. The received bio-residue(BR) was compared to the results of the former project [Høgsaa, 2015] and the results showed significant changes to spectra, especially the peaks around 1020 and 3350 cm^{-1}. The received bio-residue (BR) was not the same material as the original bio-residue investigated in former project [Høgsaa, 2015].

Therefore it was chosen to rename the new bio-residue (BR) to swine-based bio-oil (SB) and investigate the chemical composition more extensively with ATR-FTIR and GC-MS to determine the difference between the two compounds.

Spectra of the raw and dried bio-oils, bio-residue (BR), swine-based bio-oil (SB) and wood-based bio-oil (WB) are shown in figure 3.10. It was chosen to test if the drying process had affected the obtained results for the swine-based bio-oil (SB) and bio-residue (BR). However there was no significant changes of the positions and shapes of the peaks in any of the spectra. It can be observed that swine-based bio-oil (SB) had a similar spectra to bio-residue (BR), except the peaks around 1020 cm^{-1} and 3350 cm^{-1}. Peaks of 1020 and 3350 $^{-1}$ could be associated with O-C stretching(e.g. alcohols, carboxylic acids or ester)[Hosseinnezhad et al., 2015]. Another possibility could be a higher presence of amines, which also could have affect the peaks. The GC-MS analysis could confirm these possibilities.

The spectra of the wood-based bio-oil (WB) had a similar spectra, however the absence of nitrogen in its chemical composition[Pedersen et al., 2016], could account for these differences.

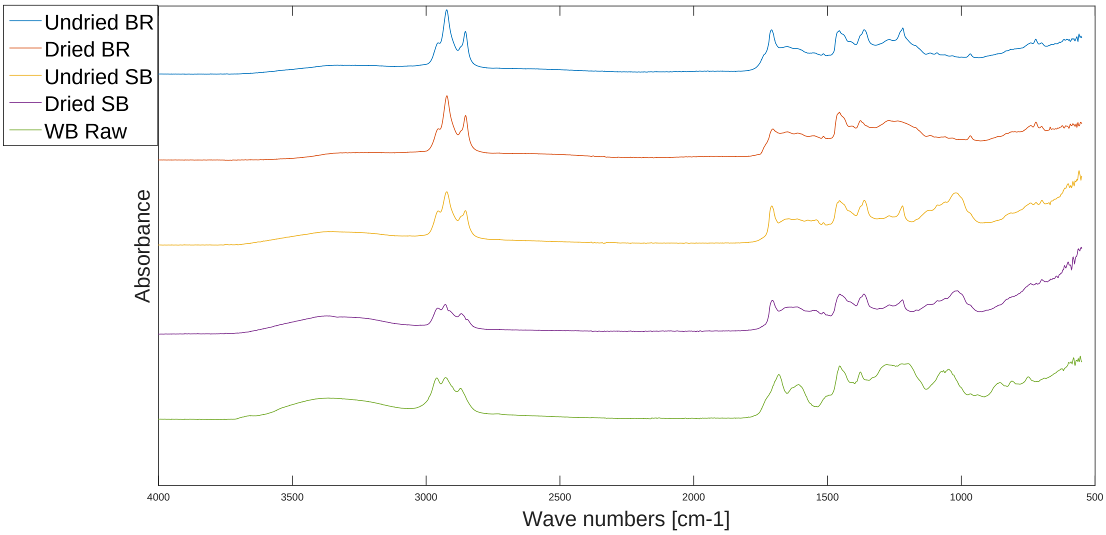

Figure 3.10. Absorbance spectra of the investigated Bio-oils.

GC-MS analysis

The results of the ATR-FTIR analysis showed that swine-based bio-oil (SB) and bio-residue (BR) had similar spectra with some changes, despite being from the same processing step. Therefore was a GC-MS analysis conducted for the bio-residue(BR) and the swine based bio-oil (SB) to investigate if the chemical composition of the material was altered. The GC-MS analysis was conducted at the Energy department - Aalborg University and the findings are reported in table 3.2 the functional groups found are listed. The program ramp from ambient temperature to 320 °C and the solvent utilized was diethyl ether.

Table 3.2. List of identified compounds in the dried bio-residue (BR) by GC-MS.

RT [min]	Identified compound	Chemical formula	C_n
4.84	2-Pentanone, 4-hydroxy-4-methyl-	$C_6H_{12}O_2$	6
8.82	Decane	$C_{10}H_{22}$	10
19.03	Tetraacetyl-d-xylonic nitrile	$C_{14}H_{17}NO_9$	14
22.26	7-Tetradecene	$C_{14}H_{28}$	14
30.44	Pentadecanoic acid	$C_{15}H_{30}O_2$	15
32.52	n-Hexadecanoic acid	$C_{16}H_{32}O_2$	16
35.93	trans-13-Octadecenoic acid	$C_{18}H_{34}O_2$	18
36.23	Octadecanoic acid	$C_{18}H_{36}O_2$	18
36.52	Dodecanamide	$C_{12}H_{25}NO$	12
37.13	N-Methyldodecanamide	$C_{13}H_{27}NO$	13
37.87	N,N-Dimethyldodecanamide	$C_{14}H_{29}NO$	14
39.57	9-Octadecenamide, (Z)-	$C_{18}H_{35}NO$	18
39.99	Octadecanamide	$C_{18}H_{37}NO$	18
40.19	1,3-Dioxocane, 2-pentadecyl	$C_{21}H_{42}O_2$	21
40.57	N-Methyldodecanamide	$C_{13}H_{27}NO$	13
40.23	N,N-Dimethyldodecanamide	$C_{14}H_{29}NO$	14
41.87	Hexadecanoic acid, 1-(hydroxymethyl)-1,2-ethanediyl ester	$C_{35}H_{68}O_5$	35
44.93	Octadecanoic acid, 2-hydroxy-1,3-propanediyl ester	$C_{39}H_{76}O_5$	39

The compounds found in the bio-residue are comparable to the results, described by Fini et al. [2011] and Hosseinnezhad et al. [2015], especially the presence of long fatty acids, amines and amides. The increased nitrogen was attributed to a higher amount of proteins, derived from the processing of the food in the dietary tract of the pigs. However there is an uncertainty on how the diet of the pigs affected the chemical composition of the obtained product during and after processing [Mills-Beale et al., 2012]. This could have affected the chemical composition of the oil and therefore the properties of bio-residue, which could explain the difference between the bio-residue (BR) and the swine-based bio-oil (SB).

The chemical composition of swine based bio-oil were investigated to ensure that the essential chemical compounds, like the long fatty acids and the amides identified in the bio-residue, are present. A secondary GC-MS analysis was conducted to assess if the drying process altered the chemical composition. The chemical composition of swine based bio-oil before and after drying showed some changes in the compounds present in material, as seen in figure 3.11. Identified compounds are listed in tables 3.3 and 3.4.

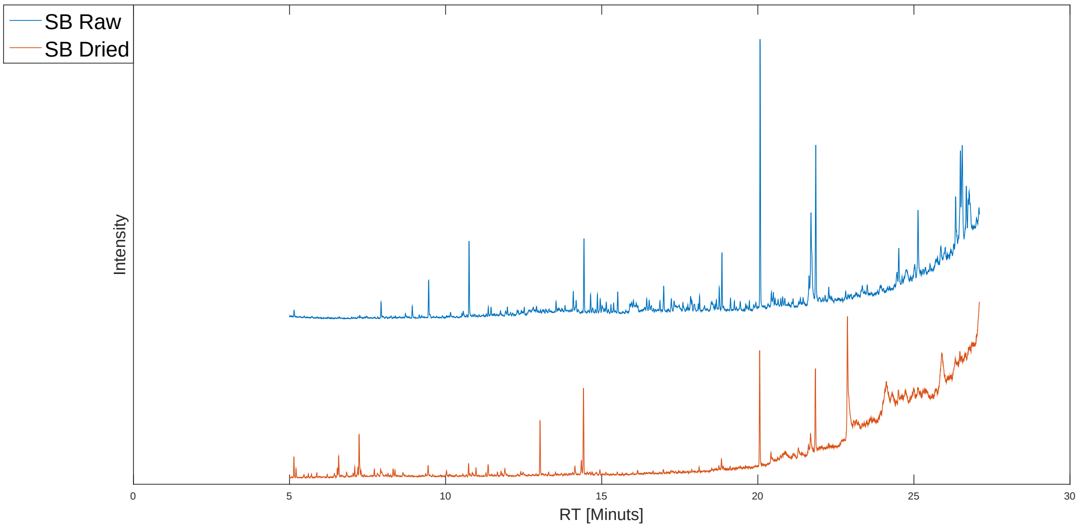

Figure 3.11. GC spectra of the raw and dried versions of the swine-based bio-oil(SB).

A byproduct of the solvent of the original conversion process[Fini, 2013], Butylated Hydroxytoluene, is present in the raw and dried swine-based bio-oil (SB). A difference in identified compounds were observed, when the swine based bio-oil (SB), raw and dried, are compared to bio-residue (BR). Bio-residue (BR) have a higher amount of amides and nitrogen based compounds present. The compounds identified in swine based bio-oil (SB) were predominantly aliphatic compounds with a polar functional group attached, e.g. long fatty acids. A small amount of aromatic compounds, e.g. phenol, were determined. The bio-residue and swine based bio-oil have difference in the chemical composition, however the polar compounds are present in both bio-oil types.

Table 3.3. List of identified compounds in the raw version of swine-based bio-oil (SB) by gas chromatography–mass spectroscopy.

RT (min)	Identified compound	Chemical formula	C_n
4.51	2,4-Dimethyl-1-heptene	C_9H_{18}	9
6.57	Hydroxylamine, O-(3-methylbutyl)-	$C_5H_{13}NO$	5
7.23	3-Hydroxybutyric acid, t-butyl ester	$C_8H_{16}O_3$	8
10.73	3-Ethylphenol	$C_8H_{10}O$	8
11.36	Phosphoric acid	H_3PO_4	0
13.02	Pentanedioic acid	$C_5H_8O_4$	5
14.35	Phenol, 2,4-bis(1,1-dimethylethyl)-	$C_{14}H_{22}O$	14
14.42	Butylated Hydroxytoluene	$C_{15}H_{24}O$	15
18.84	n-Pentanoic acid	$C_{15}H_{10}O_2$	15
20.06	Hexadecanoic acid	$C_{16}H_{32}O_2$	16
21.69	cis-9-Octadecenoic acid	$C_{18}H_{34}O_2$	18
21.84	Octadecanoic acid	$C_{18}H_{36}O_2$	18
22.87	9-Octadecenamide, (Z)-	$C_{18}H_{35}NO$	18
24.11	Sulfurous acid, pentyl tetradecyl ester	$C_{19}H_{40}O_3S$	19
24.51	Dodecanedioic acid	$C_{12}H_{22}O_4$	12
24.73	Oleic acid, 3-(octadecyloxy)propyl ester	$C_{39}H_{76}O_3$	39

Table 3.4. List of identified compounds in the dried version of swine-based bio-oil (SB) by gas chromatography–mass spectroscopy.

RT (min)	Identified compound	Chemical formula	C_n
7.93	Phenol	C_6H_6O	6
8.93	4-Piperidinone, 2,2,6,6-tetramethyl-	$C_9H_{17}NO$	9
9.46	3-Methylphenol	C_7H_8O	7
10.75	3-Ethylphenol	$C_8H_{10}O$	8
11.37	Glycerol	C_3H_{803}	3
14.43	Butylated Hydroxytoluene	$C_{15}H_{24}O$	15
14.64	3-methyl-Indole	C_9H_9N	9
15.51	2,5-dimethyl-Indole	$C_{10}H_{11}N$	10
18.85	n-Pentanoic acid	$C_{15}H_{10}O_2$	15
20.07	Hexadecanoic acid	$C_{16}H_{32}O_2$	16
21.70	cis-9-Octadecenoic acid	$C_{18}H_{34}O_2$	18
21.86	Octadecanoic acid	$C_{18}H_{36}O_2$	18
24.52	1,3-Dihydroxy-2-propanyl (9Z,12Z,15Z)-9,12,15-octadecatrienoate	$C_{21}H_{36}O_4$	21

XRD analysis

Raw halloysite nanotubes, montmorillonite, the swine-based bio-oil(SB) and the wood-based bio-oil(WB) were investigated with XRD.

The results of the X-ray diffraction of the raw halloysite and MMT, see figure 3.12, showed the following peaks. The d_{001} peak for MMT was found at 7.57, with a corresponding spacing of 11.7 Å. This measurement fits with the data sheet from the supplier [Additives and Instruments, 2015]. The halloysite nanotubes showed a d_{001}peak at 11.97, which corresponded to a interlayer spacing of 7.39 Å, which fits with dehydrated halloysite nanotubes. Spectra of the raw nanoclays can be used as a baseline to evaluate the effects of the modification process with different intercalants/surfactants.

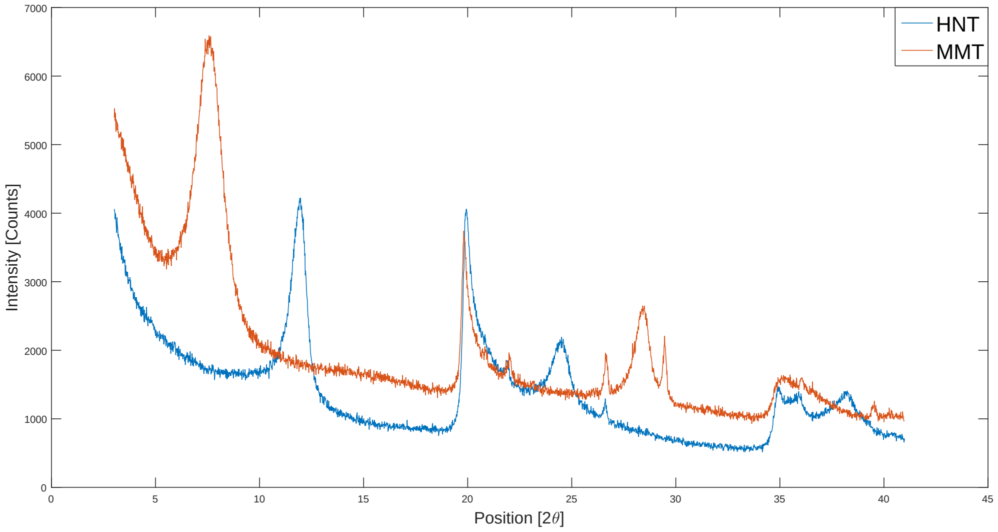

Figure 3.12. XRD analysis for raw nanoclays; MMT and HNT.

Swine-based bio-oil (SB) and wood-based bio-oil (WB) were tested with and without ultra sonic treatment to assess if there were any effects of the treatment or if the bio-oil had a crystalline structure. The wood-based bio-oil (WB) showed no crystalline structure and the results yielded amorphous signals. The swine-based bio-oil(SB) samples showed signs of a crystalline structure, with peaks at high angles, with or without treatment. The size of the found crystal structure is small and this could indicate that the bio-oil have crystalline particles. New peaks were found after the ultrasonic treatment, which could indicate the presence of the liquid crystals. These findings indicate that the swine-based bio-oil is not a ordinary bio-oil.

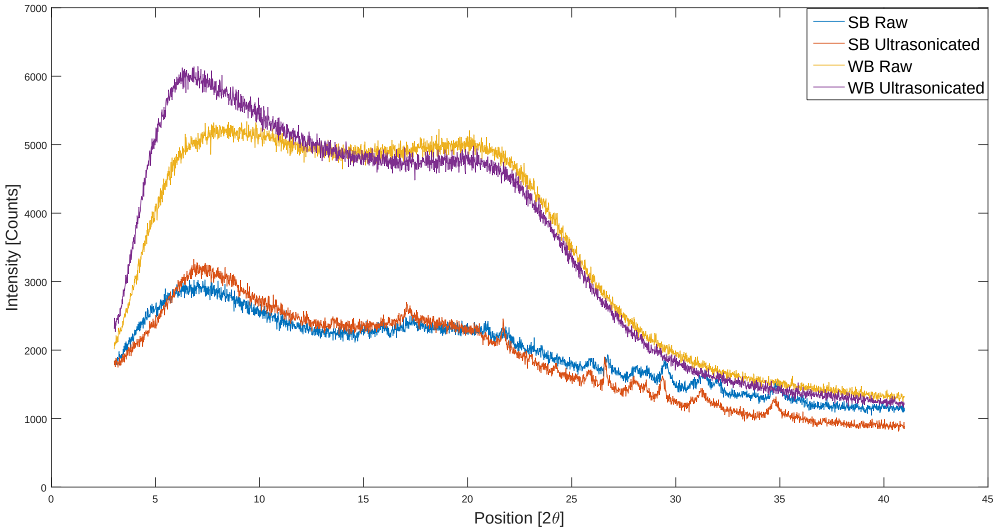

Figure 3.13. XRD analysis for the different bio-oils with/without ultrasonicated treatment.

Thermogrametric analysis

Results of the raw materials are shown in figure 3.14.

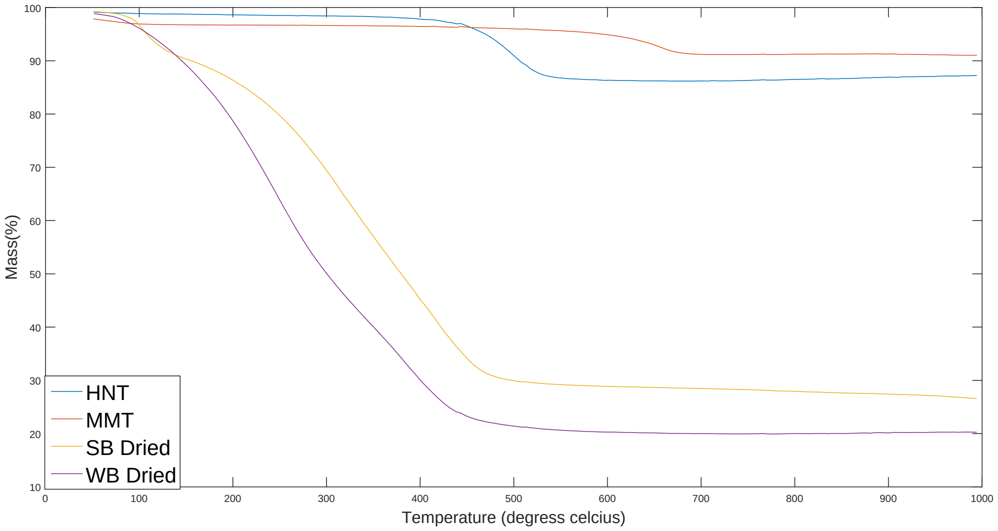

Figure 3.14. TGA measurement of weight loss, as a function of temperature, for raw nanoclays and bio-oils.

Residual mass of the clays were 87.23 % and 91.03 % for halloysite nanotubes (HNT) and montmorillonite (MMT) respectively. Due to the fact the halloysite nanotubes have a similar structure to the disordered kaolinite, a comparison to the dehydroxylation process of water in the raw clay can be established. According to Stoch and Wacławska [1981], the dehydroxylation of disordered kaolinite starts at 350-400 °C and the theoretical mass loss is 13.96 wt. %. The measured weight loss of the halloysite nanotubes (HNT) was 12.87 % and the onset temperature was 456.8 °C. The measured onset temperature of MMT was determined to be 612 °C and the residual mass to 91.03%. Swine-based bio-oil (SB) had a higher resistance to thermal degradation than wood-based bio-oil (WB) with an increase in the onset temperature of 102.3 °C. The residual mass of wood-based bio-oil (WB) was lower than swine-based bio-oil (SB) with 6.26%

3.2.3 Part conclusion

The initial characterization of the raw materials were performed to obtain baseline information for further studies. The results of the bio-residue (BR) showed that the bio-residue received in this thesis was not the same materials as the bio-residue investigated in the former project [Høgsaa, 2015]. The new bio-residue was renamed to swine-based bio-oil (SB), as a way to compare the results of the two compounds. However the results for the swine-based bio-oil (SB) showed that the material had a similar chemical composition to the bio-residue (BR) However there where some changes in the chemical structure. The swine based bio-oil still had a high presence of long fatty acids, a low content of nitrogen and oxygen compounds(e.g. amines, amides and olefins), when compared to the bio-residue (BR). FTIR analysis showed changes in the chemical composition, especially a pronounced peaks at around 1020 cm^{-1} and 3350 cm^{-1}. Peaks of 1020 and 3350 could be associated with O-C stretching(e.g. alcohols, carboxylic acids or ester)[Hosseinnezhad et al., 2015]. The changes in the chemical composition between the bio-residue(BR) and the swine-based bio-oil (SB), which were obtained from the same processing step, could indicate variations and uncertainties about the utilized conversion process for obtaining a homogenous product. The wood-based bio-oil(WB) had the desired changes in chemical composition and functional groups, when compared to the swine-based bio-oil(SB). This was confirmed with GC-MS analysis for all bio-oil types. The changes in the chemical composition could affect the potential of the swine based bio-oils as a surfactant for the selected clay types. However compared to the wood-based bio-oil(WB) ,the bio-residue (BR) and swine-based (SB) versions are similar and have the desired compounds, which are the long fatty acids and amides. These compounds have the carbxyl group (-COOH), which is believed to be the compounds which are the compounds which can facilitate the intercalation/exfoliation process as an intercalant/surfactant. However it can be difficult to asses the results of the GC-MS, because it is only the volatile phase, which is investigated and the temperature profile was only up to 300 °C. Therefore the results of the TGA analysis are essential, because swine-based bio-oil (SB), at 300 °C had a residual mass of 69.52 % of and the wood-based bio-oil(WB), mass of 50.18 %. This indicates only around 30 % and 50 % of the mass is investigated, however the TMS derivatization lowers the boiling points of some of the polar compounds. Due to the TMS process, some of the more polar compounds were included, but the mass stability of the two bio-oils are first found around 500 °C. Another drawback is the process is very demanding with regard to the operators skills and knowledge at analyzing compounds, due the different chemical reactions and understanding if the found suggestions from the library of the software, fits with the possible reactions and interaction between the raw materials. The nanoclays, montmorillonite (MMT) and halloysite nanotubes (HNT), and the bio-oils were investigated for the their crystal structure within selected angles for each clay type. The results correspond literature. The only exception was the swine bio-oil(SB), which had a crystal structure, unlike the amorphous wood based bio-oil (WB). The thermal properties were determined for baseline information, where the findings corresponded with literature. The baseline information about LLDPE was not investigated in this part, but will be described in the third part of the thesis Nanocomposites and their properties.

3.3 Modification of nanoclays

This part of the thesis is the experimental procedure and results for the modification process of different nanoclays, which are being investigated. The experimental procedure for this part is divided in two sections; preparation and processing of the materials, and the obtained results.

3.3.1 Modification of the nanoclays

The modification process for the different clays with bio-oils were conducted as follows. First step was drying to remove any excess water content, if required, from the bio-oils. Modification process is performed and completed with a secondary drying process.

Different batches were processed with the procedure with the listed ratios in table 3.5. The modified nanoclays are titled after the constituents present in the batch. Clay type is mentioned first and then intercalant/surfactant in a 1:1 ratio. The only exceptions is two MMT modified clays, which have different ratios, MMT/SB/2-1 and MMT/SB/1-2.

Table 3.5. Materials characterization.

Name	Clay	Bio-oil	Ratio
HNT/SB	HNT	SB	1:1
HNT/WB	HNT	WB	1:1
MMT/WB	MMT	WB	1:1
MMT/SB/2-1	MMT	SB	2:1
MMT/SB/1-1	MMT	SB	1:1
MMT/SB/1-2	MMT	SB	1:2

Preparation of the organo-clays

A solution-intercalation procedure is carried out for the modification process, where a solvent capable of dissolving the chosen bio-oil and swelling the selected nanoclay. This process was selected based on results obtained from an earlier study Høgsaa [2015]. Swelling were conducted to increase the interlayer distance between the clay platelets to facilitate intercalation.

A suspension of 2% nanoclay into 1:1 water:ethanol ratio was prepared using a magnetic stirrer for 25 min at 80 °C, see figure 3.15. The two component mixture of solvents was required, because the bio-residue is not solvable in pure water. The suspension was allowed to swell for approximately 24 hours.

Figure 3.15. Temperature controlled bath with magnetic stirring.

The clay suspension was reheated for 5 minutes. A second solution with 1 gram of intercalant in 10 ml of ethanol was prepared simultaneously. The suspension and solution were mixed together for 15 minutes. The mixture was ultrasonicated with an ultrasonic horn for maximum of 2 minutes, to avoid excess heating, see figure 3.16.

Figure 3.16. Setup for ultrasonification of the mixtures.

The suspension was left to settle for 24 hours before being centrifuged with 5000 rpm for 60 minutes in a Thermo Scientific Heraeus Megafuge 16. The modified nanoclay as sediment was collected and dried until mass stability, see figure 3.17. The modified nanoclays was grinded into a fine powder. The same procedure is conducted for each batch of modified nanoclays. The different modified nanoclays are investigated using different characterization methods to get base line information about the different obtained organically modified nanoclays or organo-clays.

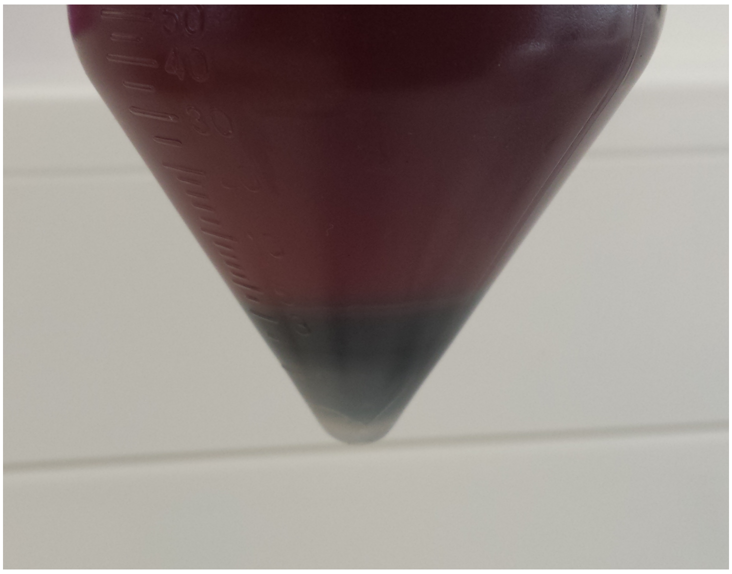

Figure 3.17. Precipitated organo-clay after the centrifugal process of one batch.

3.3.2 Results

The relevant results in this part of the project will be presented in the following sections with a discussion of the individual results.

XRD analysis

The obtained organo-clays were compared considering HNT and MMT based versions, as seen in figures 3.18 and 3.19 to assess the possible intercalation/exfoliation after the modification process. Raw nanoclay was compared to the modified versions, and the results of the bio-oils are included for comparison to investigate their possible crystalline structure.

Results of HNT based organo-clays showed no changes in the position of the d_{001} peak of the modified nano-clays after the modification process. The only changes was the intensity of the peaks, where the modified nanoclays had a higher intensity when compared to raw HNT.

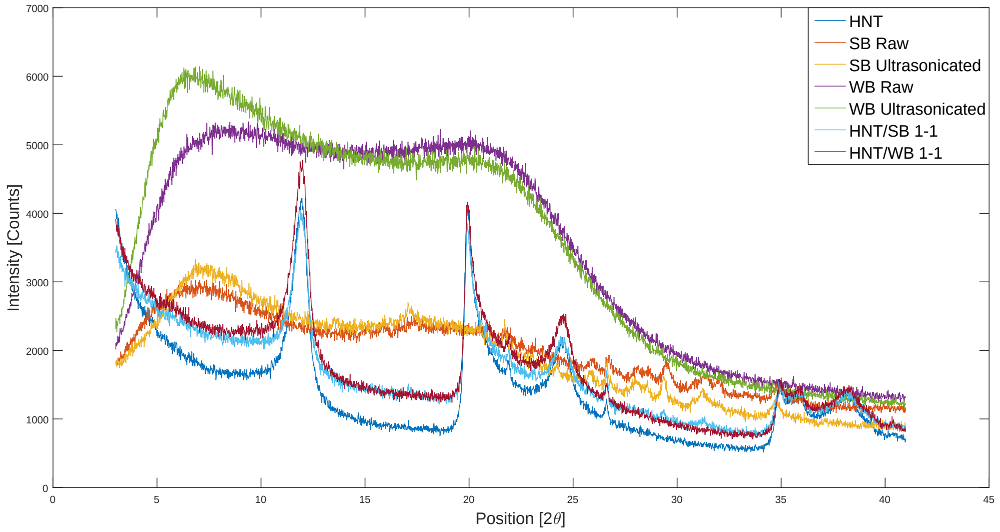

Figure 3.18. XRD analysis for HNT modified clay versions.

Results of the MMT based organo-clays showed a shift to lower angles for the d_{001} peaks of 6.57 and 6.84 for the MMT/SB and MMT/WB respectively. These angles correspondent to interlayer distances of 13.47 Å and 12.96 Å. The increase in basal d-spacing is 15.38 % and 11.11 % respectively. The peak of MMT/SB indicated a more exfoliated structure compared to the MMT/WB and the increase in the d-spacing could indicate swine-based bio-oil (SB) as an intercalant/surfactant more effective than wood-based bio-oil (WB). Another indication of the more exfoliated structure of the MMT/SB version can be seen in figure 3.19, where this peak is broad and flat compared to the sharp and high peaks of the raw MMT and the MMT/WB. An intercalated structure is a ordered structure with small changes in the interlayer spacing. Therefore is the peak higher in intensity and narrow around a specific angle. A decrease in intensity of the peak can be interpreted as a more disordered structure, where only a certain amount could be intercalated and the rest of the structure could be exfoliated A broad peak can be interpreted as a more disordered structure, where the platelets of the MMT are not parallel and therefore the size distribution is changed as a function of the parallelism between the platelets.

Table 3.6. XRD data of raw and organically modified versions of MMT.

Sample	2θ	d-spacing (Å)	d-spacing (nm)
MMT	7.57	11.69	1.17
MMT/SB 2-1	6.38	13.88	1.39
MMT/SB 1-1	6.57	13.47	1.35
MMT/SB 1-2	6.77	13.08	1.31
MMT/WB	6.84	12.96	1.30

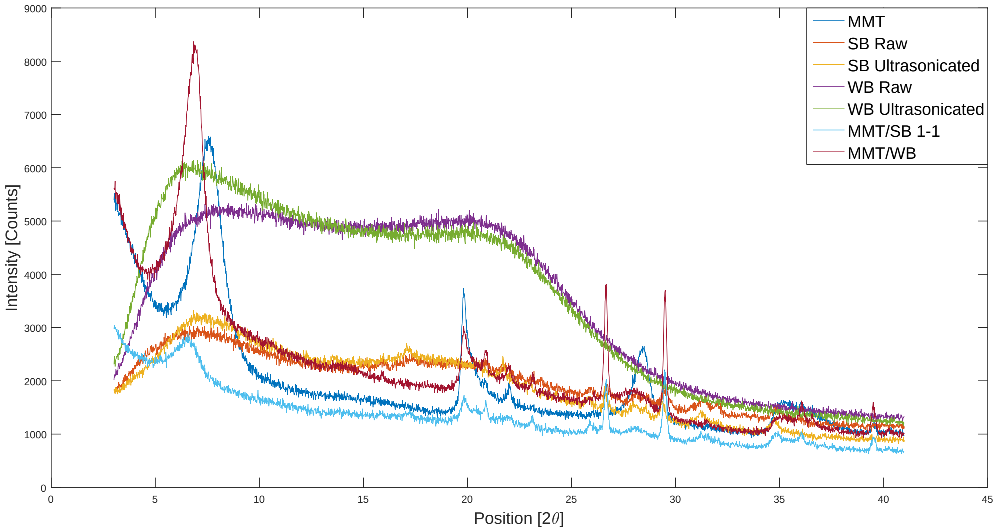

Figure 3.19. XRD analysis for MMT modified clay versions.

Obtained organo-clays with different amount of surfactant

Second batch of MMT/SB organically modified nano-clays with different amount of surfactant, are seen in figure 3.20, and the difference between all the MMT based organo-clay and the raw MMT, with regard to the angles and hereby the interlayer spacings are listed in table 3.6.

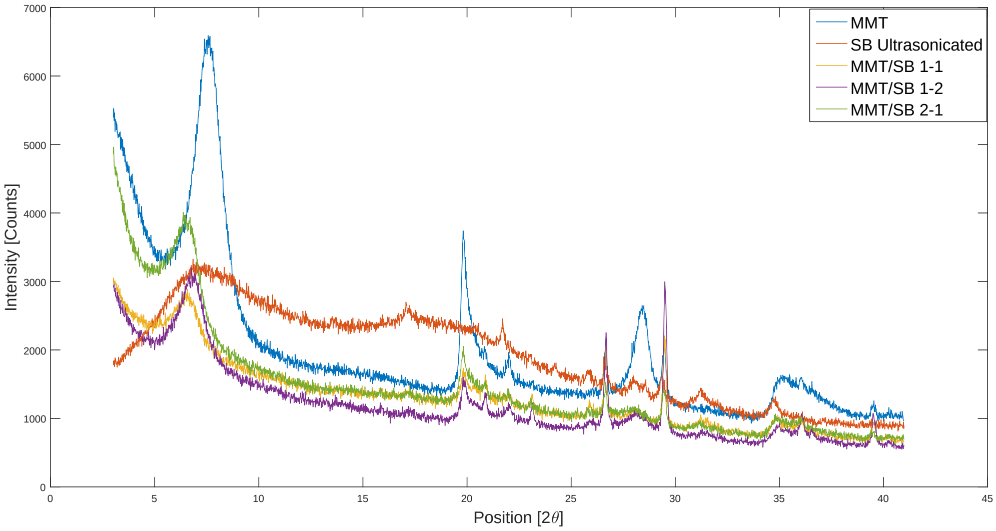

Figure 3.20. XRD analysis for MMT modified clay versions with different weight ratios.

MMT/SB 2-1 had the largest interlayer spacing compared to the two other versions. The second largest spacing is observed in MMT/SB 1-1, then MMT/SB 1-2. However the intensity of the different clay types showed the following order from highest to lowest intensity; MMT, MMT/SB 2-1, MMT/SB 1-2, MMT/SB 1-1. This could indicate that the MMT/SB 1-1 has an intercalated, partially exfoliated structure, than the rest of the organo-clays.

Attenuated Total Reflectance Fourier Transform Infrared Spectroscopy (ATR-FTIR)

The chemical interaction between the clay minerals and intercalants/surfactants were investigated. Peaks of each individual spectra were analyzed and determined with the provided software of the Spectrum One. The peaks can be utilized in the determination of relevant peaks in organically modified clays, because some of the functional groups of of the matrix and filler will be present. If a peak is not present or moved significantly after mixing, this could indicate a change of the functional group of the investigated peak and possible interaction between the nanoclay and surfactant.

Investigation of the chemical interaction between the clays and the surfactants

Results of the modified HNT nanoclays, HNT/SB and HNT/WB, are shown in figure 3.21. Position and intensity of the peaks of the modified HNT/WB was similar to raw HNT. The intensity of the peaks of 3697 cm^{-1} and 3625 were increased. The peak of 3627 in HNT/SB was still present, however a decrease in peak of 3697 cm^{-1} was observed, when compared to HNT. HNT/SB presented more peaks from the intercalant in its spectra, when compared to WB. Two new peaks were observed at 1541 and 1576 cm^{-1}, which could not be found in the spectra of halloysite (HNT) or swine-based bio-oil (SB). The peaks around 2900 cm^{-1} are reduced significantly and the peaks around 1000 cm^{-1} were increased significantly in the modified HNT/WB compared to its constituents. This could be interpreted as the surfactant is absorbed into the interior lumen of the halloysite nanotubes (HNT) and the signal of the wood-based bio-oil (WB) is shielded, which reduces the peaks around 2900 cm^{-1}.

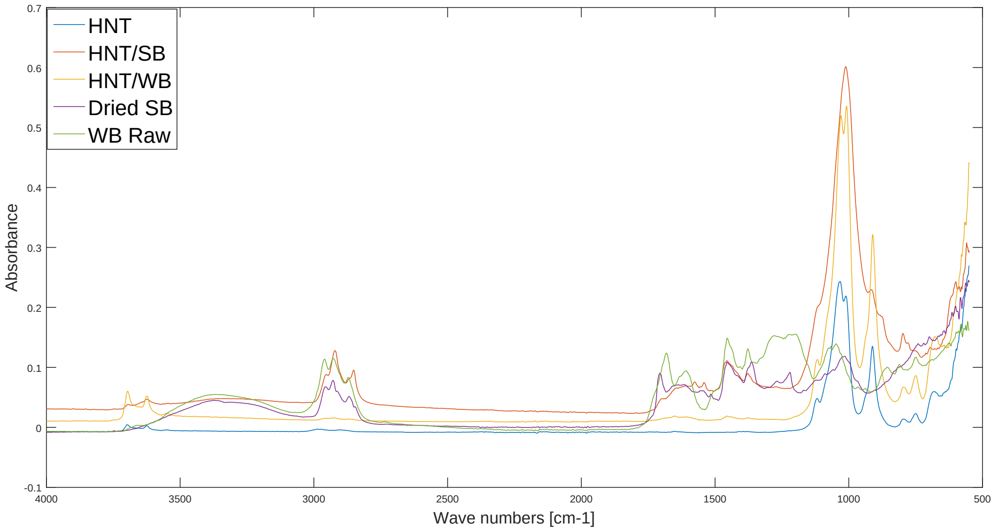

Figure 3.21. Absorbance spectra of the modified HNT nanoclays and respective raw materials.

Results of the modified MMT nanoclays are shown in figure 3.22. MMT/SB had peaks from both its constituents. The peaks around 2900 cm^{-1} and 1000 cm^{-1} showed increased intensity compared the peaks of the original materials. MMT/WB had similar trends as MMT/SB, however peaks around 2900 cm^{-1} and 1000 cm^{-1} were decreased significantly in the modified MMT/WB compared to its constituents.

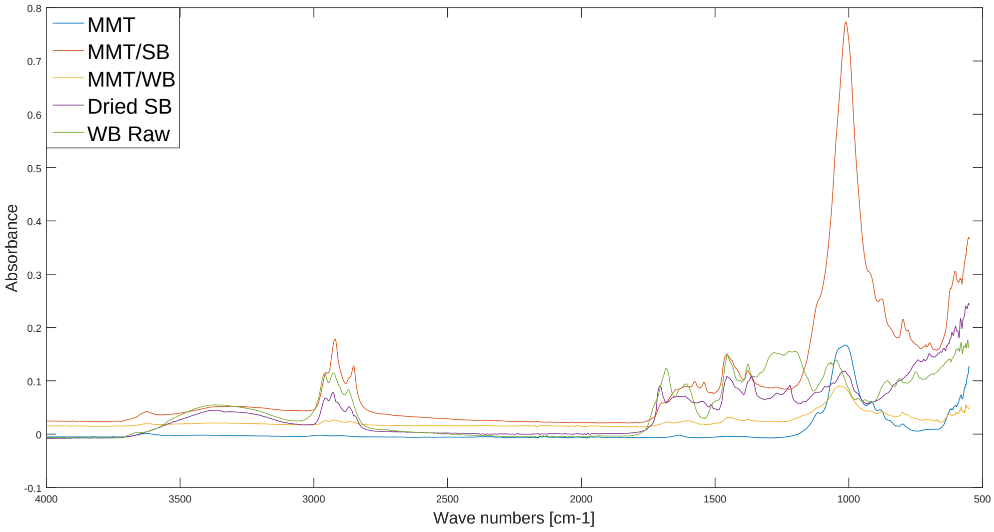

Figure 3.22. Absorbance spectra of the modified MMT nanoclays and respective raw materials.

The effect of changing amount of surfactant

Results of changing amount of surfactant in the organo-clays showed that peaks associated with swine-based bio-oil (SB) were more pronounced in MMT/SB 1-2 than MMT/SB 1-1 and MMT/SB 2-1. The same can be seen for the peaks associated with montmorillonite (MMT), except MMT/SB 2-1 had the highest peaks. Only one peak did not follow the described trend and that was the peak around 1012-1016 cm^{-1}. The highest intensity was found for the MMT/SB

1-1, which could be interpreted as a synergy effect between the clay and the swine-based bio-oil (SB) was established.

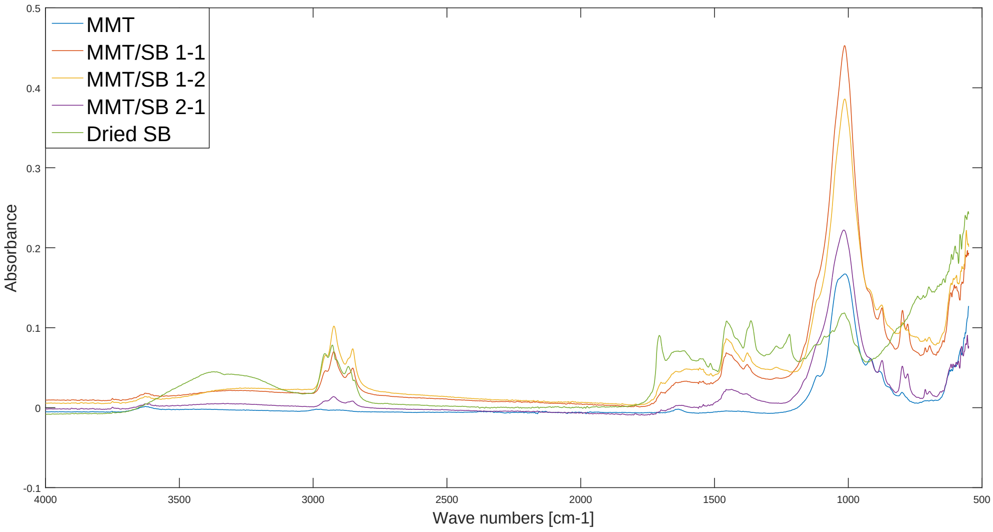

Figure 3.23. Absorbance spectra of the modified MMT nanoclays with different amount of surfactant.

Thermogrametric analysis

Results of the obtained organo-clays are shown in figures 3.24 and 3.25, and listed in tables 3.7 and 3.8. Residual mass is determined for the organoclays, because the increase in the residual mass can be an indication of the level of intercalated substance.

The onset temperature for the HNT modified nanoclays was decreased for HNT/WB and increased for the HNT/SB, when compared to the raw halloysite nanotubes (HNT). Two onset temperatures in HNT/WB and HNT/SB were registered, the first onsets temperatures are attributed unbound surfactant or unbound water in the modified clays. HNT/WB had a higher onset temperature of the primary decomposition stage, when compared to the HNT/SB. However HNT/SB had had two decompositions stages with almost equal mass loss, which could possibly indicate that some of the swine based bio-oil (SB) had interacted with the halloysHNT, which accounted for the first decomposition stage. The second decomposition stage could be pure halloysite nanotubes (HNT), which fits with the measured onset of halloysite nanotubes (HNT), which was approximately 445°C. The primary decomposition stages of HNT/WB was observed at lower onset temperatures than halloysite nanotubes (HNT), which indicates that the loss in this stage is the loss of the surfactant wood-based bio-oil (WB). The possible loss of surfactant could indicate a poor interaction between the surfactant and clay for both modified organo-clays.

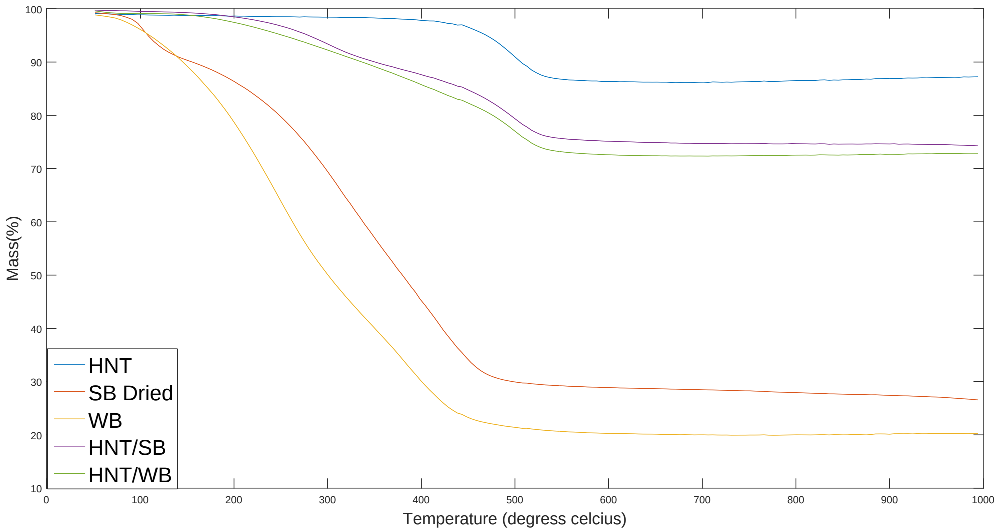

Figure 3.24. TGA measurement of weight loss, as a function of temperature, for the halloysite nanotubes (HNT), HNT modified nanoclays and bio-oils.

Table 3.7. Thermal properties of nanocomposites with modified HNT.

	Temperature range <500 °C		
Sample	Onset temp.	Mass loss	Residual mass
HNT/SB	227.0	14.58	-
	469.7	8.96	74.26
HNT/WB	84.7	0.91	-
	388.3	26.01	76.68

Montmorillonite (MMT) does not undergo thermally induced changes in the temperature range of 130-650 °C, and any mass loss in this temperature range in a organo-clay, can be attributed to the decomposition of the intercalant/surfactant within the montmorillonite [Mallakpour and Dinari, 2012]. The results of the MMT modified nanoclay showed an increase of 14.03 % in the residual mass of MMT/WB when compared to MMT/SB 1-1. The intercalated mass was 13.94 % higher for MMT/WB. Both temperatures were lower than the onset temperature of montmorillonite (MMT), which indicates that the mass loss registered can be attributed the loss of surfactant. The three nanoclays with different amount of surfactant show the same onset temperatures, however additional onset temperatures were detected. A higher amount of montmorillonite (MMT) yielded a higher residual mass.

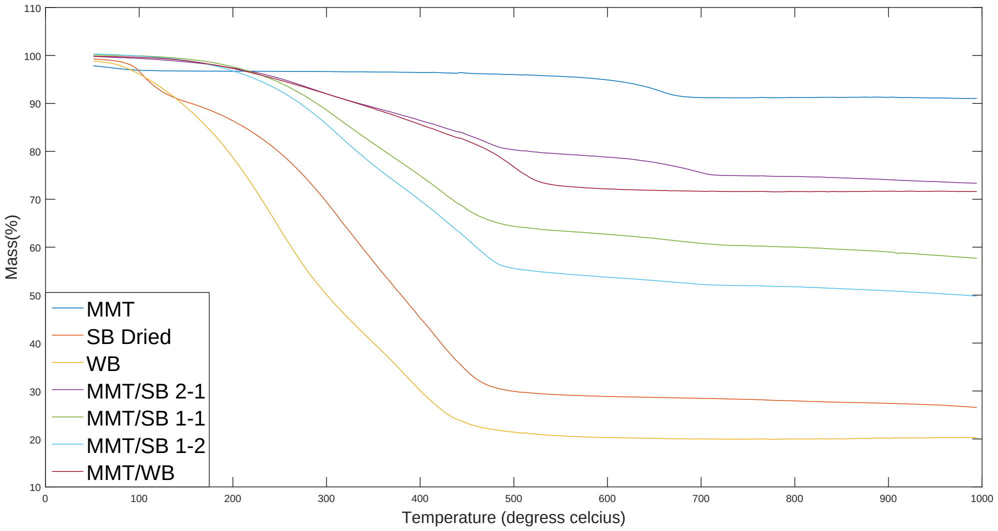

Figure 3.25. TGA measurement of weight loss, as a function of temperature, for the MMT, MMT modified nanoclays and bio-oils.

Table 3.8. Thermal properties of nanocomposites with modified MMT.

	Temperature range <650 °C		
Sample	Onset temp.	Mass loss	Residual mass
MMT/SB 1-2	227.9	40.92	-
	506.4	3.44	49.82
MMT/SB 1-1	210.4	35.95	-
	509.7	3.67	57.69
MMT/SB 2-1	227.9	10.38	-
	410.4	5.73	-
	510.2	5.27	73.33
MMT/WB	156.2	26.18	71.62

3.3.3 Part conclusion

The organic modification of the nanoclays with the different bio-oils were deemed a success for the organo-clays with montmorillonite (MMT) with increased d-spacing of 15.38 % and 11.11 % of MMT/SB 1-1 and MMT/WB respectively. This indicated that the investigated bio-oils was intercalated between the interlayer galleries of the montmorillonite (MMT). The organo-clays with different amount of swine-based bio-oil (SB) showed an increase in basal d-spacing with decreasing surfactant.

The results of the organo-clays with halloysite nanotubes (HNT) were inconclusive because the basal d-spacing was unaffected, which could be due the natural exfoliated state of the halloysite nanotubes (HNT).

The FTIR analysis indicated that the HNT/WB could possibly have absorbed the surfactant wood-based bio-oil (WB) into the interior lumen of the halloysite nanotubes (HNT). Another possibility is agglomeration of nanotubes, which shield the peaks of the surfactant. However this should have been detected by the XRD analysis as an intercalated structure. HNT/SB presented more peaks from the intercalant in its spectra, when compared to results of the HNT/WB nanocomposite. Two new peaks were observed at 1541 and 1576 cm^{-1}, which could not be found in the spectra of halloysite nanotubes (HNT) or swine-based bio-oil (SB). Results of the modified MMT nanoclays are shown in figure 3.22. MMT/SB had peaks from both its constituents. The peaks around 2900 cm^{-1} and 1000 cm^{-1} showed increased intensity compared the peaks of the original materials. MMT/WB had similar trends as MMT/SB, however peaks around 2900 cm^{-1} and 1000 cm^{-1} were decreased significantly in the modified MMT/WB compared to its constituents.

The thermogravimetric analysis showed reduced interaction between the constituents in the organo-clays. The registered mass losses were all attributed loss of surfactant.

3.4 Nanocomposites and their properties

This part of the project is the investigation of nanocomposites and their properties. This part is divided in two sections; preparation and processing of the materials, and obtained results for dispersion and properties of the nanocomposites.

3.4.1 Preparation of nanocomposites

The obtained organoclays are mixed into the linear low density polyethylene (LLDPE) with the following processing steps; compounding and extrusion. Tensile bars were processed using injection molding. A small amount of the granules are processed into film samples for optical analysis in order to investigate the dispersion.

Compounding procedure

The compounding procedure was performed on Xplore MC 15, Micro compounder with a barrel capacity of 15 ml. Selected amount of organoclay is placed into the feeder with a specified amount of pure LLDPE granules and compounded at approximately 160 °C with a screw speed of 100 RPM. The temperature profile of the barrel was set to 165 °C. The residence was approximately 180 seconds before the barrel was emptied out into strings, which were granulated after wards.

Extrusion procedure

The obtained granules were extruded in the Prism Euro-lab 16 twin screw extruder from Thermo scientific with attached water bath and granulator, see figure 3.26. The heating profile was 170 °C in all heating zones of the barrel. The granules were extruded and diluted with LLDPE to obtain nanocomposites with 2% filler content. Between each extrusion, the barrel was cleaned using approximately 20 grams of LLDPE. This procedure was performed for each batch.

The dispersion of the nanocomposites with organically modified MMT could be improved. Therefore part of nanocomposites were extruded three additional times. After each extrusion, the rheological and optical properties were investigated.

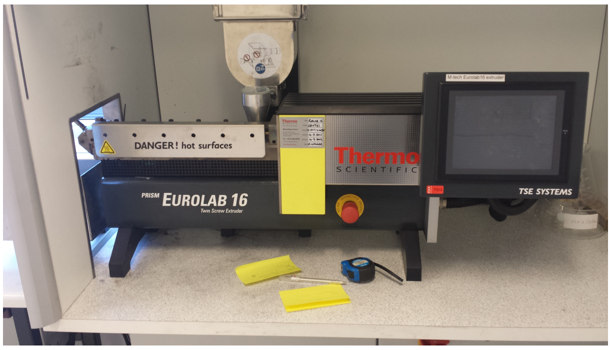

Figure 3.26. The Prism Euro-lab 16 twin screw extruder from Thermo scientific.

Injection molding procedure

Nanocomposites were injected molded in a HAAKR MiniJet Pro Piston Injection Molding System with a tensile bar mold. The mold was specified according to ISO 527-2-5A specifications. The specimens were injection molded with a temperature setting of 180 °C, a pressure of 600 bars for 20 seconds and a post pressure of 600 bars for 20 seconds. The mold temperature was 30 °C.

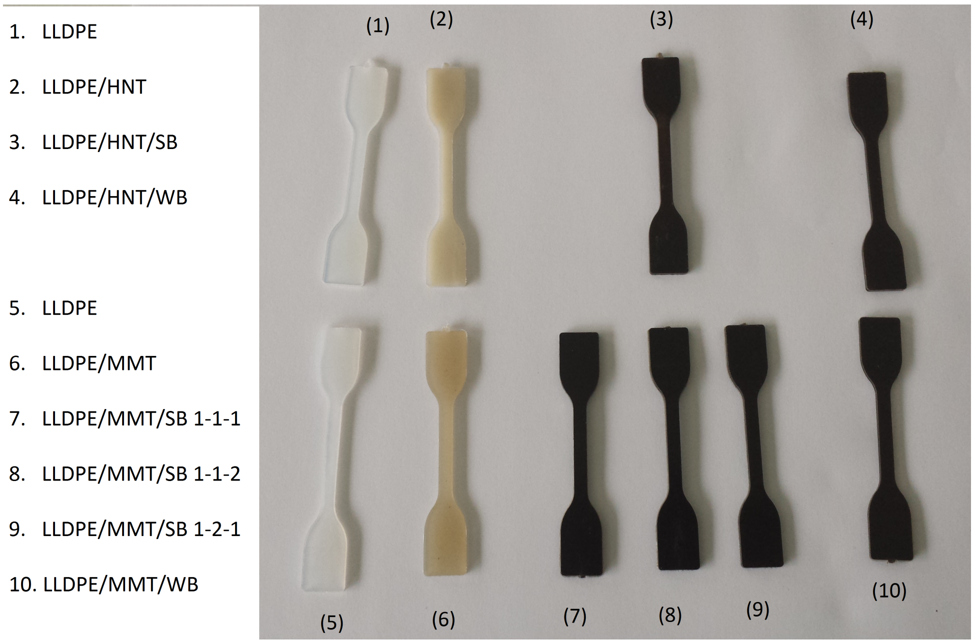

Figure 3.27. The different kinds of processed nanocomposites with numbers corresponding to title and constituents.

The nanocomposites are entitled after the constituents present in the batch. The polymer is mentioned first, then clay type and last intercalant/surfactant in a 1:1:1 ratio. The only exceptions is the two MMT modified clays, which have different ratios, MMT/SB/2-1 and MMT/SB/1-2. Nanocomposites of these organoclay are entitled as LLDPE/MMT/SB 1-2-1 and LLDPE/MMT/SB 1-1-2. The first extrusion is titled 1th and the fourth is 4th.

3.4.2 Results

Morphology and dispersion of clay, raw and modified, were investigated, as well as the thermal and mechanical properties of the nanocomposites.

XRD analysis

The XRD analysis was used to determine the degree of possible intercalation/exfoliation.

The results of the HNT based nanocomposites have similar crystal structure as the linear low density polyethylene(LLDPE), except for some changes in the intensity. A significant change can be seen in the d_{001} peaks, as seen in figure 3.28.

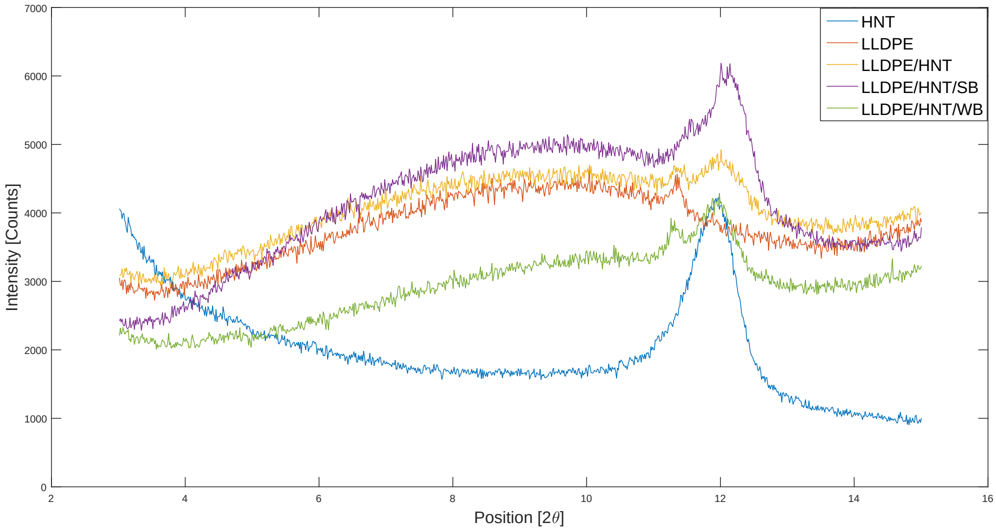

Figure 3.28. XRD analysis for HNT nanocomposites from 3-15 degrees.

There are no significant shift in the position, however the intensity is altered between the unmodified and modified nanocomposites. LLDE/HNT/SB has a higher and wider peak than LLDPE/HNT. This could indicate a more ordered structure in the modified nanocomposites. LLDPE/HNT/WB has a reduced intensity than LLDPE/HNT/SB. This loss in intensity could be interpreted as a more disordered structure compared to LLDPE/HNT/SB. A shoulder is present in all the d_{001} peaks, however this peak is attributed the LLDPE. It can be observed that this peak in the LLPDE/HNT/SB broader as compared to LLDPE/HNT and LLDPE/HNT/WB. This could indicate an interaction between polymer matrix and the modified clay.

The results of the MMT based nanocomposites have similar crystal structure as the linear low density polyethylene (LLDPE), except for some changes in the intensity. The changes can be seen in the d_{001} peaks, as seen in figure 3.29.

The modified nanocomposite shifted to lower angles of 6.67 and 6.99 for LLPDE/MMT/SB and LLDPE/MMT/WB respectively. This corresponds to basal d-spacings of 13.27 and 12.66 Å. However, when compared corresponding organo-clays, the spacings are slightly decreased. Thereby is the structure of the organoclays in the nanocomposites the same and this could indicate that the polymer LLDPE have not intercalated the clay galleries of the modified nanoclays.

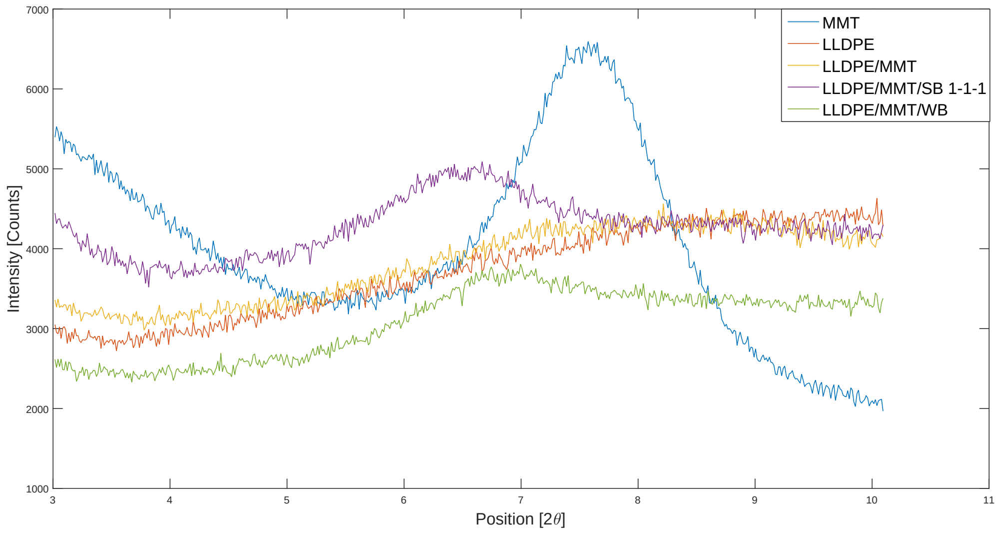

Figure 3.29. XRD analysis for MMT nanocomposites from 3-10 degrees.

The effect of surfactant on nanocomposite structure

Results of nanocomposites with different ratio of surfactant can be seen in figure 3.30. The position and spacing are listed in table 3.9. The peak position decreases with higher amount of surfactant. This indicates that nanocomposites with lower level of surfactant had a more exfoliated structure for LLDPE/MMT/SB 1-2-1 than the other mixing ratios, which had pronounced peaks with intercalated structure with increasing amount of surfactant. When comparing the nanocomposites with the corresponding organo-clays, see table 3.9, an interesting result can be observed for the interlayer spacing of LLDPE/MMT/SB 1-1-2 nanocomposite. The interlayer spacing was increased with approximately 4.36 %, which could indicate that the polymer matrix had intercalated the organo-clay.

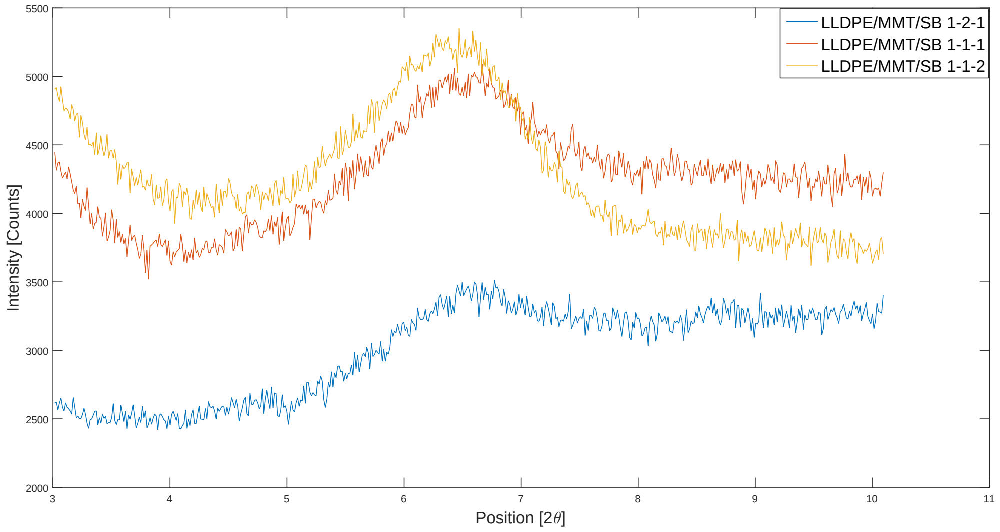

Figure 3.30. XRD analysis for MMT nanocomposites with different mixing ratio from 3-10 degrees.

The effect of additional extrusions

Results of effects of additional extrusion of MMT modified nanocomposites can be seen in figure 3.31. The position and spacing are listed in table 3.9. The swine based LLDPE/MMT/SB 1-1-1 and the wood based LLDPE/MMT/WB had obtained a more exfoliated structure in the fourth extrusion compared to the first extrusion. Insignificant changes had occurred in LLDPE/MMT/SB 1-2-1, while the only changes between the first and fourth extrusion of LLDPE/MMT/SB 1-1-2 was the decrease in intensity. Results of the extrusions of the different nanocomposites could be interpreted as a specific ratio, between surfactant and clay, is required to obtain an exfoliated structure. The results of the interlayer spacings of the nanocomposites showed that the longer mixing time yield higher spacing for the nanocomposites with MMT with different amount of surfactant. LLDPE/MMT/SB 1-1-1 had an increased interlayer spacing with higher mixing time, and the spacing was higher than the spacing of the corresponding organoclay MMT/SB 1-1. This indicates that the polymer possibly intercalated the interlayer galleries of the organoclay. The nanocomposite LLDPE/MMT/WB had a decreased interlayer spacing with increasing mixing time. The

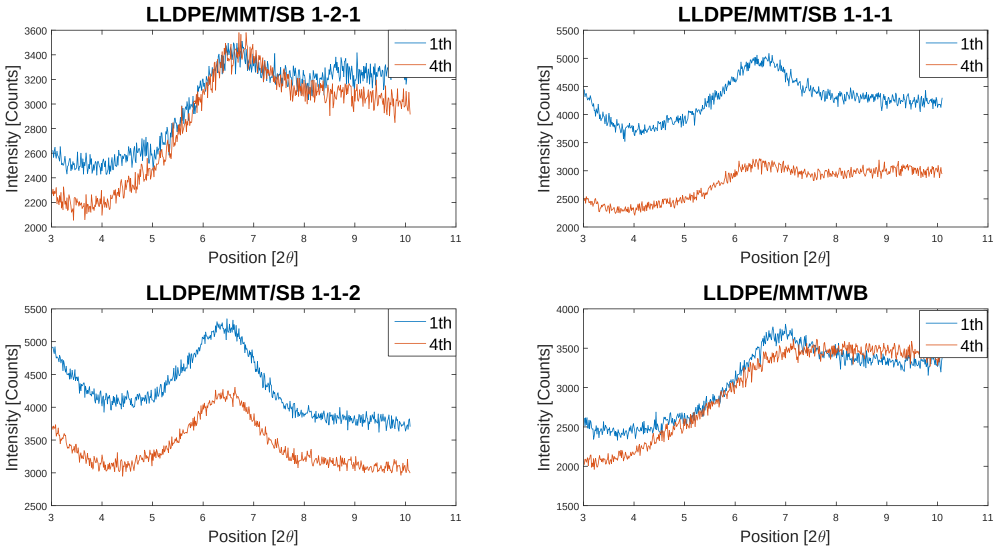

Figure 3.31. XRD analysis for MMT nanocomposites for 1th extrusions and 4th extrusions.

Table 3.9. XRD data of raw and organically modified versions of MMT.

Sample	2θ	d-spacing (Å)	d-spacing (nm)
MMT	7.57	11.69	1.17
LLDPE/MMT	8.22	10.78	1.08
MMT/SB 1-1	6.57	13.47	1.35
LLDPE/MMT/SB 1-1-1 1th. Ex.	6.67	13.27	1.33
LLDPE/MMT/SB 1-1-1 4th. Ex.	6.48	13.65	1.37
MMT/SB 1-2	6.77	13.08	1.31
LLDPE/MMT/SB 1-1-2 1th. Ex.	6.48	13.65	1.37
LLDPE/MMT/SB 1-1-2 4th. Ex.	6.63	13.34	1.33
MMT/SB 2-1	6.38	13.88	1.39
LLDPE/MMT/SB 1-2-1 1th. Ex.	6.77	13.07	1.31
LLDPE/MMT/SB 1-2-1 4th. Ex.	6.70	13.20	1.32
MMT/WB	6.84	12.96	1.30
LLDPE/MMT/WB 1th. Ex.	6.99	12.66	1.27
LLDPE/MMT/WB 4th. Ex.	7.15	12.38	1.24

Optical analysis

The different films produced for microscopy are shown in figure 3.32. The films with modified organoclay had a darker color, when compared the film with raw clay. The film of the pure polymer and raw clay were translucent. The modified nanocomposite films had visible dark agglomerates. The nanocomposites films with unmodified clay had no visible agglomerates. Based on this, the bio-oils could contain particles. This correlates with XRD analysis of the raw bio-oils, which showed a crystal structure in the swine based bio-oil (SB).

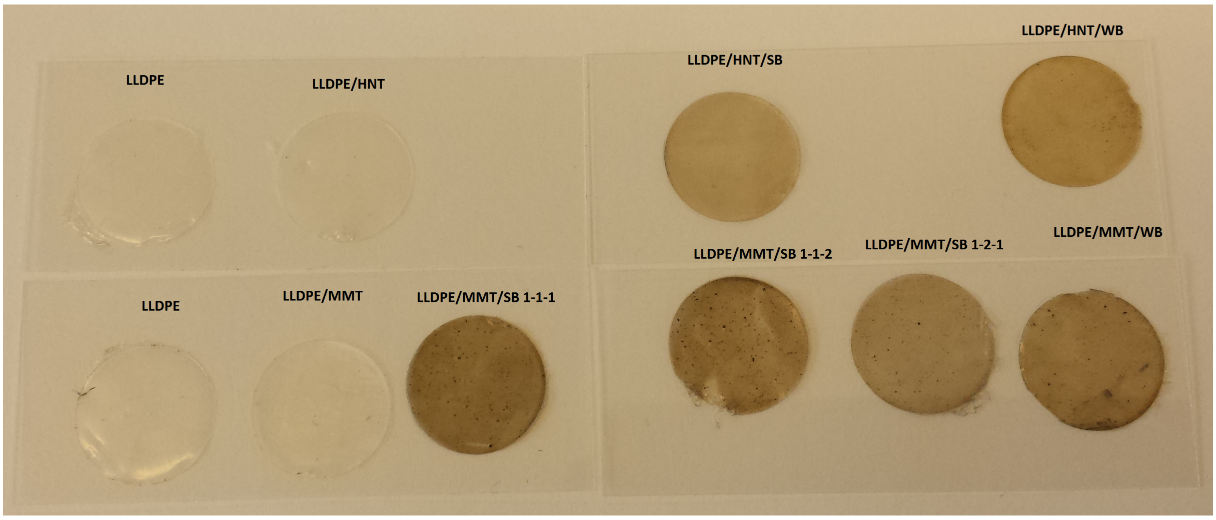

Figure 3.32. Processed films of the different kinds of processed nanocomposites.

Particle size analysis

Results of the particle analysis of the swine-based bio-oil (SB) and wood-based bio-oil (WB) are listed in table 3.10. The average diameter of the particles are determined with three repetitions.

The average diameters were between 1.58-1.78 μm and 0.85-0.92 μm for swine-based bio-oil(SB) and wood-based bio-oil(WB) respectively. These could be the observed particles in the films.

Investigation of dispersion

Table 3.10. Particle size analysis for swine-based bio-oil (SB) and wood-based bio-oil (WB).

Sample	Average diameter in [nm]	Average diameter in [μm]
SB 1	1620	1.62
SB 2	1584	1.58
SB 3	1779	1.78
WB 1	873.2	0.87
WB 2	852.5	0.85
WB 3	923.1	0.92

The films were investigated under microscope and results of the different types are shown in figures 3.33 and 3.34. present the raw polymer LLDPE, the unmodified nanocomposites LLDPE/HNT or LLDPE/MMT and the modified nanocomposites with swine -based bio-oil (SB) and wood-based bio-oil (WB). The results of analysis showed that the raw polymer had flaws in the surface of the film. This can be seen as dark gray spots. Striations can be observed, which are from the produced mold. The HNT unmodified nanocomposite showed no agglomerates; only flaws from the mold. The modified nanocomposites showed light brown and dark particles. The edges of the dark particles had a brownish hue. This could indicate that the particles are agglomerates of the modified nanoclay. The results of the particles analysis supporters the presence of agglomerates, due to increased size of some of the particles

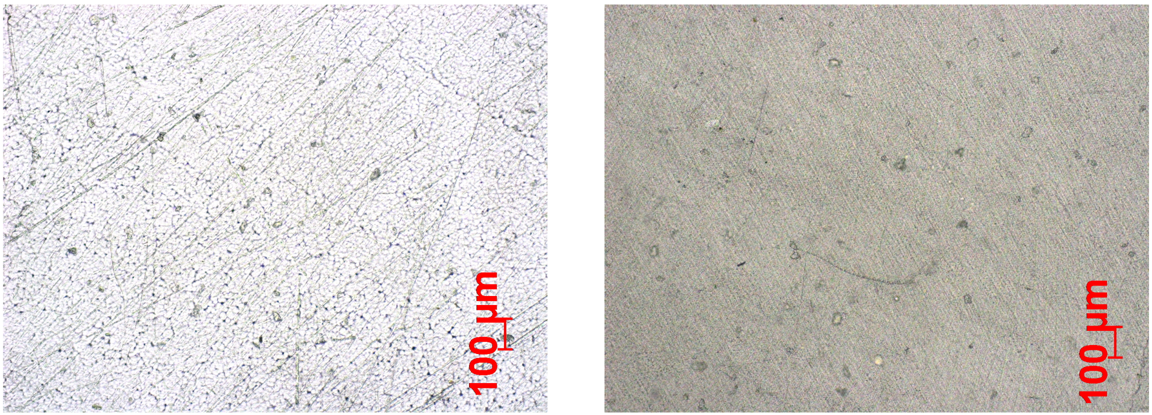

(a) Pure LLDPE .(b) LLDPE mixed with 2% WT HNT

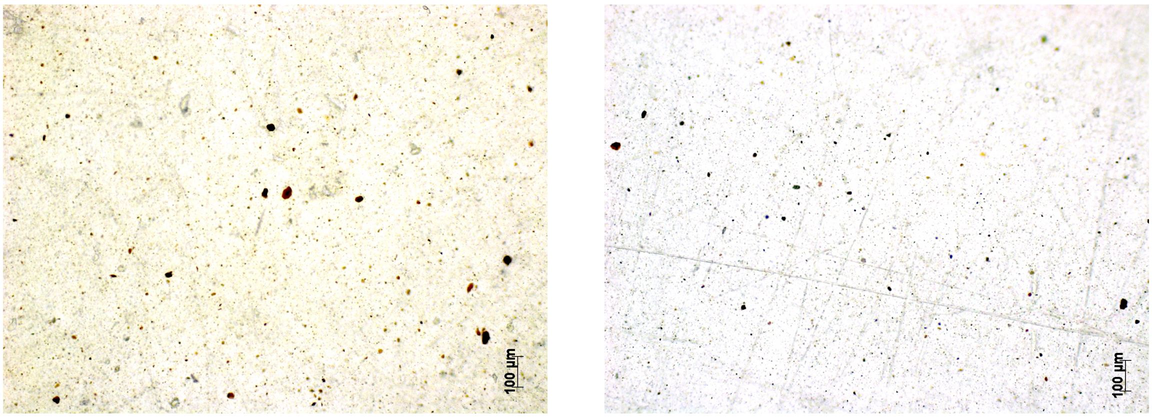

(c) LLDPE mixed with 2% WT HNT/WB (d) LLDPE mixed with 2% WT HNT/SB

Figure 3.33. Samples of pure LLDPE and HNT modified versions under 10X magnification.

The nanocomposite with unmodified MMT showed no agglomerates; only flaws from the mold. The nanocomposites with modified MMT showed a mix of light brown and dark particles.

Compared to the nanocomposites, with modified HNT, the nanocomposites with modified MMT have more agglomerates.

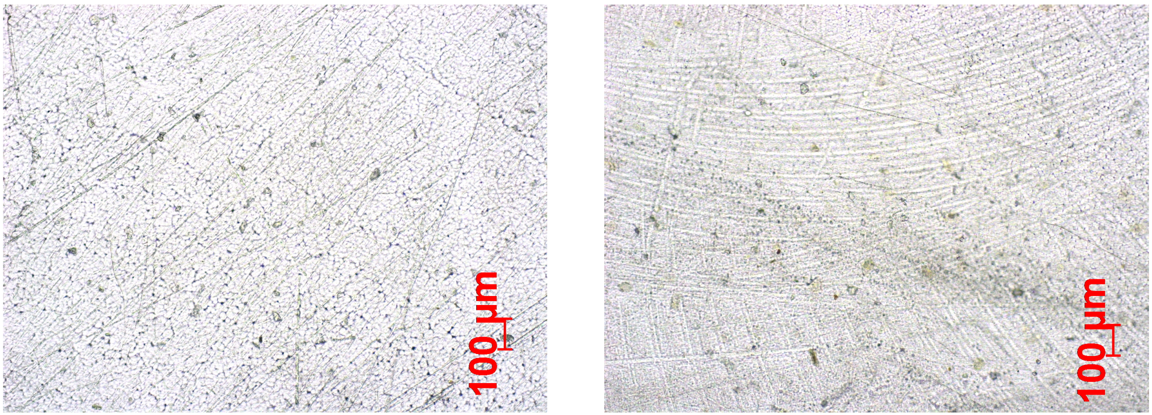

(a) Pure LLDPE (b) LLDPE mixed with 2% WT MMT

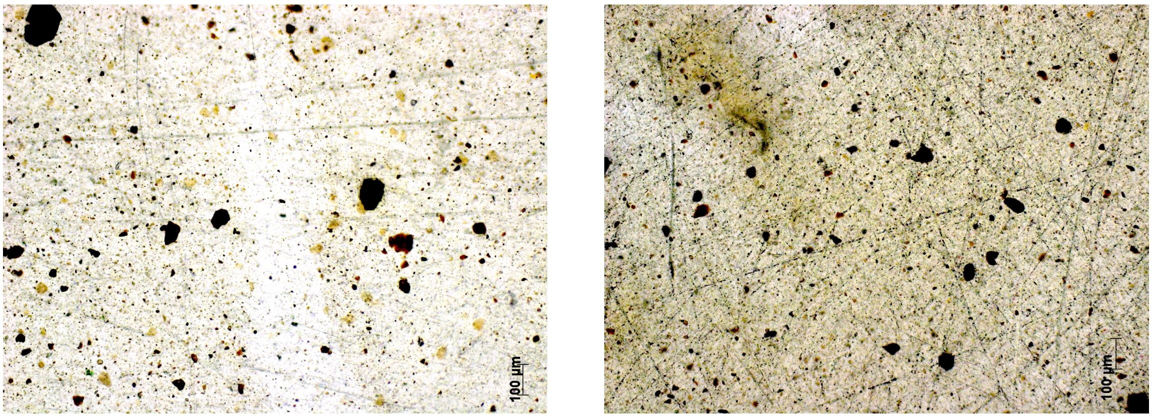

(c) LLDPE mixed with 2% WT MMT/WB (d) LLDPE mixed with 2% WT MMT/SB 1-1

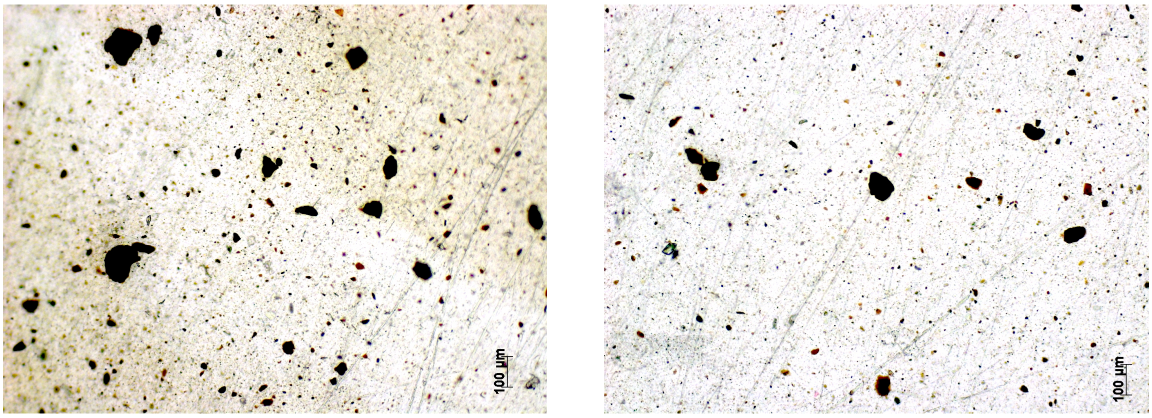

(e) LLDPE mixed with 2% WT MMT/SB 1-2 (f) LLDPE mixed with 2% WT MMT/SB 2-1

Figure 3.34. Samples of pure LLDPE and MMT modified versions under 10X magnification.

The effect of extrusions on dispersion

In figures; 3.37, 3.35, 3.36 and 3.38, the films of the nanocomposites with MMT are showed. Each figure show pictures corresponding to each extrusion in order to evaluate the effect of supplementary processing.

Determination of size distribution of agglomerates and particles were attempted with imaging software. However, these analysis were deemed inconclusive, due to flaws in the obtained films.

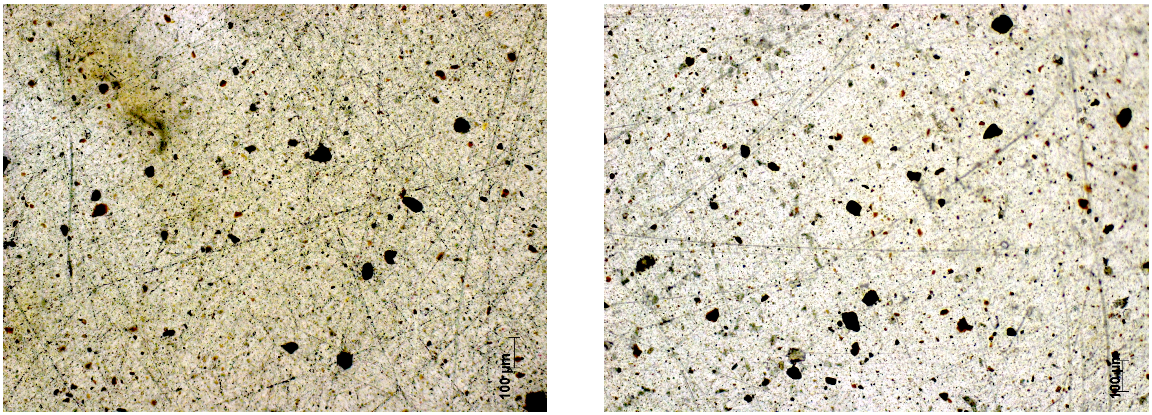

(a) 1 extrusion of LLDPE mixed with 2% WT MMT/SB 1-1.

(b) 2 extrusion of LLDPE mixed with 2% WT MMT/SB 1-1.

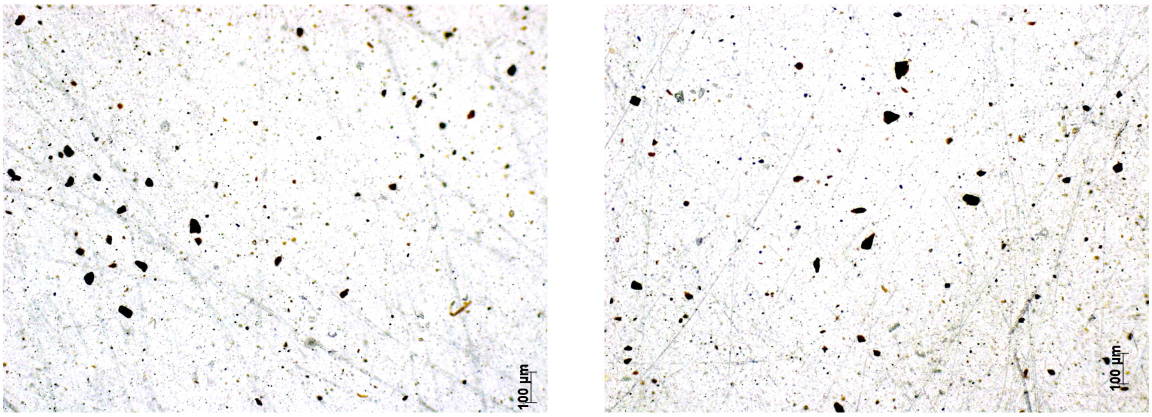

(c) 3 extrusion of LLDPE mixed with 2% WT MMT/SB 1-1.

(d) 4 extrusion of LLDPE mixed with 2% WT MMT/SB 1-1.

Figure 3.35. Samples of LLDPE/MMT/SB 1-1-1 modified versions under 10X magnification after several extrusions.

These flaws distorted the results of the size distribution in the software. Therefore the effects of additional extrusions on the dispersion could not be determined.

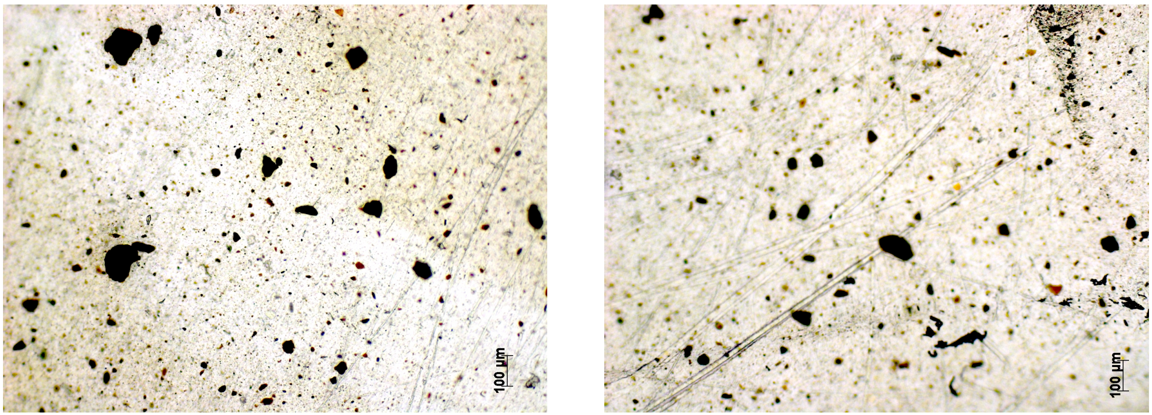

(a) 1 extrusion of LLDPE mixed with 2% WT MMT/SB 1-2.

(b) 2 extrusion of LLDPE mixed with 2% WT MMT/SB 1-2.

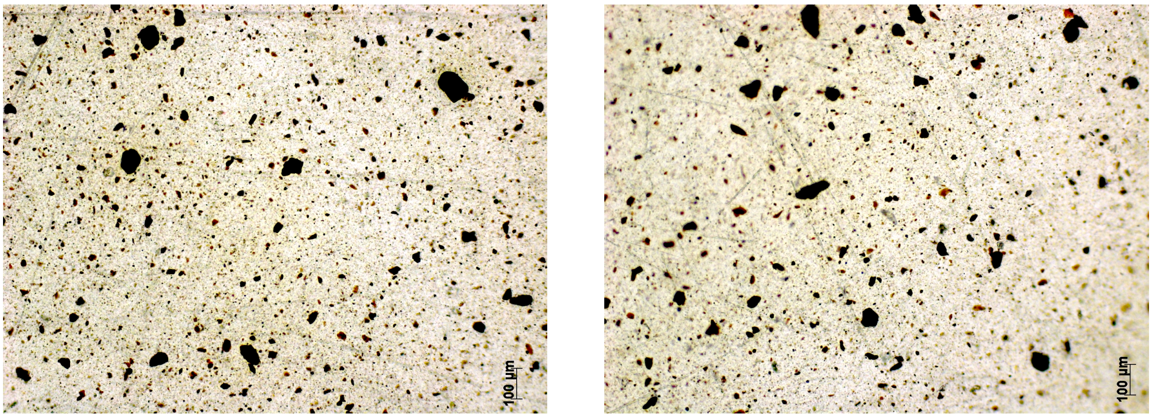

(c) 3 extrusion of LLDPE mixed with 2% WT MMT/SB 1-2.

(d) 4 extrusion of LLDPE mixed with 2% WT MMT/SB 1-2.

Figure 3.36. Samples of LLDPE/MMT/SB 1-1-2 modified versions under 10X magnification after several extrusions.

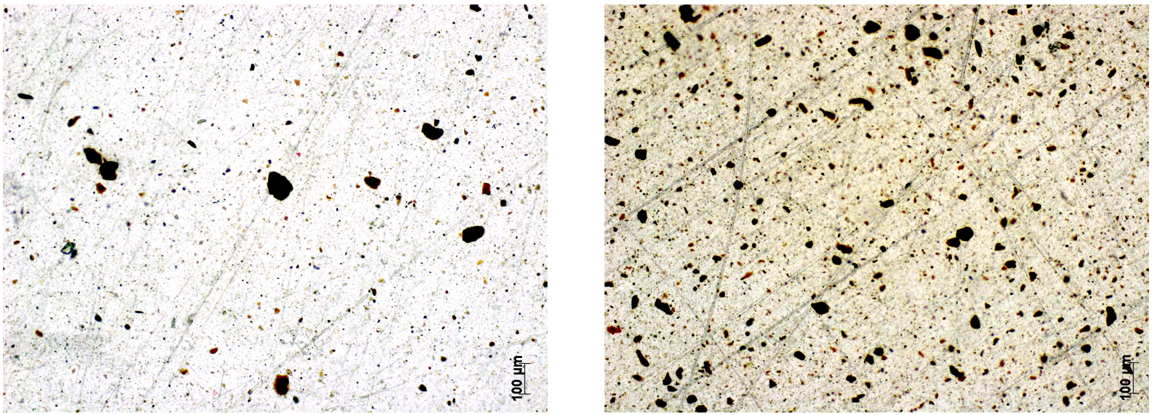

(a) 1 extrusion of LLDPE mixed with 2% WT MMT/SB 21.

(b) 2 extrusion of LLDPE mixed with 2% WT MMT/SB 21.

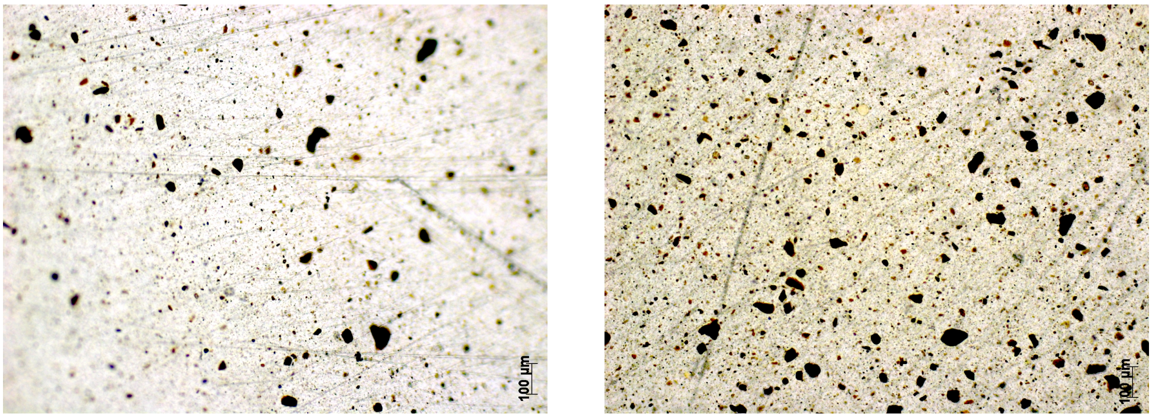

(c) 3 extrusion of LLDPE mixed with 2% WT MMT/SB 21.

(d) 4 extrusion of LLDPE mixed with 2% WT MMT/SB 21.

Figure 3.37. Samples of LLDPE/MMT/SB 1-2-1 modified versions under 10X magnification after several extrusions.

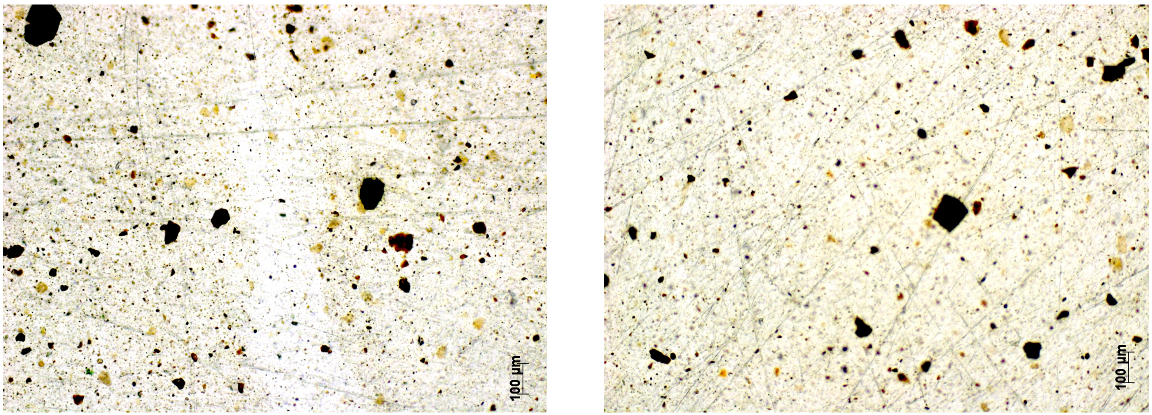

(a) 1 extrusion of LLDPE mixed with 2% WT MMT/WB.

(b) 2 extrusion of LLDPE mixed with 2% WT MMT/WB.

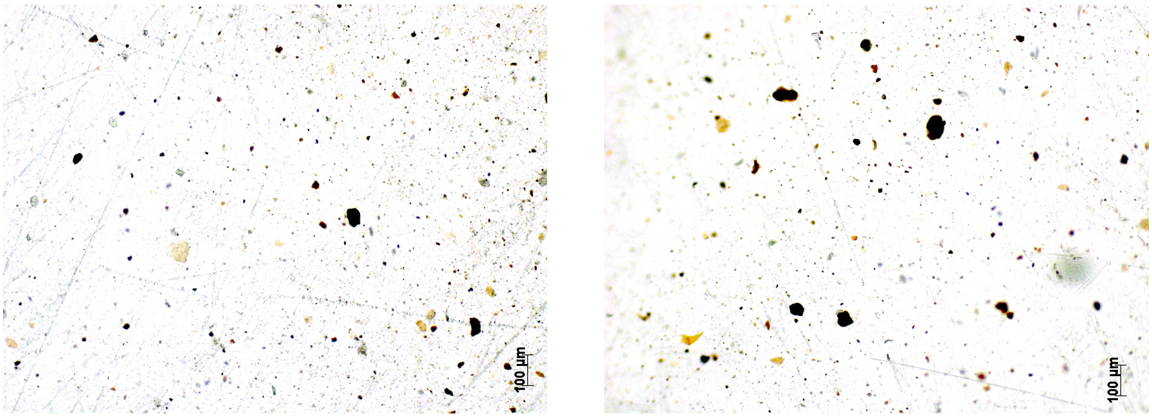

(c) 3 extrusion of LLDPE mixed with 2% WT MMT/WB.

(d) 4 extrusion of LLDPE mixed with 2% WT MMT/WB.

Figure 3.38. Samples of LLDPE/MMT/WB modified versions under 10X magnification after several extrusions.

Attenuated total reflectance fourier transform infrared spectroscopy (ATR-FTIR)

The peaks of interest for the dispersion process are the peaks around 1000-1200 for the montmorillonite (MMT) [Cole, 2008]. Therefore these peaks will be investigated more extensively. All spectra are normalized to the peak 1456 cm^{-1} and the spectrum of LLDPE is subtracted to assess the peaks of interest. The results of the normalized spectra the nanocomposites with 1th and 4th extrusions with modified MMT are shown in figure 3.39.

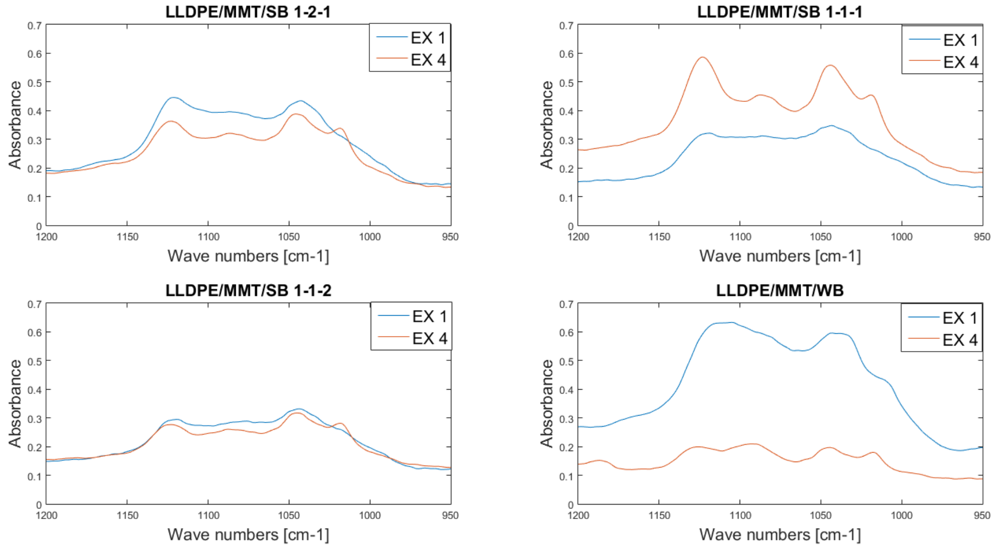

Figure 3.39. Normalized and subtracted absorbance spectra of the nanocomposites with modified montmorillonite (MMT) and different amount of surfactant for 1th and 4th extrusions.

The peak of II (1080 cm^{-1}) is reported to narrow in bandwidth and shift to higher angles with increasing intercalation/exfoliation. There is a relation between the four peaks, where the peaks II (1080 cm^{-1}) and III (1048 cm^{-1}) gets more prominent, compared to the two other peaks I (1120 cm^{-1}) and II (1025 cm^{-1}), with increasing intercalation/exfoliation [Cole, 2008].

The registered peaks for the nanocomposites with modified MMT are listed in table 3.11.

Table 3.11. Intercalation/exfoliation peaks (I-IV), described by Cole [2008], and compared to the normalized and subtracted peaks of the nanocomposites with modified MMT with 1th and 4th extrusions.

Sample	Peak I 1120 cm^{-1}	Peak II 1080 cm^{-1}	Peak III 1048 cm^{-1}	Peak IV 1025 cm^{-1}
LLLDPE/MMT/SB 1-2-1 1th	1122	1086	1043	1017
LLLDPE/MMT/SB 1-2-1 4th	1123	1087	1046	1019
LLLDPE/MMT/SB 1-1-1 1th	1119	1086	1043	1021
LLLDPE/MMT/SB 1-1-1 4th	1123	1087	1044	1019
LLLDPE/MMT/SB 1-1-2 1th	1119	1076	1044	1020
LLLDPE/MMT/SB 1-1-2 4th	1123	1088	1045	1018
LLLDPE/MMT/WB 1th	1115	1084	1043	1012
LLLDPE/MMT/WB 4th	1126	1093	1045	1018

The results of the II peaks of all the 4.th extrusions of the nanocomposites shows narrower peaks compared with corresponding the 1th extrusion peaks, as seen in figure 3.39. The positions of the II peaks of the 4th extrusions of the nanocomposites are all shifted to higher angles. This could interpreted as higher degree of intercalation/exfoliation. The nanocomposite with a higher amount of surfactant LLDPE/MMT/SB 1-1-2 and the wood-based LLDPE/MMT/WB had the highest shifts in angles. The area/intensity ratio between the four peaks are difficult to assess, because the results indicates more pronounce peaks of all 4 peaks of all nanocomposites with 4th extrusion, when compared the 1th extrusion peaks. Especially the I and VI becomes more distinct after the additional extrusions. To assess the area more precisely a peak fitting process with a de-convolution, as described by Cole [2008], has to be performed. This is not performed in this thesis, however this could be an viable option for more information about the intercalation/exfoliation state of the nanocomposites.

Thermal stability of nanocomposites

Thermal properties of the nanocomposites were investigated to asses the thermal stability.

Results of nanocomposites with halloysite nanotubes (HNT) are shown and listed in figure 3.40 and table 3.12. When compared to the pure polymer matrix, the organically modified nanocomposites with halloysite nanotubes(HNT) were found to have some improvements in thermal properties with higher degradation onset temperatures and high char content. The modified nanocomposites have an increase in the onset temperature by approximately 3 and 8 °C for the swine based LLDPE/HNT/SB and the wood based LLDPE/HNT/WB respectively. The only exception was the nanocomposite with unmodified HNT, as seen in figure 3.40. It can be seen that LLDPE/HNT has two decomposition ranges, where the first is between 300-360 °C with a mass loss of 12.27 %. The second decomposition occurs between 400-500 °C, which is in the range of the primary decomposition of the polymer and the other nanocomposites. The initial mass loss at lower temperature indicates a poor compatibility between the halloysite nanotubes (HNT) and the linear low density polyethylene (LLDPE). An other indication of the bad interaction is the lower residual mass of the unmodified nanocomposite, when compared to the modified nanocomposites.

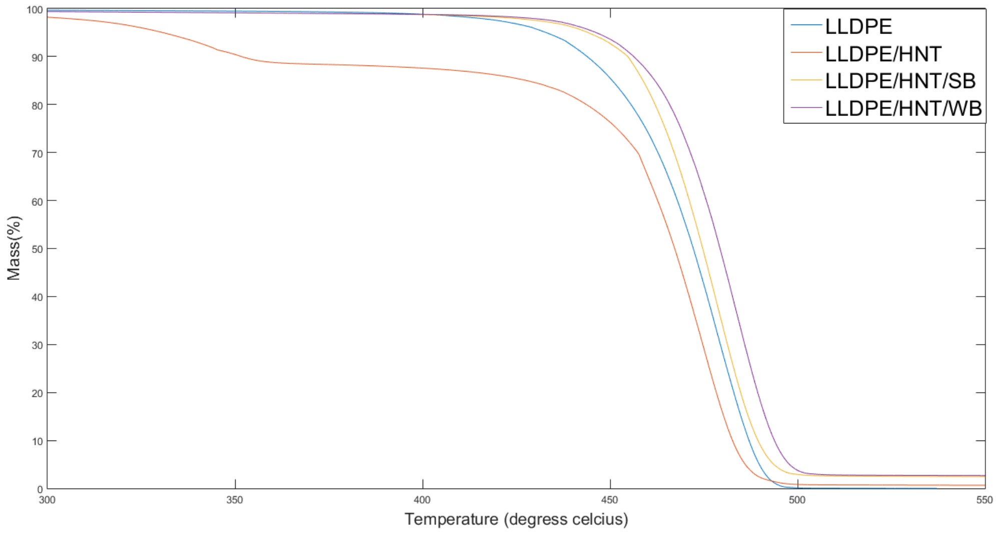

Figure 3.40. TGA measurement of weight loss, as a function of temperature, for the nanocomposites with halloysite nanotubes(HNT).

Table 3.12. Thermal properties of nanocomposites with halloysite nanotubes (HNT).

	Temperature range				
	<360 °C		360-500 °C		
Sample	Onset temp. [°C]	Mass loss [%]	Onset temp. [°C]	Mass loss [%]	Residual mass [%]
LLDPE	-	-	455.01	99.3178	0
LLDPE/HNT	319.96	11.21	431.96	87.98	0.73
LLDPE/HNT/SB	-	-	458.31	96.16	2.40
LLDPE/HNT/WB	-	-	463.03	95.31	2.60

Results of nanocomposites with montmorillonite (MMT) are shown and listed in figure 3.41 and table 3.13. It can be seen in figure 3.41, that the nanocomposites with montmorillonite (MMT) has one decomposition reaction around 320-500 °C. The onset temperature, mass loss and the residual mass are listed in table 3.13. Residual mass was reduced for LLLDE/MMT with 1 % , when compared to modified nanocomposites with approximately 2 %. The onset temperature is lower for the nanocomposite with unmodified montmorillonite (MMT) and increased for the nanocomposites with modified montmorillonite (MMT). The reduced onset temperature and reduced residual mass for the nanocomposites with unmodified montmorillonite (MMT) indicates a poor compatibility between the hydrophobic LLDPE and the hydrophyllic montmorillonite (MMT). Nanocomposites with modified MMT had an increases in the onset temperature and hereby the improved thermal stability. The increase in onset temperature was approximately 5 and 7 °Cfor LLDPE/MMT/SB 1-1-1 and LLDPE/MMT/WB respectively. The residual mass was lower for the wood based nanocomposite LLDPE/MMT/WB than the swine based LLDPE/MMT/SB 1-1-1.

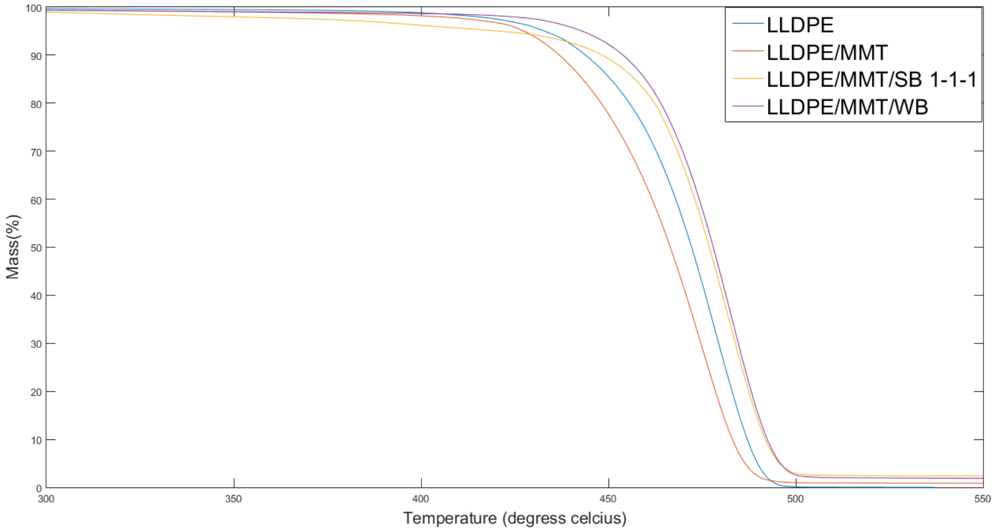

Figure 3.41. TGA measurement of weight loss, as a function of temperature, for the nanocomposites with montmorillonite (MMT).

Table 3.13. Thermal properties of nanocomposites wit montmorillonite (MMT).

	Temperature range 320-500 °C		
Sample	Onset temp. [°C]	Mass loss [%]	Residual mass [%]
LLDPE	455.01	95.71	0
LLDPE/MMT	447.42	95.65	0.82
LLDPE/MMT/SB 1-1-1	459.98	91.34	2.13
LLDPE/MMT/WB	461.50	92.27	1.70

The effect of surfactant on nanocomposite thermal stability

Results of changing the amount of surfactant is seen in figure 3.42. There are registered one primary decomposition stage at approximately 440-500 °C for all LLDPE/MMT/SB nanocomposites. From table 3.14, it can be observed that the onset temperature is reduced for the LLDPE/MMT/SB 1-1-1 than the other nanocomposites. There is a trend in the results of the residual mass were the mass is increased with increasing amount of surfactant.

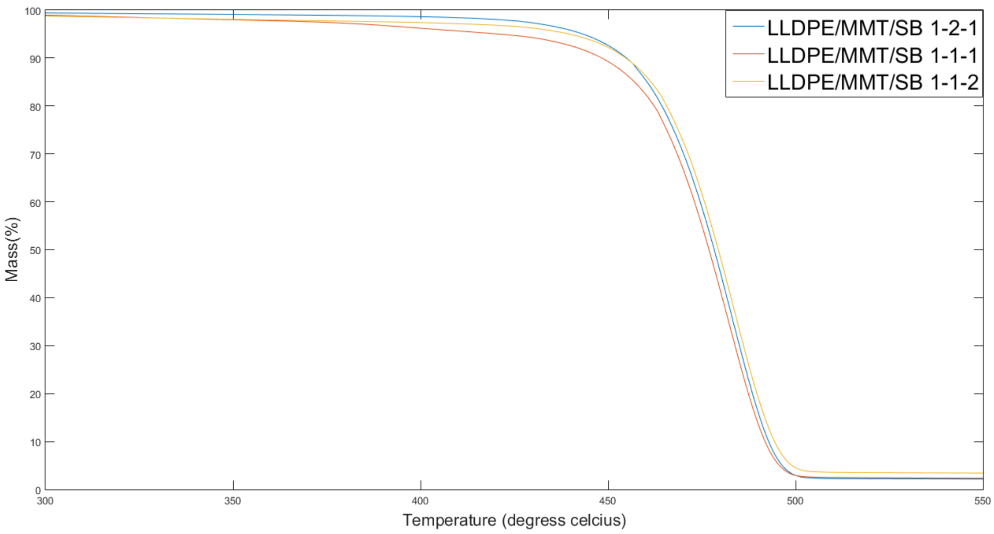

Figure 3.42. TGA measurement of weight loss, as a function of temperature, for the nanocomposites with modified montmorillonite (MMT) and different amount of surfactant.

Table 3.14. Thermal properties of nanocomposites with modified montmorillonite (MMT) and different amount of surfactant.

	Temperature range 320-500 °C		
Sample	Onset temp. [°C]	Mass loss [%]	Residual mass [%]
LLDPE/MMT/SB 1-2-1	461.73	94.41	2.06
LLDPE/MMT/SB 1-1-1	459.98	91.34	2.14
LLDPE/MMT/SB 1-1-2	462.79	94.20	3.25

Oscillatory rheometry

The rheological properties of the nanocomposites were investigated for each type. An initial amplitude sweep was conducted and the strain(γ) was chosen to be 5% to ensure that the investigated materials remained within the linear visco elastic regime. It was decided to perform a single measurement on each batch of the modified nanocomposite, due to a high amount of agglomerates present in them, as observed in the optical analysis.

The initial testing of visco elastic properties

The results for storage and loss moduli and complex viscosity measurements for the different processed nanocomposites are shown in figures 3.43,3.44, 3.45 and 3.46.

The results for the HNT modified nanocomposites indicated that LLLDE/HNT showed an increase in the storage modulus compared to the raw polymer and the organically modified nanocomposites. At lower angular frequencies there was observed an increase in the storage modulus in modified nanocomposites. The effect of the changes can be seen in the complex viscosity, there is a small increase between the raw polymer LLDPE and the modified nanocomposites, as seen in figure 3.44. However the biggest increase is registered in the unmodified LLDE/HNT nanocomposite. This is interesting because the modified versions should in theory yield better results. This could indicate that the modification of the HNT based nanocomposites was not able to reach a pseudo-solid-like behavior, which increase the viscosity at low angular frequencies. In nanocomposites with polymeric matrix materials and clay fillers, the low frequency solidification behavior can be used as an indicator of the state of particle dispersion where a big increase in the viscosity, at low angular frequencies, is associated with a better clay dispersion rate[Klitkou, 2012].

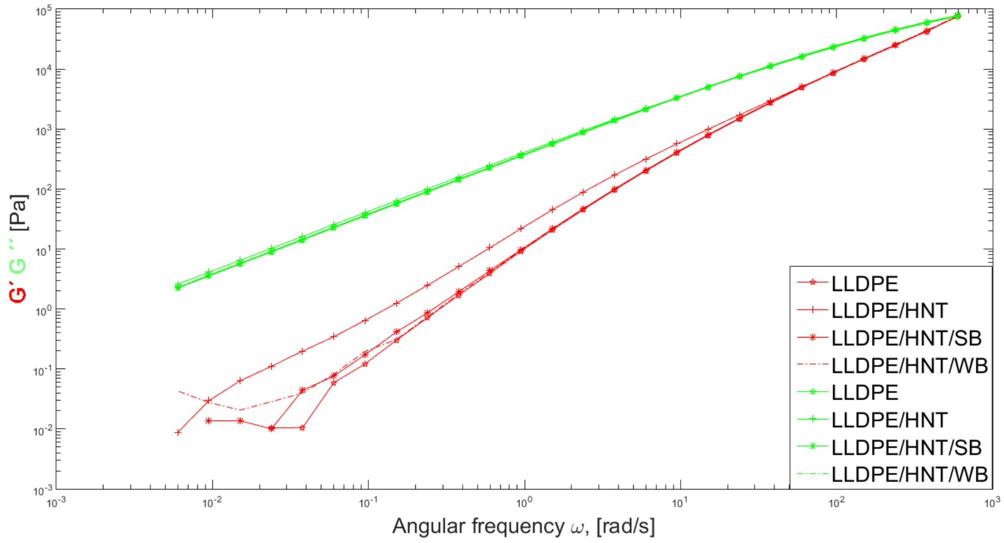

Figure 3.43. Storage(G´) and loss(G´´) modulus, as a function of angular frequency ω, for the nanocomposites with HNT.

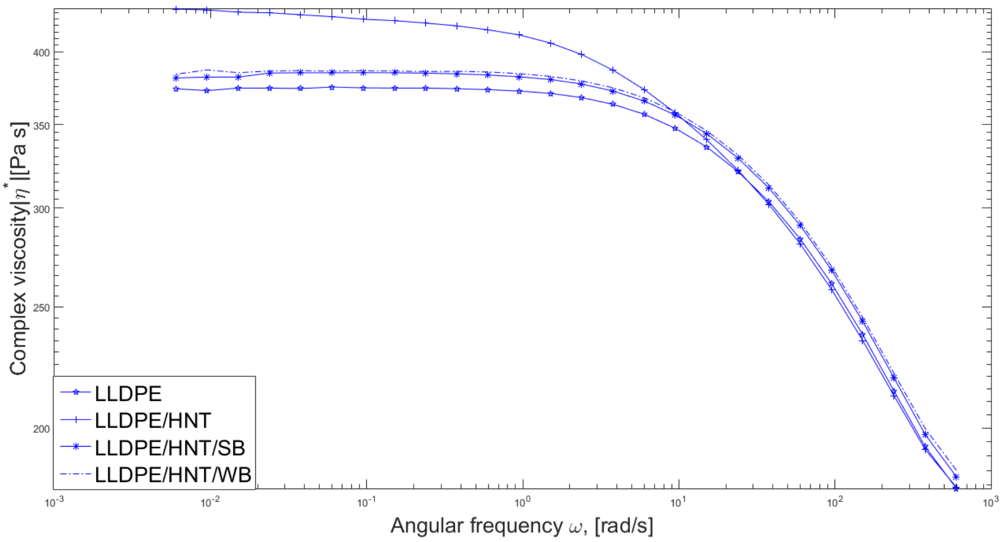

Figure 3.44. Complex viscosity $\eta*$, as a function of angular frequency ω, for the nanocomposites with HNT.

The rheological results for the MMT modified nanocomposites indicated that the storage moduli of all the organically modified clays started to plateau at lower angular frequencies. There was increase in the storage moduli in the following sequence; LLDPE/MMT/SB 1-1-1, LLDPE/MMT/WB, LLDPE/MMT/SB 1-2-1, LLDPE/MMT/SB 1-1-2. The unmodified nanocomposite LLDPE/MMT and the raw LLDPE did not have the same tendency to plateau as the modified versions. The complex viscosity showed increase in the viscosity with a plateau at lower angular frequencies. All the nanocomposites had a little higher viscosity compared to the raw LLDPE. The most interesting result was observed for nanocomposite LLDPE/MMT/SB 1-1-2. The measurement showed a higher increase at higher angular frequencies with a tail, that finds a plateau at lower angular frequencies. This indicates a inaction between the modified filler and the polymer.

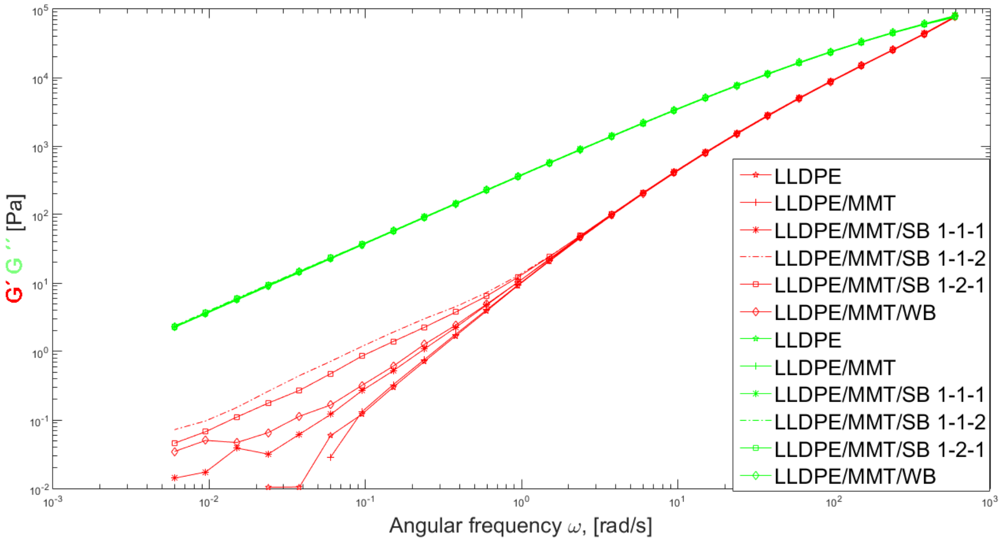

Figure 3.45. Storage(G´) and loss(G´´) modulus, as a function of angular frequency ω, for the nanocomposites with MMT.

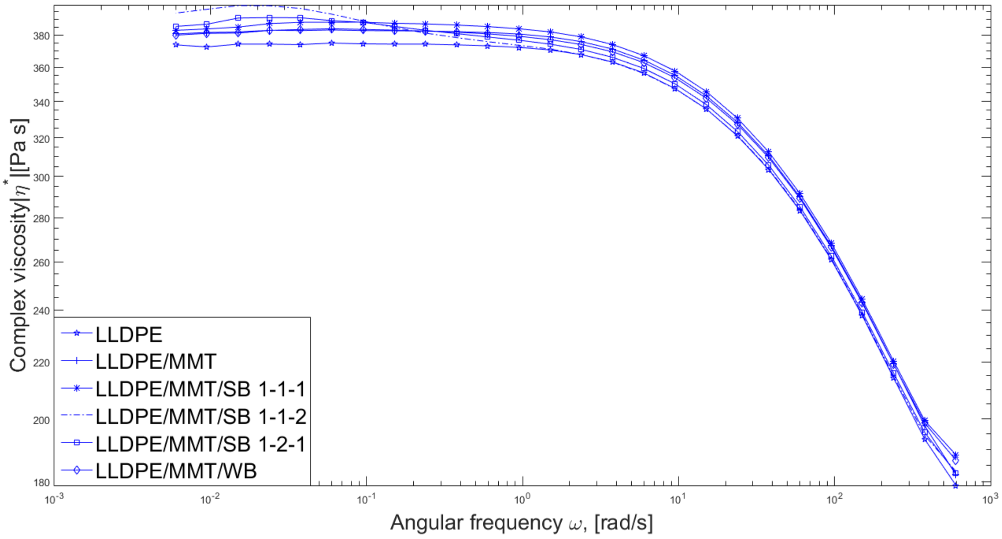

Figure 3.46. Complex viscosity $\eta*$, as a function of angular frequency ω, for the nanocomposites with MMT.

The effects of extrusion on dispersion of nanoclay

The rheological properties of the MMT modified nanocomposites were tested to assess if it was possible to achieve a better clay dispersion in the nanocomposites using multiple extrusions. It can be seen in figures 3.47 and 3.48, that the storage moduli of all nanocomposites at lower angular frequencies is a plateau. This can be perceived as an interaction between the filler material and the polymer matrix material. However the changes in the complex viscosity between the different extrusions were small. Only the results of the 1th and 3th extrusion of the LLDPE/MMT/SB 1-1-2 showed an significant increase in the complex viscosity at lower angular frequencies. This increase is a sign of better dispersion, however the result is misleading, because the 2th and 4th extrusion is reduced to a lower level of viscosity.

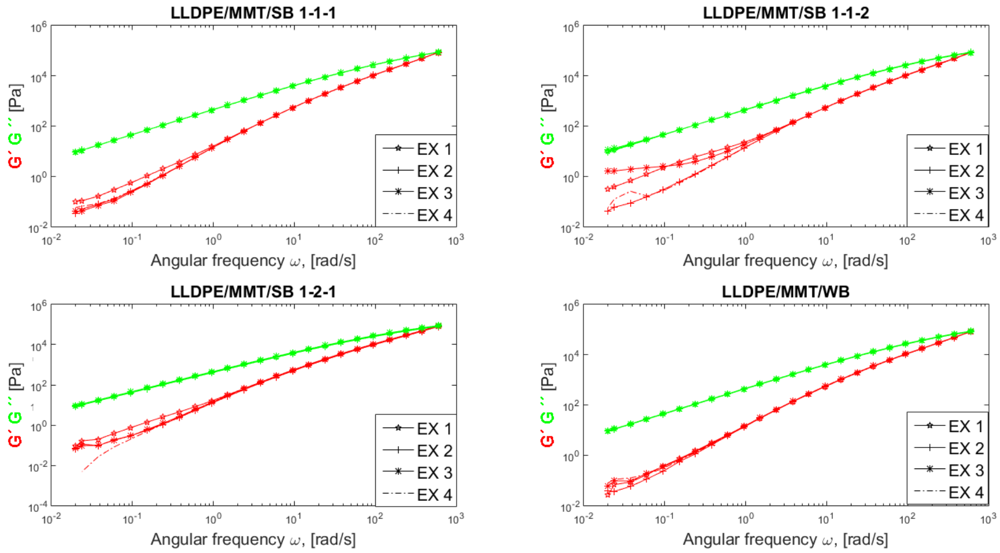

Figure 3.47. Storage(G´) and loss(G´´) modulus, as a function of angular frequency ω, for the 4 extrusions(EX) of the nanocomposites with MMT.

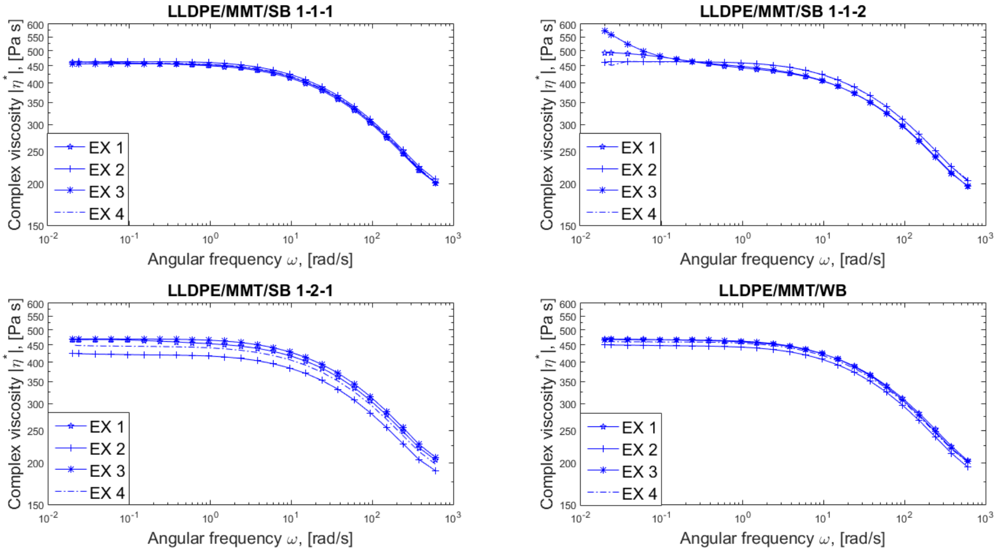

Figure 3.48. Complex viscosity $\eta*$, as a function of angular frequency ω, for the 4 extrusions(EX) of the nanocomposites with MMT.

Uni-axial tensile test

The tensile properties of the nanocomposites were investigated with focus on the young's modulus, maximum strain at yield (σ_{yield}) and break ($\sigma_{Atbreak}$) and the corresponding elongation at yield (ϵ_{yield}) and break ($\epsilon_{Atbreak}$). The results are based on two repetitions for each sample type, except for LDPE/MMT/WB 1 th. had only one repetition, due to a poor sample. The obtained stress-strain curves for the pure polymer LLDPE, and the nanocomposites, unmodified and modified, are shown in the following figures 3.49 and 3.50. All of the curves exhibits an elastic region followed by yielding, which is accompanied with neck propagation. Necking is improved with strain hardening and completed with failure at break. The failure at break is registered as a decrease in stress. These kinds of curves are reported by other studies for linear low density polyethylene (LLDPE) [Durmuş et al., 2007].

Nanocomposites with raw and modified HNT

Young's modulus of nanocomposites were increased approximately 116-129 % for the nanocomposites with unmodified HNT, when compared to the raw polymer LLDPE. The increase in young's modulus were approximately 11-30% and 23 % for LLDPE/HNT/SB and LLDPE/HNT/WB respectively. The stiffness could be attributed the reinforcing affect of halloysite nanotubes (HNT). The tensile stress, and corresponding elongation, of nanocomposites are close to the values of the pure polymer.

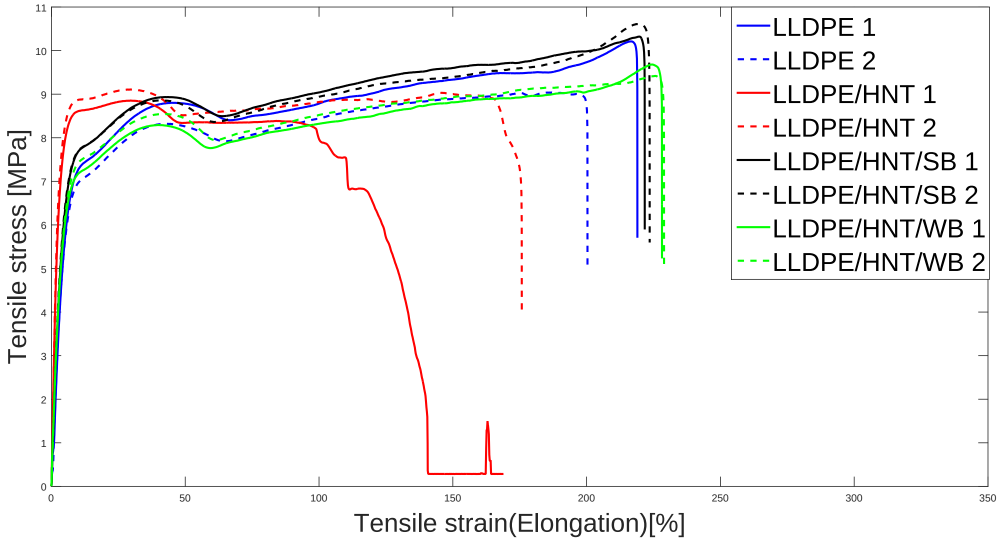

Figure 3.49. Tensile stress-strain curves of the nanocomposites with halloysite nanotubes (HNT). Each types of nanocomposites has two repetitions, where the lines are (-) and (–) are the first and second respectively

Table 3.15. Uni-axial testing results of the nanocomposites with halloysite nanotubes (HNT).

Sample	σ_{yield} [MPa]	ϵ_{yield} [%]	$\sigma_{Atbreak}$ [MPa]	$\epsilon_{Atbreak}$ [%]	Youngs modulus [MPa]
LLDPE 1	8.80	44.81	10.21	216.47	150.62
LLDPE 2	8.32	43.13	9.04	187.46	149.95
LLDPE/HNT 1	8.85	29.63	8.39	84.13	324.14
LLDPE/HNT 2	9.11	29.63	9.03	145.64	344.49
LLDPE/HNT/SB 1	8.93	43.48	10.32	219.64	167.07
LLDPE/HNT/SB 2	8.86	40.81	10.61	218.64	195.49
LLDPE/HNT/WB 1	8.29	40.13	9.68	224.63	185.61
LLDPE/HNT/WB 2	8.55	41.98	9.42	225.81	185.76

However the nanocomposites with unmodified HNT had a reduced elongation at yield and break. This could be attributed aggregation of the filler in the matrix material, which due to a poor compatibility and therefore a poor dispersion between the polymer matrix and halloysite nanotubes (HNT). The nanocomposites with modified HNT show some increases in the tensile stress and elongation at break, when compared to the pure polymer. The small increase in the nanocomposites with modified HNT could have been achieved due to an improved compatibility and a higher dispersion. Similar results for modified HNT in LLDPE are reported by Pedrazzoli et al. [2015].

Nanocomposites with raw and modified MMT

The results of nanocomposites with montmorillonite (MMT) are shown in figure 3.50 and listed in table 3.16. Young's modulus of nanocomposites were increased approximately 35-39 % for the nanocomposites with unmodified MMT, when compared to the raw polymer LLDPE. The increase in young's modulus were approximately 47-62 % and 40 % for LLDPE/MMT/SB 1-1-1 and LLDPE/MMT/WB respectively.

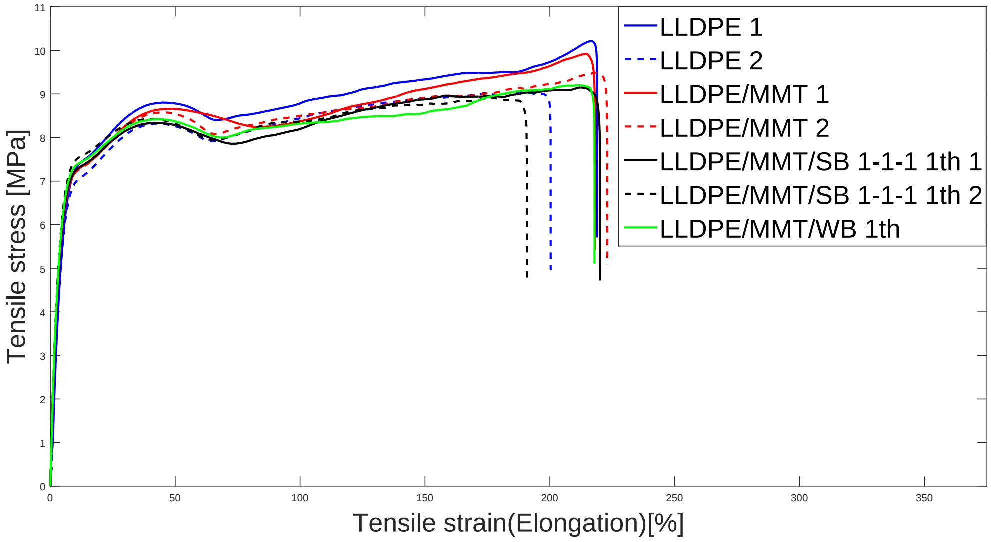

Figure 3.50. Tensile stress-strain curves of the nanocomposites with montmorillonite (MMT). Each types of nanocomposites has two repetitions, where the lines are (-) and (–)are the first and second respectively. LLDPE/MMT/WB has only 1 sample, due to a failed repetition.

The tensile stress and elongation at yield and break showed inconclusive results where the results are not significantly improved or reduced when compared to the pure polymer LLDPE. The improvement of Young modulus of the nanocomposite with modified MMT could be interpreted as an improved compatibility or in interaction between the polymer, the surfactant and the filler materials. However the insignificant changes in the tensile stress and elongation could be also be interpreted as the opposite with a poor compatibility.

Table 3.16. Uni-axial testing results of the nanocomposites nanocomposites with montmorillonite (MMT).

Sample	σ_{UT} [MPa]	ϵ_{UT} [%]	$\sigma_{Atbreak}$ [MPa]	$\epsilon_{Atbreak}$ [%]	Youngs modulus [MPa]
LLDPE 1	8.80	44.81	10.21	216.47	150.62
LLDPE 2	8.32	43.13	9.04	187.46	149.95
LLDPE/MMT 1	8.66	49.13	9.92	214.13	203.06
LLDPE/MMT 2	8.58	44.64	9.49	218.81	209.37
LLDPE/MMT/SB 1-1-1 1	8.34	41.47	9.15	212.81	219.81
LLDPE/MMT/SB 1-1-1 2	8.43	39.97	8.91	176.47	243.13
LLDPE/MMT/WB 1	8.42	42.81	9.20	210.81	210.32

The effects of changing the amount of surfactant

The results of changing amount of surfactant are shown in figure 3.51 and listed in table 3.17. It can be observed that tensile stress at yield and break decreased with decreasing amount of surfactant. The results of the elongations and Youngs modulus showed no clear trends.

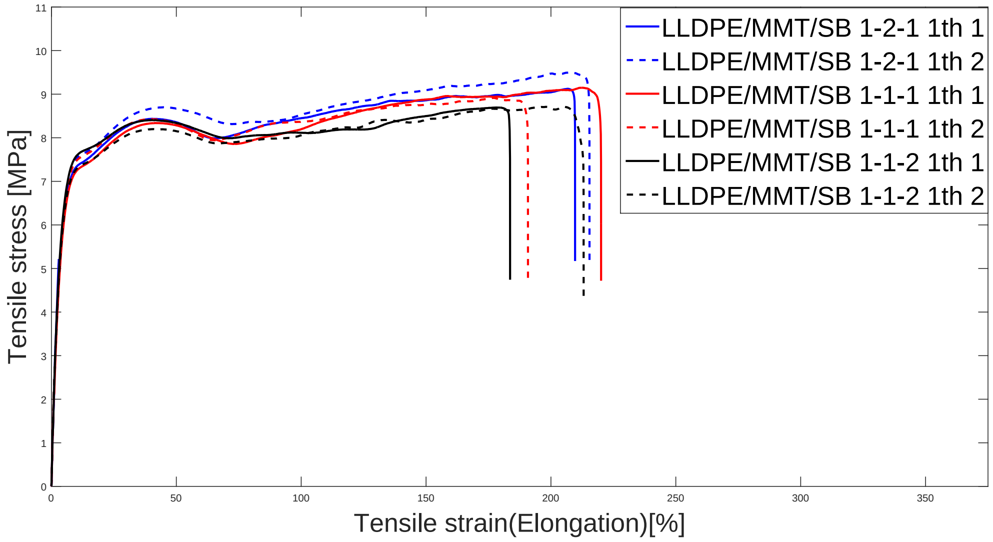

Figure 3.51. Tensile stress-strain curves of nanocomposites with modified montmorillonite (MMT) and different amount of surfactant.

Table 3.17. Uni-axial testing results of the nanocomposites with modified montmorillonite (MMT) and different amount of surfactant.

Sample	σ_{UT} [MPa]	ϵ_{UT} [%]	$\sigma_{Atbreak}$ [MPa]	$\epsilon_{Atbreak}$ [%]	Youngs modulus [MPa]
LLDPE/MMT/SB 1-2-1 1	8.44	40.48	9.12	206.81	206.66
LLDPE/MMT/SB 1-2-1 2	8.70	44.98	9.49	206.48	221.03
LLDPE/MMT/SB 1-1-1 1	8.34	41.47	9.15	212.81	219.81
LLDPE/MMT/SB 1-1-1 2	8.43	39.97	8.91	176.47	243.13
LLDPE/MMT/SB 1-1-2 1	8.41	40.14	8.69	178.31	198.96
LLDPE/MMT/SB 1-1-2 2	8.20	41.64	8.71	205.43	241.96

The effect of extrusions on tensile properties

Attempt at improving the tensile properties were attempted with additional extrusions for the nanocomposites with modified MMT. The results of changing amount of surfactant are shown in figure 3.52 and listed in table 3.18.

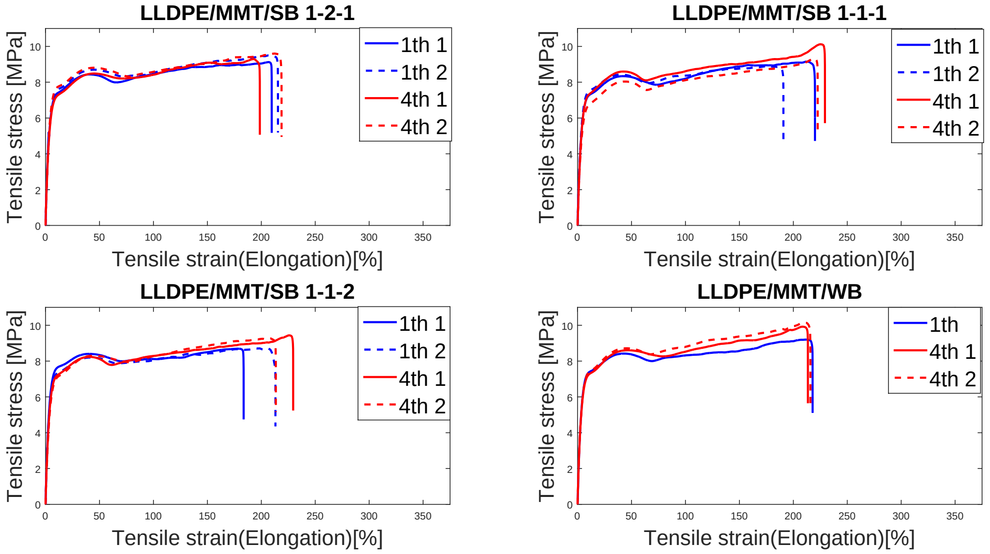

Figure 3.52. Tensile stress-strain curves of the nanocomposites with modified MMT with 1th and 4th extrusion. Each types of nanocomposites has two repetitions, where the lines are (-) are the first and second respectively. LLDPE/MMT/WB 1.th has only 1 sample, due to a failed repetition.

All the nanocomposites, which were loaded with the swine-based MMT/SB had reduced Young's modulus and increased yield strength after additional extrusions. According to Durmus et al. [2008] good adhesion or compatibility at the polymer-filler interphase and the reinforcing effect of a filler is usually indicated by a increase in the yield stress and Young's modulus. The results of the swine based nanocomposites could indicate a poor compatibility due to the reduced Young's modulus. However the results of wood-based LLDPE/MMT/WB nanocomposites shows both an increase in Young's modulus and yield stress after 4 extrusions. This could indicate a better dispersion and compatibility.

Table 3.18. Uni-axial testing results the nanocomposites with modified MMT with 1th and 4th extrusion..

Sample	σ_{UT} [MPa]	ϵ_{UT} [%]	$\sigma_{Atbreak}$ [MPa]	$\epsilon_{Atbreak}$ [%]	Youngs modulus [MPa]
LLDPE/MMT/SB 1-2-1 1	8.44	40.48	9.12	206.81	206.66
LLDPE/MMT/SB 1-2-1 2	8.70	44.98	9.49	206.48	221.03
LLDPE/MMT/SB 1-2-1 4th 1	8.49	44.47	9.30	192.97	219.18
LLDPE/MMT/SB 1-2-1 4th 2	8.81	44.48	9.60	212.31	196.74
LLDPE/MMT/SB 1-1-1 1	8.34	41.47	9.15	212.81	219.81
LLDPE/MMT/SB 1-1-1 2	8.43	39.97	8.91	176.47	243.13
LLDPE/MMT/SB 1-1-1 4th 1	8.60	42.31	10.12	225.15	189.45
LLDPE/MMT/SB 1-1-1 4th 2	8.04	44.81	9.32	219.14	200.47
LLDPE/MMT/SB 1-1-2 1	8.41	40.14	8.69	178.31	198.96
LLDPE/MMT/SB 1-1-2 2	8.20	41.64	8.71	205.43	241.96
LLDPE/MMT/SB 1-1-2 4th 1	8.24	40.14	9.44	226.14	217.24
LLDPE/MMT/SB 1-1-2 4th 2	8.30	44.47	9.25	200.97	203.39
LLDPE/MMT/WB 1	8.42	42.81	9.20	210.81	210.32
LLDPE/MMT/WB 4th 1	8.61	46.30	9.23	208.30	217.29
LLDPE/MMT/WB 4th 1	8.72	44.97	10.15	210.31	220.51

3.4.3 Part conclusion

The results of all the characterization techniques were to determine the degree of dispersion and the compatibility, because good dispersion means good compatibility and yields improved properties of the nanocomposites. The thermal properties showed improved thermal stability for the nanocomposites with modified nanoclays. There is a trend in the results of the residual mass were the mass is increased with increasing amount of surfactant for the nanocomposites with MMT/SB organo-clay.

The visco-elastic properties showed the reinforcing effect of a filler, however no secondary filler interaction with the polymer was not observed. The most interesting result was observed for nanocomposite LLDPE/MMT/SB 1-1-2. The measurement showed an higher increase at higher angular frequencies with a tail, that finds a plateau at lower angular frequencies. This indicates an interaction between the modified filler and the polymer. However this was the exception in the obtained results, and thereby can be results of the visco-elastic properties be interpreted as a poor compatibility and dispersion between the modified nanoclays and the polymer.

The tensile properties showed reduced or poor improvements when compared to the pure polymer. This indicates a poor compatibility with the selected modified nano-clays. However the results of wood-based LLDPE/MMT/WB nanocomposites shows both an increase in Young's modulus and yield stress after 4 extrusions. This could indicate a better dispersion and compatibility.

The FTIR analysis of the nanocomposites with modified MMMT showed that all showed a more intercalated/exfoliated structure with higher mixing time. The nanocomposite with a higher amount of surfactant LLDPE/MMT/SB 1-1-2 and the wood-based LLDPE/MMT/WB had the highest shifts in angles. The XRD analysis supported these results, where the interlayer spacing increased with higher mixing time and amount of surfactant for the nanocomposites with MMT/SB organo-clay, where the polymer intercalated the organoclay. However the nanocomposite with MMT/WB organo-clay had a decrease in the interlayer spacing, which contradicts the results for the ATR-FTIR analysis.

The attempts at improving the dispersion of the nanocomposites with additional extrusions showed some improvements in the intercalation, the dispersion and the compatibility, however the changes were small. Further work have to be conducted to investigate how to improve the dispersion further.

Discussion 4

This chapter focus on the discussion of the obtained experimental results of the performed experiments, when compared to the theory described in the literature study, to investigate the chosen problem statements.

The initial characterization of the raw materials was performed to obtain a baseline for further processing. All the materials, except the bio-residue (BR), yielded no surprising results. The received bio-residue (BR) had a different chemical composition and was renamed to swine-based bio-oil (SB). The results for the swine-based bio-oil (SB) showed that the material had a similar compounds, with differences, to the bio-residue (BR) described in the former project Høgsaa [2015]. However the changes in the chemical structure was significant. This was proven with ATR-FTIR and GC-MS analysis. The swine-based bio-oil (SB) still had a high presence of long fatty acids, a low content of nitrogen and oxygen compounds (e.g. amines, amides and olefins), when compared to the bio-residue (BR). These changes could change the possible interactions with filler materials and polymer matrix. A study into how conversion process affects the chemical structure of the bio-residue (BR) and the swine based bio-oil (SB) would be recommended if bio-oil should be used as intercalant at an industrial / commercial level. There were uncertainties regarding changes in the chemical composition and how this will affect the modification process of the investigated organo-clays.

The modification process was performed with a solution-intercalation blending process with ultrasonification for both nanoclays and surfactants. The results of the characterization methods indicated that the modification process was a success for the montmorillonite clays, where the structure of the clays were intercalated/exfoliated for both types of surfactant. The analysis of the chemical structure of organo-clays with HNT was inconclusive, due the natural exfoliated state of the halloysite nanotubes (HNT). The FTIR analysis indicated that the HNT/WB could possibly have absorbed the surfactant wood-based bio-oil (WB) into the interior lumen of the halloysite nanotubes (HNT). Another possibility is agglomeration of nanotubes, which shield the peaks of the surfactant. However this should have been detected by the XRD analysis as an intercalated structure. HNT/SB presented more peaks from the intercalant in its spectra, when compared to wood-based bio-oil (WB). Two new peaks were observed at 1541 and 1576 cm^{-1}, which could not be found in the spectra of halloysite nanotubes (HNT) or swine-based bio-oil (SB). MMT/SB had peaks from both its constituents. The peaks around 2900 cm^{-1} and 1000 cm^{-1} showed increased intensity compared the peaks of the original materials. MMT/WB had similar trends as MMT/SB, however peaks around 2900 cm^{-1} and 1000 cm^{-1} were decreased significantly in the modified MMT/WB compared to its constituents. It was attempted to determine the interactions between the selected surfactants and the nano-clays, however this was unsuccessful. The nano-clays with modified montmorillonite had peaks from both the clay and the surfactant in the area, described by Cole [2008], which made it difficult to determine the degree of intercalation/exfoliation with this technique for the organo-clays. The organic modification of the selected nano-clays was successful, however it is still unclear, which functional or polar group of the surfactants, which facilitated the intercalated state, was produced in the organo-clays. The intercalation mechanism could be a dipole-dipole interaction, a cation-exchange or a mixture of both. The presence of the hydroxy groups (-OH) in the surfactants and the nanoclays could have attracted each other for a dipole-dipole interaction. The improved intercalated/structure of organoclays with swine based bio-oil (SB) could also have been facilitated by some of the nitrogen rich compounds with a cation-exchange.

A way to improve the possibility on how assess the interactions could be to wash the obtained organo-clay for excess surfactant or tailoring the surfactant for a specific filler or polymer. A washing process of the organo-clays, where the excess surfactant is removed, could enable easier processing and compatibility with a chosen polymeric material and the filler material. The cleaned organo-clay version can be used to assess and determine the intercalation mechanism between organo-clay - filler and between organoclay - polymer material. Another viable options for improving the properties and the compatibility between the modified nanoclays could be to tailor specific bio-oils from different origins, to be compatible with selected polymers or fillers. These options could improve the potential of the usage of the bio-oils. To tailor the bio-oils, more studies have to be conducted in order to investigate which functional groups of the bio-oil, which can facilitate the intercalation/exfoliation mechanism and improve the compatibility and dispersion. A bio-oil is complex mixture of different compounds and it is selected compounds of the bio-oil, which can be used effectively as an intercalant. Therefore a separation and cleaning process to extract specific compounds could help determine, which kinds of mechanisms can improve the compatibility and increase the desired properties of the nanocomposites.

The problem statement for the nanocomposites was to investigative if the obtained organo-clays is compatible with linear low density polyethylene. The results of the nanocomposites with the different organo-clays showed mixed results. The nanocomposites with unmodified nanoclay, both with montmorillonite (MMT) and halloysite nanotubes (HNT), had reduced mechanical and thermal properties when compared to the results of the pure polymer. This fits with findings of the literature study. The nanocomposites with modified organo-clay had the same or slightly improved mechanical and thermal properties when compared to the pure polymer. This shows that the compatibility between the constituents was slightly improved. However compared to results of other studies [Pedrazzoli et al., 2015; Zhang and Sundararaj, 2006] with similar material systems, the compatibility was poor, based on the obtained properties. The results could be attributed to usage of bio-oils, which is a complex mixture of compounds. The other studies utilized pure compounds as compatibilizers. Therefore a small fraction of the bio-oils, could facilitate the interaction between the organo-clay and the polymer matrix. This would explain the reduced compatibility.

The improvement in the thermal properties was significant, based on the low clay loading of 2 % Wt with several degrees in the onset temperature and residual mass. The nanocomposites with MMT/SB organo-clay showed a higher thermal stability by increasing the amount of surfactant. This finding could be attributed to a nucleating effect on the crystallinity of the polymer by the surfactants.

The results of XRD and ATR-FTIR analysis showed possible intercalation of the polymer in the interlayer of the galleries of the organo-clays with MMT/SB with higher amount of surfactant and mixing time. However these results could be attributed to the reduction of agglomerated particles, which was observed in the obtained nanofilms. Further studies have to be conducted to determine how to improve the compatibility and dispersion between LLDPE and the selected investigated organo-clays. There are different ways to improve the properties of the nanocomposites. One option could be to increase the amount of organo-clay in the nanocomposites. A study into how the amount of the surfactant affects the chemical structure and properties would be needed. A secondary surfactant, which can facilitate further exfoliation after intercalation have taken place could be an option. A study into the mixing properties and setting would be a highly viable solution, especially based on the results in this thesis, where the nanocomposites with modified MMT/SB organo clay had improved exfoliation and thermal properties. A more polar polymer matrix material, which could be more compatible with organo-clay.

Conclusion 5

The purpose of this thesis was to investigate if bio-oils could be used as compatibilizers for LLDPE. The modification process, solution-intercalation blending with ultrasonication, was deemed a success for modified MMT nanoclays with intercalated, partly exfoliated structure for both the swine-based bio-oil (SB) and the wood-based bio-oil (WB). This was supported by the various characterization techniques utilized. The results of the XRD analysis indicated that swine-based bio-oil (SB) is more effective as an intercalant than the wood-based bio-oil (WB). The nanoclays with modified HNT showed inconclusive results due to the natural exfoliated state of the halloysite nanotubes (HNT). However the FTIR analysis showed interactions between the surfactant and the nanoclays. Therefore it was not clear which functional groups of the nanoclays and the different surfactants facilitated the interactions.

The compatibility between the hydrophobic LLDPE and modified nanoclays showed poor compatibility, which was evident by the high agglomeration in the produced nanofilms. Another indication was the unchanged basal d-spacing of the nanocomposites with modified nanoclay, which indicated that the polymer matrix had not intercalated the interlayer galleries of the montmorillonite. The thermal properties of the nanocomposites with modified nanoclay showed improvements in the thermal stability. However the mechanical properties was slightly improved, when compared to the pure polymer. The nanocomposites with unmodified nanoclay showed severely reduced and the nanocomposite with modified nanoclay had slightly improved properties, or close to the properties of the pure polymer. The modified nanoclays were deemed not compatible with the LLDPE, when compared to the results of other studies [Pedrazzoli et al., 2015; Zhang and Sundararaj, 2006; Hotta and Paul, 2004].

Attempts at improving the dispersion by additional extrusions was a mixed success with some improvements, but further studies are needed to determine how the longer mixing time affects the chemical structure.

However the results of the modification with both surfactants were promising, and a more polar polymer like Poly(ethylene oxide)(PEO) could possibly have facilitated more improved mechanical and thermal properties. An other option is to increase the filler loading of the nanocomposites, because the results of the montmorillonite could possibly be improved significantly with higher clay loading. The nanocomposites with halloysite nanotubes (HNT) should have according to literature have a clay loading of 5-10%, and montmorillonite (MMT) 2-5 % for improved mechanical and thermal properties.

Bibliography

Additives and Instruments, December 2015. BYK Additives and Instruments. *Cloisite NA+ product data*. ALTANA, 2015. URL https://www.byk.com/en/additives/additives-by-name/cloisite-na.php.

As' habi, Jafari, Khonakdar, Kretzschmar, Wagenknecht, and Heinrich, 2013. Ladan As' habi, Seyed Hassan Jafari, Hossein Ali Khonakdar, Bernd Kretzschmar, Udo Wagenknecht, and Gert Heinrich. *Effect of clay type and polymer matrix on microstructure and tensile properties of PLALLDPEclay nanocomposites*. Journal of Applied Polymer Science, 130(2), 749–758, 2013.

Barnes, 2000. Howard A. Barnes. *A handbook of elementary rheometry*. The University of Wales Institute of Non-Newtonian Fluid Mechanics, Penglais, Aberystwyth, Dyfed, Wales, SY23 3BZ, 2000. ISBN 0-9538032-0-1.

Brydson, 1999. John Andrew Brydson. *Plastics materials*. Butterworth-Heinemann, 1999.

Cambridge Polymer Group. Cambridge Polymer Group. *Small Amplitude Oscillatory Shear Rheometry*. URL http://www.campoly.com/educational-resources/application-notes/.

Carli, Crespo, and Mauler, 2011. Larissa N Carli, Janaina S Crespo, and Raquel S Mauler. *PHBV nanocomposites based on organomodified montmorillonite and halloysite: the effect of clay type on the morphology and thermal and mechanical properties*. Composites Part A: Applied Science and Manufacturing, 42(11), 1601–1608, 2011.

Ceramicindustry, 2005. Ceramicindustry. *Improving Zirconia Ceramics through Thermoanalytical Characterization*, 2005. URL http://www.ceramicindustry.com/articles/87505-improving-zirconia-ceramics-through-thermoanalytical-characterization. no available author.

online, April 2016. The Essential chemical industry online. *Poly(ethylene)*. The university of York, 2016. URL http://www.essentialchemicalindustry.org/polymers/polyethene.html.

Cole, 2008. Kenneth C Cole. *Use of infrared spectroscopy to characterize clay intercalation and exfoliation in polymer nanocomposites*. Macromolecules, 41(3), 834–843, 2008.

Durmus, Kasgoz, and Macosko, 2007. Ali Durmus, Ahmet Kasgoz, and Christopher W Macosko. *Linear low density polyethylene (LLDPE)/clay nanocomposites. Part I: Structural characterization and quantifying clay dispersion by melt rheology*. Polymer, 48(15), 4492–4502, 2007.

Durmuş, Woo, Kaşgöz, Macosko, and Tsapatsis, 2007. Ali Durmuş, Maybelle Woo, Ahmet Kaşgöz, Christopher W Macosko, and Michael Tsapatsis. *Intercalated linear low density polyethylene (LLDPE)/clay nanocomposites prepared with oxidized polyethylene as a new type compatibilizer: structural, mechanical and barrier properties*. European Polymer Journal, 43(9), 3737–3749, 2007.

Durmus, Kaşgöz, and Macosko, **2008**. Ali Durmus, Ahmet Kaşgöz, and Christopher W Macosko. *Mechanical Properties of Linear Low-density Polyethylene (LLDPE)/clay Nanocomposites: Estimation of Aspect Ratio and İnterfacial Strength by Composite Models.* Journal of Macromolecular Science®, Part B: Physics, 47(3), 608–619, 2008.

Fini, **September 20 2013**. Elham H Fini. *Preparation and uses of bio-adhesives*, 2013. US Patent App. 14/032,445.

Fini, Kalberer, Shahbazi, Basti, You, Ozer, and Aurangzeb, **2011**. Elham H Fini, Eric W Kalberer, Abolghasem Shahbazi, Mufeed Basti, Zhanping You, Hasan Ozer, and Qazi Aurangzeb. *Chemical characterization of biobinder from swine manure: Sustainable modifier for asphalt binder.* Journal of Materials in Civil Engineering, 23(11), 1506–1513, 2011.

Fini, Al-Qadi, You, Zada, and Mills-Beale, **2012**. Elham H Fini, Imad L Al-Qadi, Zhanping You, Boubacar Zada, and J Mills-Beale. *Partial replacement of asphalt binder with bio-binder: characterisation and modification.* International Journal of Pavement Engineering, 13(6), 515–522, 2012.

Gorrasi, **2015**. Giuliana Gorrasi. *Dispersion of halloysite loaded with natural antimicrobials into pectins: Characterization and controlled release analysis.* Carbohydrate polymers, 127, 47–53, 2015.

Høgsaa, **December 2015**. Bjarke Hangstrup Høgsaa. *Investigation of materials from biorenewable resources.* AAU, 2015.

Hosseinnezhad, Fini, Sharma, Basti, and Kunwar, **2015**. Shahrzad Hosseinnezhad, Ellie H Fini, Brajendra K Sharma, Mufeed Basti, and Bidhya Kunwar. *Physiochemical characterization of synthetic bio-oils produced from bio-mass: a sustainable source for construction bio-adhesives.* RSC Advances, 5(92), 75519–75527, 2015.

Hotta and Paul, **2004**. S Hotta and DR Paul. *Nanocomposites formed from linear low density polyethylene and organoclays.* Polymer, 45(22), 7639–7654, 2004.

Irani, Ismail, and Ahmad, **2013**. Maryam Irani, Hanafi Ismail, and Zulkifli Ahmad. *Preparation and properties of linear low-density polyethylene-g-poly (acrylic acid)/organo-montmorillonite superabsorbent hydrogel composites.* Polymer Testing, 32(3), 502–512, 2013.

Jia, Luo, Guo, Yang, Du, and Jia, **2009**. Zhixin Jia, Yuanfang Luo, Baochun Guo, Bingtao Yang, Mingliang Du, and Demin Jia. *Reinforcing and flame-retardant effects of halloysite nanotubes on LLDPE.* Polymer-Plastics Technology and Engineering, 48(6), 607–613, 2009.

Jin, Seol, and Kim, **2009**. Dong-Woo Jin, Sung-Mok Seol, and Gue-Hyun Kim. *New compatibilizer for linear low-density polyethylene (LLDPE)/clay nanocomposites.* Journal of applied polymer science, 114(1), 25–31, 2009.

K.Fukushima, D.Tabuani, and G.Camino, **November 2008**. K.Fukushima, D.Tabuani, and G.Camino. *Nanocomposites of PLA and PCL based on montmorillonite and sepiolite.* Materials Science and Engineering C, pages 1433–1441, 2008.

Khederlou, Bagheri, and Shojaei, **2014**. Kh Khederlou, R Bagheri, and A Shojaei. *A mathematical method for XRD pattern interpretation in clay containing nano composites.* Applied Surface Science, 318, 90–94, 2014.

Khunova, Kristof, Kelnar, and Dybal, 2013. V Khunova, J Kristof, I Kelnar, and J Dybal. *The effect of halloysite modification combined with in situ matrix modifications on the structure and properties of polypropylene/halloysite nanocomposites.* eXPRESS Polymer Letters, 7(5), 2013.

Klitkou, 2012. Rasmus Klitkou. *Mechanical Response of Polypropylene/Clay Nanocomposites.* Videnbasen for Aalborg UniversitetVBN, Aalborg UniversitetAalborg University, Det Teknisk-Naturvidenskabelige FakultetThe Faculty of Engineering and Science, Institut for ProduktionDepartment of Production, 2012.

Lampman et al., 2003. Steve Lampman et al. *Characterization and failure analysis of plastics.* ASM International, 2003.

Liu, Guo, Du, Cai, and Jia, 2007. Mingxian Liu, Baochun Guo, Mingliang Du, Xiaojia Cai, and Demin Jia. *Properties of halloysite nanotube–epoxy resin hybrids and the interfacial reactions in the systems.* Nanotechnology, 18(45), 455703, 2007.

Mallakpour and Dinari, 2012. Shadpour Mallakpour and Mohammad Dinari. *Biomodification of cloisite Na+ with L-methionine amino acid and preparation of poly (vinyl alcohol)/organoclay nanocomposite films.* Journal of Applied Polymer Science, 124(5), 4322–4330, 2012.

Abolfazl Maneshi, Joao BP Soares, and Leonardo C Simon, 2006. Abolfazl Maneshi, Joao BP Soares, and Leonardo C Simon. A Single-Gallery Model for the In Situ Production of Polyethylene-Clay Nanocomposites. In *Macromolecular Symposia*, volume 243, pages 277–286. Wiley Online Library, 2006.

Marchante, Marcilla, Benavente, Martínez-Verdú, and Beltran, 2013. V Marchante, A Marcilla, V Benavente, Francisco Miguel Martínez-Verdú, and MI Beltran. *Linear low-density polyethylene colored with a nanoclay-based pigment: Morphology and mechanical, thermal, and colorimetric properties.* Journal of Applied Polymer Science, 129(5), 2716–2726, 2013.

Mills-Beale, You, Fini, Zada, Lee, and Yap, 2012. Julian Mills-Beale, Zhanping You, Elham Fini, Boubacar Zada, Chee Huei Lee, and Yoke Khin Yap. *Aging Influence on Rheology Properties of Petroleum-Based Asphalt Modified with Biobinder.* Journal of Materials in Civil Engineering, 26(2), 358–366, 2012.

Newport, 2015. Newport. *Introduction to FTIR Spectroscopy*, 2015. URL `http://www.newport.com/store/genContent.aspx/Introduction%ADto%ADFT%ADIR%ADSpectroscopy/405840/1033`. no available author.

Oldham, Fini, and Chailleux, 2015. Daniel J Oldham, Ellie H Fini, and Emmanuel Chailleux. *Application of a bio-binder as a rejuvenator for wet processed asphalt shingles in pavement construction.* Construction and Building Materials, 86, 75–84, 2015.

Önal and Sarıkaya, 2008. Müşerref Önal and Yüksel Sarıkaya. *The effect of organic cation content on the interlayer spacing, surface area and porosity of methyltributylammonium-smectite.* Colloids and Surfaces A: Physicochemical and Engineering Aspects, 317(1), 323–327, 2008.

Panalytical, 2015. Panalytical. *X-ray diffractometers*, 2015. URL `http://www.panalytical.com/Xray-diffractometers.htm`. no available author.

Paul and Robeson, 2008. DR Paul and LM Robeson. *Polymer nanotechnology: nanocomposites.* Polymer, 49(15), 3187–3204, 2008.

Pavlidou and Papaspyrides, 2008. S Pavlidou and CD Papaspyrides. *A review on polymer–layered silicate nanocomposites.* Progress in polymer science, 33(12), 1119–1198, 2008.

Peacock, 2000. Andrew Peacock. *Handbook of polyethylene: structures: properties, and applications.* CRC Press, 2000.

Pedersen, Grigoras, Hoffmann, Toor, Daraban, Jensen, Iversen, Madsen, Glasius, Arturi, et al., 2016. Thomas Helmer Pedersen, IF Grigoras, Jessica Hoffmann, Saqib Sohail Toor, Iulia Maria Daraban, Claus Uhrenholt Jensen, SB Iversen, RB Madsen, M Glasius, Katarzyna Ratajczyk Arturi, et al. *Continuous hydrothermal co-liquefaction of aspen wood and glycerol with water phase recirculation.* Applied Energy, 162, 1034–1041, 2016.

Pedrazzoli, 2013. D Pedrazzoli. *Viscoelastic behaviour and fracture toughness of linear-low-density polyethylene reinforced with synthetic boehmite alumina nanoparticles.* Express Polymer Letters, 7(8), 652–666, 2013.

Pedrazzoli, Pegoretti, Thomann, Kristóf, and Karger-Kocsis, 2015. Diego Pedrazzoli, Alessandro Pegoretti, Ralf Thomann, János Kristóf, and József Karger-Kocsis. *Toughening linear low-density polyethylene with halloysite nanotubes.* Polymer Composites, 36(5), 869–883, 2015.

Perkin Elmer, 2004. Perkin Elmer. *ATR accessories*, 2004. URL `http://shop.perkinelmer.com/Content/technicalinfo/tch_atraccessories.pdf`. no available author.

Poppe, Paskevich, Hathaway, and Blackwood, 2001. LJ Poppe, VF Paskevich, JC Hathaway, and DS Blackwood. *A laboratory manual for X-ray powder diffraction.* US Geological Survey Open-File Report, 1(041), 1–88, 2001.

Potarniche, Vuluga, Christiansen, Radovici, and Kristensen, 2013. Catalina-Gabriela Potarniche, Zina Vuluga, Jesper de Claville Christiansen, Constantin Radovici, and Peter Kjaer Kristensen. *Influence of two compatibilizers on clay/PP nanocomposites properties.* Polymer Engineering & Science, 53(2), 403–409, 2013.

Qiu, Chen, and Qu, 2006. Longzhen Qiu, Wei Chen, and Baojun Qu. *Morphology and thermal stabilization mechanism of LLDPE/MMT and LLDPE/LDH nanocomposites.* Polymer, 47(3), 922–930, 2006.

Rafiei and Ghomi, 2013. Behrouz Rafiei and F Ahmadi Ghomi. *Preparation and characterization of the Cloisite Na+ modified with cationic surfactants.* Journal of Crystallography and Mineralogy, 21(2), 25–31, 2013.

Rawtani and Agrawal, 2012. Deepak Rawtani and YK Agrawal. *Multifarious applications of halloysite nanotubes: a review.* Rev. Adv. Mater. Sci, 30, 282–295, 2012.

Rooj, Das, Stöckelhuber, Mukhopadhyay, Bhattacharyya, Jehnichen, and Heinrich, 2012. Sandip Rooj, Amit Das, Klaus Werner Stöckelhuber, Nabaneeta Mukhopadhyay, Arup R Bhattacharyya, Dieter Jehnichen, and Gert Heinrich. *Pre-intercalation of long chain fatty acid in the interlayer space of layered silicates and preparation of montmorillonite/natural rubber nanocomposites.* Applied Clay Science, 67, 50–56, 2012.

Ryu and Chang, 2005. Sung Hun Ryu and Young-Wook Chang. *Factors affecting the dispersion of montmorillonite in LLDPE nanocomposite.* Polymer Bulletin, 55(5), 385–392, 2005.

Saad and Dimitry, 2012. ALG Saad and OIH Dimitry. *Studies of particle dispersion in plasticized poly (vinyl chloride)/montmorillonite nanocomposites.* Journal of Applied Polymer Science, 123(3), 1407–1420, 2012.

Stevens, 1999. Malcolm P. Stevens. *Polymer Chemistry-An introduction.* Oxford, 3th edition, 1999. ISBN 978-0-19-512444-6.

Stoch and Wacławska, 1981. Leszek Stoch and I Wacławska. *Dehydroxylation of kaolinite group minerals: I. Kinetics of dehydroxylation of kaolinite and halloysite.* Journal of Thermal Analysis and Calorimetry, 20(2), 291–304, 1981.

Truss and Yeow, 2006. Rowan W Truss and Tay Kiah Yeow. *Effect of exfoliation and dispersion on the yield behavior of melt-compounded polyethylene–montmorillonite nanocomposites.* Journal of applied polymer science, 100(4), 3044–3049, 2006.

Uddin, 2008. Faheem Uddin. *Clays, nanoclays, and montmorillonite minerals.* Metallurgical and Materials Transactions A, 39(12), 2804–2814, 2008.

Walters, Fini, and Abu-Lebdeh, 2014. Renaldo C Walters, Elham H Fini, and Taher Abu-Lebdeh. *Enhancing Asphalt Rheological Behavior And Aging Susceptibility Using Bio-Char And Nano-Clay.* American Journal of Engineering and Applied Sciences, 7(1), 66–76, 2014.

Xi, Frost, He, Kloprogge, and Bostrom, 2005. Yunfei Xi, Ray L Frost, Hongping He, Theo Kloprogge, and Thor Bostrom. *Modification of Wyoming montmorillonite surfaces using a cationic surfactant.* Langmuir, 21(19), 8675–8680, 2005.

Yuan, Southon, Liu, Green, Hook, Antill, and Kepert, 2008. Peng Yuan, Peter D Southon, Zongwen Liu, Malcolm ER Green, James M Hook, Sarah J Antill, and Cameron J Kepert. *Functionalization of halloysite clay nanotubes by grafting with γ-aminopropyltriethoxysilane.* The Journal of Physical Chemistry C, 112(40), 15742–15751, 2008.

Yuan, Tan, and Annabi-Bergaya, 2015. Peng Yuan, Daoyong Tan, and Faïza Annabi-Bergaya. *Properties and applications of halloysite nanotubes: recent research advances and future prospects.* Applied Clay Science, 112, 75–93, 2015.

Zhang and Sundararaj, 2006. Mingqian Zhang and Uttandaraman Sundararaj. *Thermal, rheological, and mechanical behaviors of LLDPE/PEMA/clay nanocomposites: effect of interaction between polymer, compatibilizer, and nanofiller.* Macromolecular Materials and Engineering, 291(6), 697–706, 2006.

Investigation of materials from bio-renewable resources A

A.1 Introduction

The idea of converting biomass into sustainable materials and energy has gathered a lot of attention in the last couple of decades. Especially the process of converting biomass into bio-fuel, bio-oil and other byproducts of the conversion process have been researched extensively. A detailed search in the research databases shows the bio convertible materials and bio-renewable materials, which are suitable to be converted into bio oil and bio-fuel, have many different sources from grown materials; like corn, starch, rice straws, coconut peals and shells, and micro algae to pure waste products like manure from life stock. The potential gain of converting wasted bio mass like manure is immense, not only due to the environmental aspects of removing CO_2 emissions and greenhouse gases and reducing the potential spills, that could pollute the ecosystems surrounding the production facility and the ground water of the region. Another gain of the conversion process is of great importance for the agricultural industry, which have been subjected to increasing regulations and hereby forced to downsize their production facilities to meets the regulations, due to excess manure and waste. If the wasted biomass is converted into bio-oil by non-expensive conversion methods, the farmers can increase their production and gain a supplementary income. The obtained bio-oil can be used and processed for many applications (e.g. new materials processes directly from the oil or the obtained byproducts of the applied conversions process).

A new exciting application, of converting biomass into new resources, is the conversion of swine manure into bio-adhesives. The Agricultural and Technical State University of North Carolina (NC A&T) has researched and developed a patented method, which can convert liquefied swine manure into bio-adhesives with different properties. One of the patented bio-adhesives can be converted trough filtration and fractionation into a bio-binder, which is analogous to bitumen in properties. This has gained a lot of attention from the road and highway construction industry, because this industry is looking for more sustainable and economic viable alternatives for the petroleum based bitumen, which is used in the current construction process. Research has been conducted of the bio-binder's potential as a partial replacement for the conventional asphalt binder(PG 64-22). The initial results were promising and the bio-binder has shown to improve the rheological and mechanical properties as an partial modifier in the conventional binder, but only at a weight fraction of 5-10 %. Some research have gone into the properties of the bio-binder and the bio-oil, which is obtained in the conversion process. The bio-adhesive, which is investigated in this project, is a bio-residue. The material is one of the conversions steps between earlier mentioned bio-oil and the bio-binder.

One of this project's main focuses is to gain a deeper understanding of production processes and the properties obtained; a characterization of the bio-residue, which were produced at NC A&T facilities from swine manure. The is achieved with a literature study of the available materials(e.g. articles, patent, studies) and selected experiments chosen from the study, to obtain a baseline knowledge of the material to evaluate the effects of a possible addition of a nanofiller.

Another aim of the literature study is to investigate if it is possible to improve the rheological and mechanical properties of the bio-residue with the addition of a nanofiller(e.g. montmorillonite, a clay particle material) to obtain a nanocomposite. Alternatively the bio-residue can be used as a intercalant to obtaining a modified silicate or organoclay(organically modified clay) for further processing at a later time. A literature study on the montmorillonite, and its structure(e.g intercalation, exfoliation, dispersion) and properties(e.g. viscosity and thermal) will be conducted to determine the appropriate further processing.

A.2 Investigated materials

In the following chapter, a small literature study on the conversion process of swine manure into bio-residue from NC A&T is compiled from different sources (e.g. articles and patents) to get a better understand of the process to obtaining the bio-residue, which is being investigated in this project. Then a study of montmorillonite, with focus on the structure and morphology, is investigated.

A.2.1 Bio-residue

The process on how obtain the bio-residue and other bio-adhesives is described in a international filled patent application WO 2014/047462 A1, also titled as PREPARATION AND USES OF BIO-ADHESIVES [Fini, 2013]. The following sections are primary based in this source.

Conversion process

According to the filled patent, the process from NC A&T can be used to convert swine or poultry manure into different bio-adhesives. A schematic of the different steps of the conversion process is illustrated in figure A.1, where the full conversion process is illustrated with all the obtained products and a partial conversion process, where the direct conversion path to the bio-residue is illustrated in figure A.2.

From bio-mass into bio-oil The process starts with animal slurry waste, with a liquid phase of up to 80%, whic is comprised primarily of water, and solid phase, which is subjected to a thermochemical conversion process (TCC). The TCC process can be performed by three different processes; Pyrolysis, gasification and liquefaction. The three processes are different ways to convert bio-mass into bio-oil and other byproducts. According to Fini et al. [2011], the process of pyrolysis, is where bio-mass is degraded by thermal reactions at elevated temperatures with the absence of oxygen. This process yields a volatile phase and a carbonaceous (carbon-rich) char.

The gasification process is where biomass is converted to into carbon monoxide, hydrogen or carbon dioxide gases in an oxygen depleted environment with thermal decomposition, which can be used to power electric or mechanical equipment.

The final process is liquefaction, where biomass is converted with a high-pressure thermal decomposition process, which utilizes reactive carbon monoxide or hydrogen gases as carrier gases to produce oil, char, liquid fuel and bitumen. The process of liquefaction has been refined in recent years with the employment of heat and pressure to improve the efficiency of the conversion process.

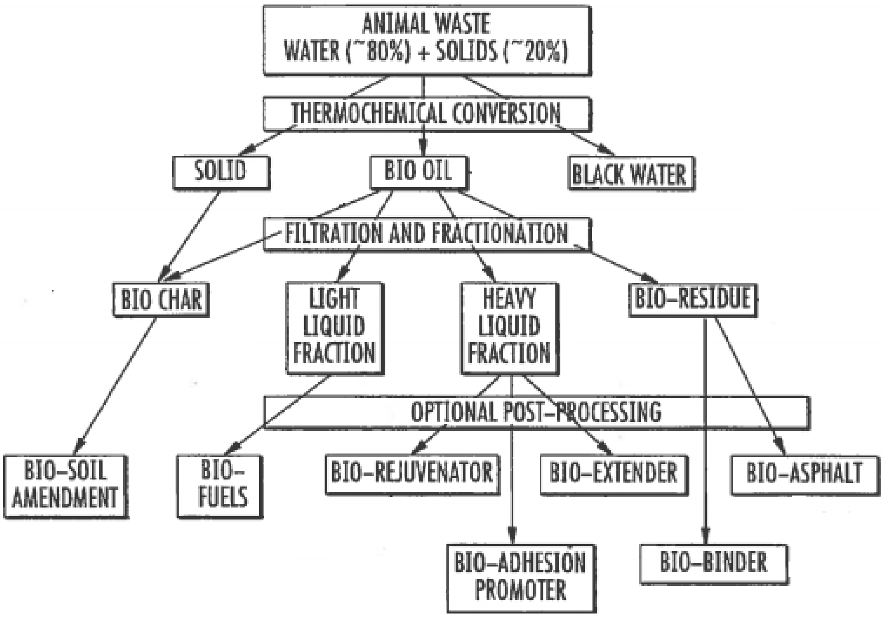

Figure A.1. Full conversion process from swine manure into bio-adhesives [Fini, 2013].

In the patented process from NC A&T, it is the thermal liquefaction with heat and pressure, which have been utilized to convert the swine manure into bio-oil. According to Fini [2013], the pressure is between 15-20 MPa and the temperature is up to 350 °C in an anaerobic environment within a reactor(e.g. an autoclave). The mixture is purged with nitrogen gas three times to ensure an oxygen free, but pressurized environment. The reactor is heated and held for a specific residence time of 15-80 minutes, depending on the pressure and temperature settings. Then the reactor is rapidly cooled down to room temperature with a recycled ice-water cooling coil. The gas pressure in the reactor is released and a sticky residue remains in the reactor.

The sticky residue, described in the process, is isolated with the addition of a solvent (e.g. acetone/toulene mixture or pure acetone) to yield a solid phase in the mixture. An aqueous phase of the mixture is also obtained and is removed through a filtration process. The aqueous phase is called black water, and contains nutrients, but no pathogens. Therefore it is described as a great fertilizer. The remaining substance in the mixture is the solid phase and the bio-oil. The mixture is described as an energy-dense, but crude oil, which have properties similar to a petroleum based oil.

Post processing products The solid and bio-oil can be filtered and fractionation additionally to obtain bio-char. The bio-char can be used for bio-soil amendment, because bio-char is comprised of an insoluble organic material, which is full of nutrients and minerals (e.g. nitrogen, phosphorus, potassium, calcium and carbon). Additional filtration and fractionation produces a light liquid fraction, a heavy liquid fraction and bio-residue from the bio-oil. These three products can be further processed into other bio products(e.g. bio-fuels, a bio-rejuvenator, a bio-adhesion promoter, a bio-extender, a bio-binder and bio-asphalt).

From bio-oil to bio-residue In this project, the main focus is the conversion process to the bio-residue, which is illustrated in figure A.2. From the schematic, it can be seen that the bio-residue is converted from the the bio-oil into the bio-binder and bio-asphalt. The bio-residue can be filtrated, then followed by polymerization and then lastly, fractional distillation into the bio-binder. The bio-residue is described as a dark black/brownish, sticky substance with no odors at room temperature, but a has small scent of sulfur at elevated temperatures.

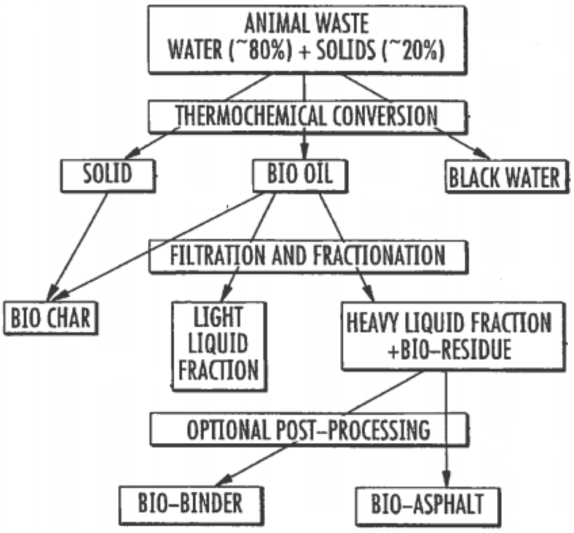

Figure A.2. Direct conversion process from swine manure into bio-residue.

The production setup

A schematic of an possible processing setup, for the conversion of the raw swine manure to the desired bio-adhesives, is illustrated in figure A.3. This setup can be set up for a continuous or batch production, depending on the need. A mixture of bio-oil, bio-char and a solvent (e.g. acetone) is loaded in a filtration tank and filtrated. After the filtration process, where the bio-char is removed, the remaining substance is transferred into a vacuum chamber for distillation. The pressure and heat is applied and monitored. The substance can be fractionated into different compounds; a solid, a light liquid, a heavy liquid or bio-residue. These compounds can be condensed via a condenser in an additional step.

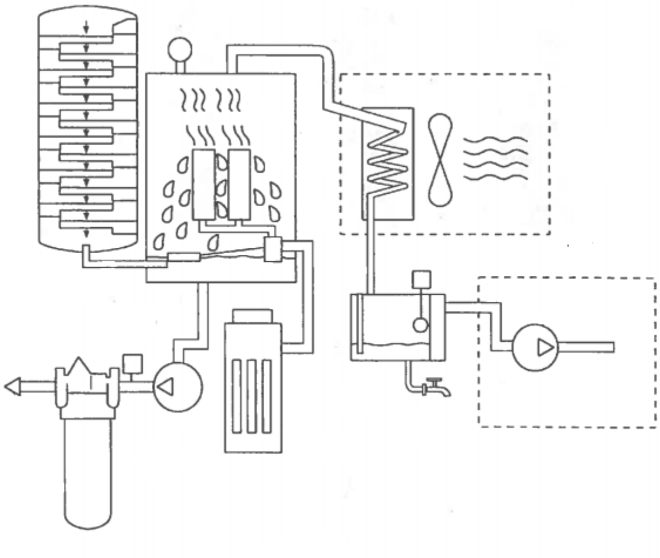

Figure A.3. Possible setup for the conversion process.

Another additional process is to pump the heavy liquid/bio-residue into a desiccator, and transfer the mixture into a isolation chamber, for separate processing. The bio-residue, is trough filtration and fractional distillation, converted into the bio-binder.

Potential gains and drawbacks of the conversion

The economic potential, of the conversion process, is valued high, because the market for bio-renewable energy and bio-conversion is gigantic. The potential for hog farmers to convert one of their biggest obstacles, the excess manure, into new materials is difficult to asses directly. However the bio-binder's potential, when compared to the conventional binders, has been estimated to material production price \$0.13/L. to a price 0.53/L respectively. However the bio-binder has only been proven to be a partial replacement of the conventional binders at low weight fractions[Fini et al., 2011]. The environmental gain is high, because of the reduced emissions of green gases and all the potential dangers of spoils and pollution[Fini et al., 2011]. Results of the moisture resistance of conventional binders has been reported to increase with the addition of the bio-binder as a partial replacement, even at small weight fractions. The low molecular weight of the bio-binder could have a softening effect and this would be beneficial, when utilizing recycled asphalt in the new mixture. The recycled aged asphalt has a higher stiffness than the un-aged asphalt, due to oxidation and weathering, and this could lead to a higher risk of cracking damage. Obtained results of mixing the bio-binder with recycled asphalt have shown to reduce the stiffness of the new mixture, which decrease the risk of cracking damage, due to the lower stiffness. This could led to increased use of recycled asphalt in the highway construction industry [Oldham et al., 2015]. The pure bio-oil, as shown in figure A.1 for the conversion process, can converted into a lot of different application and the full potential is not fully explored at this time.

In a study of the conversion process from NC A&T, it was found there were drawbacks of the conversion process from NC A&T and the obtained products[Mills-Beale et al., 2012]. Firstly, the process is costly in the electric energy needed to produce swine manure into bio oil. There could maybe be a way to utilize some of the byproducts(e.g. bio-fuel and bio-gas) to be looped back to power the production, which would enhance the potential and gain of the whole process. Secondly, there is an uncertainty on how the diet of the pigs affected the chemical composition of the obtained product during and after processing. The final drawback was that it was found that an unpleasant odor of sulfur occurred when the bio-binder was heated to elevated temperatures[Mills-Beale et al., 2012].

Properties

Several studies have gone into the investigation of the properties(e.g. thermal, rheological properties and chemical composition) of the bio-oil and the bio-binder respectively. In this section, selected information about the properties is highlighted.

The importance of the bio-oil and bio-binder are that the properties of it allow it to be a partial replacement in conventional asphalt binders. Some of the properties of the bio-residue and the bio-binder should be analogues, because the distillation and filtration are primarily performed to remove the water content. A chemical characterization of the bio-binder was conducted in Fini et al. [2011]. The characterization was conducted with elemental analysis, SARA analysis, gas chromatography-mass spectrometry(GC-MS), nuclear magnetic resonance(NMR), Fourier-transform infrared spectroscopy(FTIR)and Aspaltene determinator(AD). The essential findings of the characterization study showed that the bio-binder had some similar properties compared to conventional binder, but differed greatly with other properties. The elemental analysis showed that the bio-binder had more oxygen and nitrogen, compared to the conventional binder, as seen in table A.1. According to Fini et al. [2011], the enhanced content of oxygen and nitrogen could form polar functional groups with aggregate surface, which have shown to possibly improved resistance against moisture damage.

Table A.1. Chemical composition of the bio-binder and bituminous binder Fini et al. [2011].

Component (percent by weight)	Bio-binder	AAD-1
C	72.58	81.6
H	9.76	10.8
N	4.47	0.77
O	13.19	0.9

The SARA analysis showed, that the distribution of saturated, aromatic, resins and asphaltenes compounds of conventional binders are different compared to the bio-binder. The bio-binder has a higher resin content, but lower saturated compounds and almost no aromatic compounds[Fini et al., 2011]

Table A.2. Comparison of SARA components of bio-based binder and bituminous binders [Fini et al., 2011].

SARA component	Adhesive type	Saturated compounds	Aromatic compounds	Resin	Asphaltenes
Percentage (percent by weight)	Bio-binder from swine manure	2.48	1.67	45.87	43.39
Percentage (percent by weight)	Air-blown aspalt binder (the most brittle asphalt binder)	10.4	52.7	28.4	7.0
Percentage (percent by weight)	AAD-1 (the softest asphalt binder)	8.6	41.3	25.1	20.5

The FTIR analysis of the bio-binder sample was carried out by utilizing a solvent, carbon disulfide(CS2), and the resulting spectra is illustrated in figure A.4. According to Fini et al. [2011], the solvent overwhelmed the two spectral regions between 1.400-1.600 cm^1 and 2.200-2.400 cm^1. These peaks have to been excluded from the spectral determination. An other study, conducted by Oldham et al. [2015], showed the same results in the spectra, where the excluded peaks were also not present.

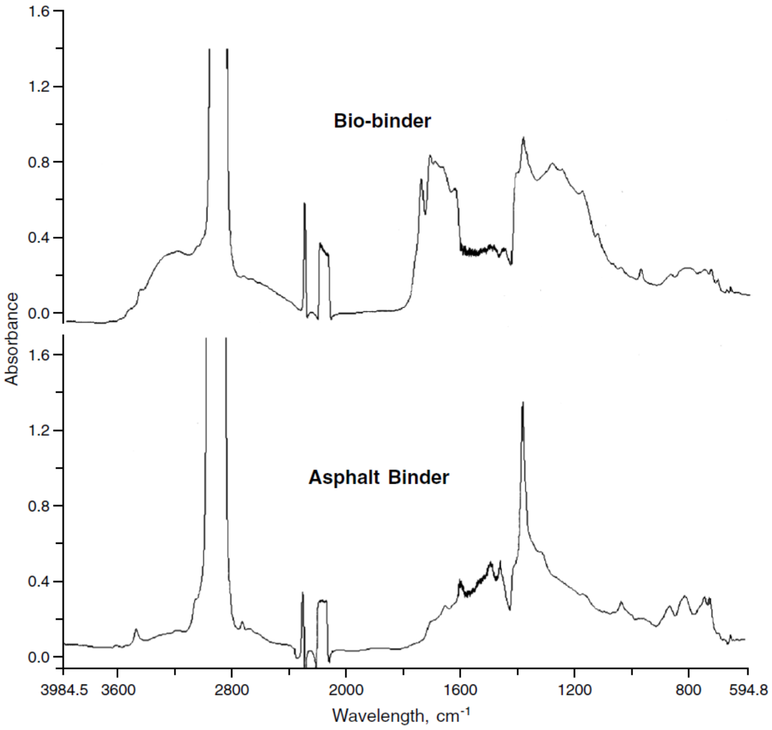

Figure A.4. FTIR spectra of a conventional binder and the bio-binder [Fini et al., 2011].

It can be seen in figure A.4, that the two spectra of the two binders differs from each other.The peaks and regions assigned to C-H and C-C bonds are different in the ranges 600–900 and 2700–3000 cm^{-1}. According to Fini et al. [2011], this reflects the differences between the two binders, due to their respective origins. The large shoulder next to the twin peaks at 3.000–3.300 cm^{-1} are amines, alcohols and olefins, which is supported by the other results of the characterization process .The peaks at 1.600 and 1.800 cm^{-1} are nitrogen- and oxygen-containing organic molecules (e.g. carbonyl, aldehyde, amine, and nitrosyl functionalists). The peaks between 920-1.400 cm^{-1} could be defined as olefinic carbons, amines, sulfur-containing organics, and other organics. According to Fini et al. [2011], the reason for the more complex mixture of functionalized organics in the bio-binder, compared to conventional petroleum binders, is due to the increased concentration of nitrogen, oxygen, and sulfur in the bio-binder. A full analysis of all the functional groups of the bio-binder has not been published to this author's knowledge.

The gas chromatography-mass spectrometry(GC-MS) analysis showed the presence of olefins and complex mixtures of compounds within the bio-binder. The nuclear magnetic resonance(NMR) supports the presence of complex structured compounds in the bio-binder. According to Fini et al. [2011], the following compounds are present in the bio-binder; hexadecanamide, hexadecanoic acid, tetradecanal o-methyloxime, 2-tridecanone, o-methyloxime, n-butyl octadecanamide, octadecanoic acid, cholest-7-ene, cholest-3-ene, cholest-4-ene, and vitamin-E.

According to Oldham et al. [2015], the bio-binder is highly polar and and enriched in olefin and amide functional groups. However the lack of aromatic and high molecular weight asphaltenes, and the high content of straight-chain aliphatic and polar functional groups, could contribute to a brittle state of the raw material, due to the many polar functional groups in the material[Fini et al., 2011].

The characterization techniques showed that the bio-binder could be compatibility with the conventional binders, but the lower molecular weight of the bio-binder could have a softening effect, when mixed with the conventional binder in low weight fractions. This effected the rheological properties, where the viscosity decreased with the addition of the bio-binder in conventional binders [Fini et al., 2011]. The rheological properties of the pure bio-binder have to this author's knowledge have not been tested directly, but only as partial modifiers in conventional binders in several studies [Fini et al., 2011] [Walters et al., 2014] [Fini et al., 2012].

In one study, performed by Hosseinnezhad et al. [2015], the properties of the bio-oil were compared to other bio-oils, which were obtained from other bio-masses (e.g. wood pellets(WS), corn stovers(CS) and miscanthus(MS)). The chemical composition was investigated by the means of Attenuated Total Reflectance Fourier Transform Infrared spectroscopy (ATR-FTIR), which yielded an interesting result. The properties within the plant-based bio-oil showed similar aromatic and aliphatic functional groups, as listed in table A.3, but the bio-oil obtained from swine manure had some different functional groups present within its spectra. Some of these changes were attributed to that the plant-based materials had been digested and altered by the intestinal tracks of the target animal in this case pigs. The bio-oil obtained from the swine manure showed a high content of long fatty acid chains. These were attributed to the presence of lipids in the food stock.

Table A.3. Functional groups for MS, CS and WP [Hosseinnezhad et al., 2015].

Wavenumber(cm^{-1})	Functional group
3400-3200	-OH stretching
3000-2800	Aliphatic CH stretching
1700-1710	Aromatic carbonyl/carboxyl C=0 stretching
1514-1560	Aromatic C=C ring stretching
1454	Aliphatic CH deformation
1370	Aliphatic CH_3 deformation
1250-1270	Aromatic CO- and phenolic -OH stretching
1010-1014	Ether or alcohol C-O stretching
770-780	Aliphatic CH deformation

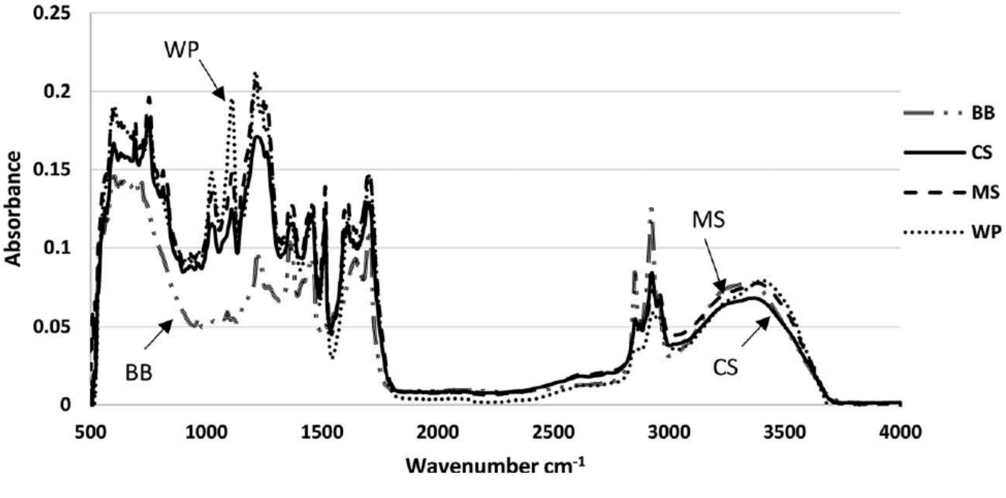

Figure A.5. FT-IR spectra of bio-oil samples [Hosseinnezhad et al., 2015].

The selected bio-oil from the swine manure had also a higher content of nitrogen present compared to the plant-based derived bio-oils, which increased the PH level closer to a neutral state of 5.97 compared to the plant-based, which had between 2.8–2.95. The increased nitrogen was attributed to a higher amount of proteins. The elemental compositions of the four bio-oils have been illustrated in table A.4.

Table A.4. Physio chemical properties of bio-oils [Hosseinnezhad et al., 2015].

Bio-oil	pH	Density ($g\ ml^{-1}$)	Higher heating value ($Mj\ kg^{-1}$)	C	H	N	O	Ash content (wt%)
BB	5.97	0.96	31	63.44	8.36	3.53	14.33	10.34
WP	2.80	1.23	26	61.05	6.93	0.21	24.97	6.84
CS	2.87	1.25	27	61.60	7.28	0.96	20.89	9.27
MS	2.95	1.05	28	65.77	7.31	0.67	24.11	2.14

The amount of carbon and hydrogen measured in all four bio-oils were of similar values and therefore were not a factor in the properties. The bio-oil from swine manure showed a higher increase in nitrogen and a lower amount of oxygen compared to the plant-based versions. The physical properties (e.g. volatility and viscosity) are related to the molecular weight of the bio-oils by the fact the higher the molecular weight, the higher is the viscosity. Therefore all the bio-oils can be listed ranging from the highest to the lowest by their molecular weight in table A.5.

Table A.5. Molecular weight for bio-oils [Hosseinnezhad et al., 2015].

Name of the bio-oil	M_n	M_w
CS	137	960
MS	192	1035
WP	192	610
BB	1011	2978

The literature study of the bio-oil and the bio-binder indicated that the materials have complex organic structures and functional groups. The importance of this is it can serve as a reference point from the literature to support the experimental results, obtained later in the project.

A.2.2 Montmorillonite

Montmorillonite is a clay mineral, which have been investigated for some decades, due its ability to improve mechanical, thermal and barrier properties of matrix materials. This has made the clay materials significantly useful for nanocomposites, where a small addition of the nanofiller can improve the properties significantly. The reason for clays' unique ability to improve properties, can be found in the dimensions and chemical structure of the clays. Montmorillonite, or layered silicate, is found in nature, as rocks or powder, with micron-sized flaky particles with typical dimension of the particles, which varies from 10 μ m to 0.1 mm. These particles are agglomerates of smaller particles with dimensions varying from 1 to 10 μm. The thickness of each individual layer is around 1 nm. The lateral dimensions can vary from around 300 nm to several micrometers, depending on the type of layered silicate, which are used [Maneshi et al., 2006]. Each clay particle is composed of many of these layers, stacked together in an assembly, which called a tactoid. The particles can be described as consisting of aggregates of tactoids, or stacks of platelets. The closely packed layers are held together, due the charges of the molecules within the structure of the designated clay. The structure of montmorillonite can be explained as platelets within an inner octahedral layer, which is dominated by aluminum oxides, with some magnesium molecules replacing some of aluminum molecules. This layer is sandwiched between two silicate tetrahedral layers, or silicon oxides [Paul and Robeson, 2008]. The resulting structure are illustrated in figure A.6.

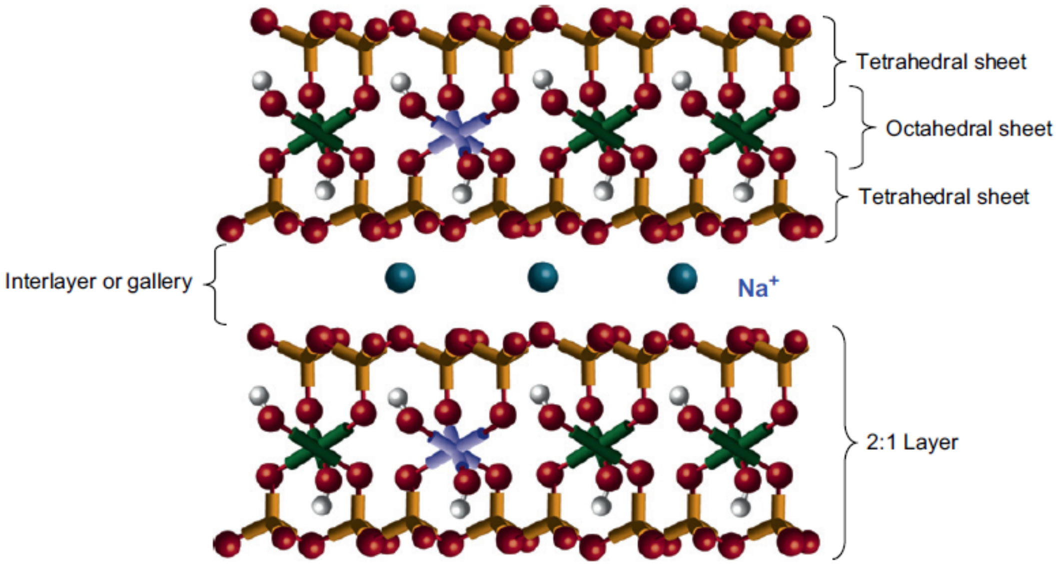

Figure A.6. Molecular structure of Cloisite Na+ [Uddin, 2008].

The layers are bonded together by oxygen molecules into a 2:1 layered structure, which comprised an individual platelet. The platelets are held together by Van der Waals forces, electrostatic forces, or by hydrogen bonding. The effect of these forces is that the layers create negative charges, due to the electron charges within the molecules. Sodium montmorillonite has sodium cations Na+ placed within the space between platelets. The difference in valences between the aluminum and magnesium molecules creates negative charges in the space, known as the gallery, between the platelets. The negative cations are balanced by positive counter ions (e.g. sodium ions), located in the galleries. The positive interlayer charges can be categorized as a cation exchange capacity (CEC), which has the capabilities of absorbing ions into the selected gallery or modifying the surface of the individual clay platelet [Klitkou, 2012]. Montmorillonite is reported to swell, when submerged in water. This is due to the hydration of the sodium ions, which causes the galleries or spacing between the platelets to expand. Natural or unmodified montmorillonite are difficult to disperse in polymers, because montmorillonite is hydrophylic and polymers are hydrophobic. According to Paul and Robeson [2008], the sodium ions can be exchanged with organic cations to form an organoclay. Organoclay is modified clay, which is treated have a more reactive surface or cation exchange rate, which increases the chance for better dispersion in a matrix material. There are different states of dispersion for clay in matrix materials; immiscible, where the clay particle consists of large agglomerates with no interaction of the matrix material, intercalated structure consisting of isolated stacks with an intercalant in the gallery of the clays, exfoliated structure with single clay platelets without orientation or structure of the platelets are integrated into the matrix material.[Klitkou, 2012].

The modification treatment of the montmorillonite increases the miscibility of the modified clay into a hydrophobic matrix material. The process of converting hydrophylic montmorillonite clay organophilic is called compatibilization, or intercalation, where a intercalant is an organic or semiorganic chemical capable of entering the montmorillonite clay galleries, and bond to the surface of the platelets [Uddin, 2008]. The intercalated organic cations will act as pillars, which permanently increases the interlayer spacing between the inorganic layers of montmorillonite

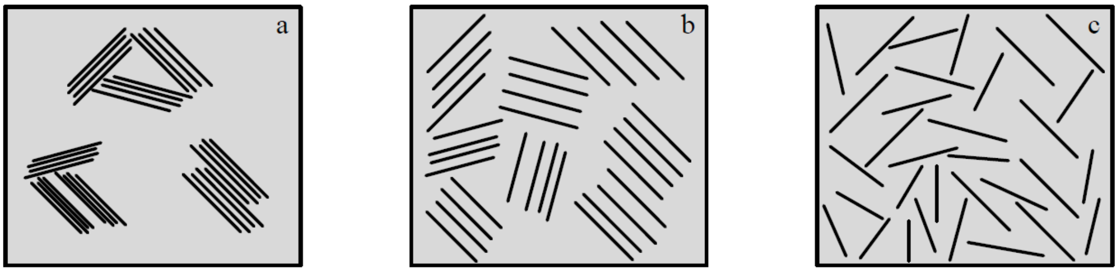

Figure A.7. Possible dispersion states for clay-containing polymeric nanocomposites [Klitkou, 2012]

[Önal and Sarıkaya, 2008]. If the electrostatic forces between the platelets are reduced or potentially severed, the resulting structure of montmorillonite is known as intercalated or exfoliated structure respectively. Intercalants, or surfactants, which are used primarily for cation-ion exchange are ammonium cations.These quaternary ammonium ions replaces the sodium cations in the interlayer gallery of the montmorillonite. The ammonium cations may have hydrocarbon tails, which are amphiphilic, which consists of two parts of the molecule; hydrophyllic and lipophilic. Therefore these groups can be used as bridges between matrix materials and the clay[Paul and Robeson, 2008]. Another interaction between the filler and the matrix material for intercalation, can be achieved with a dipole-dipole attraction, where the polar groups(e.g. OH or COOH) of the matrix material forms hydrogen bonds with the oxygen groups of montmorillonite. The Na+ cation remains within the interlayer galleries[Potarniche et al., 2013].

The state of intercalation and dispersion can be determined directly and indirectly by various characterization techniques. In his studies with montmorillonite and polypropylene, Klitkou [2012]showed that the conventional TEM and XRD could be supported by FTIR and Oscillatory rheometry, in determining the morphology of the investigated nanocomposites and the interphase between its utilized constituents. The XRD can be used to quantifying the inter-layer spacing of the montmorillonite, where the change of the spacing indicates the different stages; immiscible, intercalation and exfoliation. This is illustrated for pure oregano clay in figure A.8.

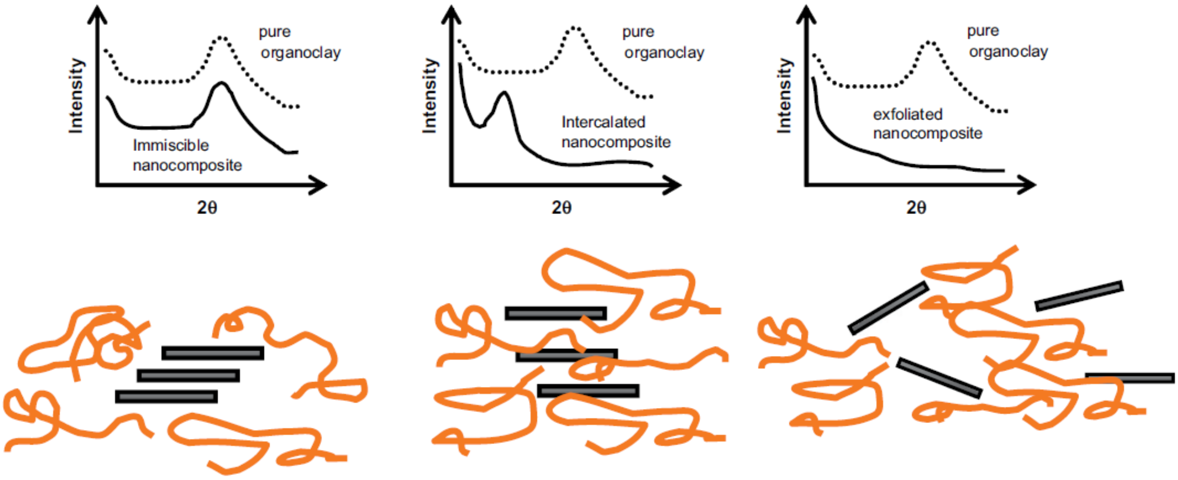

Figure A.8. Illustration of different states of dispersion of organoclays in polymers with regard to XRD [Paul and Robeson, 2008].

The organoclay has a characteristic peak, which with Bragg's law, can indicate the spacing between the platelets. This spacing is known as d-spacing or d_{001}. The placement of the peak determines the state of dispersion, where no shift of the peak is interpreted as immiscible and no intercalant had penetrated the galleries of the clays. If the peak shifts to a lower angle, or larger d-spacing, this is generally interpreted as intercalation of matrix material (e.g. polymers or other species) into the galleries of montmorillonite. If the peak is absent, it can be interpreted as exfoliation. However, this is not conclusive evidence and the results have to be supported by other characterization methods. If the peak shift to higher angles, it can be interpreted as loss of unbound surfactant from the gallery, or degradation of the utilized surfactant[Paul and Robeson, 2008].

Another technique for investigation of clay dispersion and state of intercalation/exfoliation in polymeric/clay nanocomposites is FTIR. The idea behind this technique, which were first described by Cole [2008], is that montmorillonite has four distinct peaks in the region from 1150-1000 cm^{-1}, and corresponds to four Si-O stretching modes in the montmorillonite. These four peaks(1120, 1080, 1048, 1025) are affected with regard to the state of intercalation of the clay particles. The peak of 1080 cm^{-1} is reported to narrow in bandwidth and shift to higher angles with increasing intercalation/exfoliation. There is a relation between the four peaks, where the peaks 1080 and 1048 $^{-1}$ gets more prominent, compared to the two other peaks 1120 and 1025 $^{-1}$, with increasing intercalation/exfoliation [Klitkou, 2012]. The spectra illustrated in figure A.9 are the results of the PP/OMMT nanocomposites, which were investigated. The four peaks are clearly present in both of the normalized spectra.

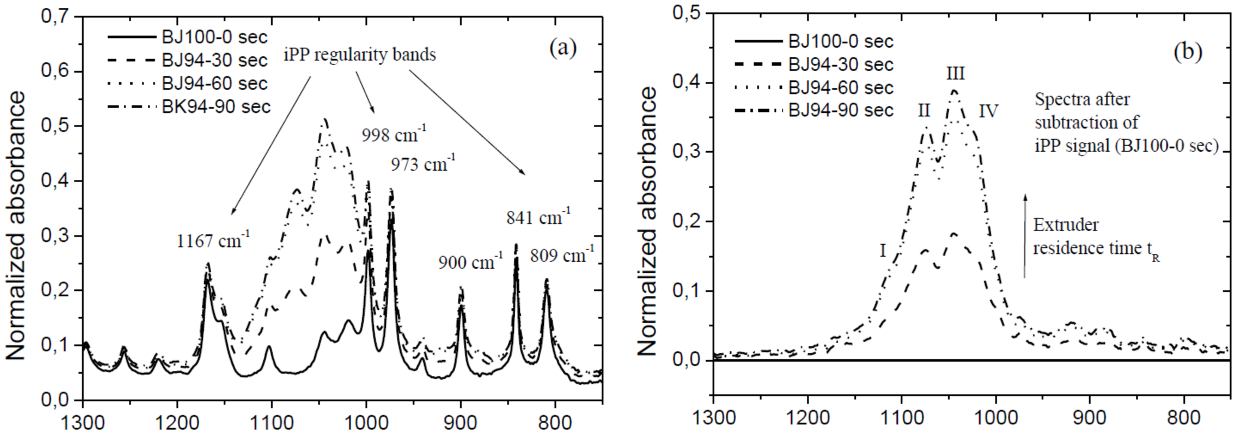

Figure A.9. Normalized absorbance spectrum for the polypropylene nanocomposite, where (a) is the raw signal, and (b) is a subtracted signal [Klitkou, 2012].

The FTIR analysis can be used to characterize the functional groups of the montmorillonite. According to Rafiei and Ghomi [2013], the significant peaks of Cloisite Na+ is characterized by stretching and bending bands of O-H and Si-O, bending bands of Al-O and bending bands of Mg-O. In table A.6, the different bands and their ranges are listed.

Table A.6. Significant peaks and band ranges for Cloisite Na+[Rafiei and Ghomi, 2013].

Type	Vibration mode	Range [cm^{-1}]
O-H	Stretching	3100-3700
O-H	Bending	1600-1700
Si-O	Stretching	1040
Si-O and Al-O	Bending	400-600

This can be utilized in the determination of relevant peaks in organically modified clays or matrix materials with addition of nanoclay, because some of the functional groups of of the matrix and filler will be present. If a peak is not present after mixing, this could indicate a change of the functional group of the investigated peak.

The changes of the rheological properties of various liquids, with the addition of clay particles, is well established[Klitkou, 2012]. In nanocomposites, if a plateau in the storage modulus(G´) at low frequencies is located, this indicates a build-up of complexity viscosity($\eta*$. This build-up of complex viscosity is associated with filler dispersion and activation with the affected melt network. The rheological measurements are an indirect method to determineng compatibility between the matrix material and filler [Klitkou, 2012]. The addition of the organically modified nanoclay to bio-binder had on effect on the viscosity, where the addition of the clay in small weight fraction of 2-4% increased the viscosity, is reported by Walters et al. [2014].

The thermal properties of the organoclay can be evaluated by TGA and DSC. According to Xi et al. [2005], the decomposition of an organoclay takes place in four steps: water desorption, dehydration, desurfactant and dehydroxylation. The molecular environment, in which the surfactant is intercalated in the organoclays, is another effect, which will affect the decomposition temperature. There are registered three different environments, where the first is surfactant cations intercalated into the clay interlayers through cation exchange and bound to surface sites via electrostatic interaction. The second, is where surfactant (cations and/or molecules) are physically adsorbed on the external surface of the clay. The last environment, is where the surfactant molecules are located within the clay interlayer. Montmorillonite does not undergo thermally induced changes in the temperature range of 170-500 °C, therefore the registered mass loss in the temperature range can be attributed to the decomposition, or evaporation, of the surfactant for organoclay with montmorillonite. The results of the study, conducted by Xi et al. [2005], showed the potential for interpreting the possible molecular environment or intercalation state, of the bio-residue in the Na-montmorillonite utilized in this project. In the study, conducted by Xi et al. [2005], the montmorillonite from Wyoming was untreated and modified using octadecyltrimethylammonium bromide, a cationic surfactant.

A.2.3 Compatibility between the bio-residue and montmorillonite

There is not present a lot of information about the comparability between montmorillonite and the investigated bio-oil, bio-binder or bio-residue. However in one study, performed by Walters et al. [2014], the oxidative aging of asphalt were investigated, showed that the aging could be reduced by the additions of nano-clay and bio-char. This study is the only one to the authors's knowledge, where the bio-binder was mixed with montmorillonite. The filler materials(e.g. nano-clay and bio-char) were mixed within the asphalt to reduce the deterioration of the asphalt, caused by the oxidative aging. The idea was to enhance and strengthen the rheological properties to extend the service life of the pavements. The bio-char in question was obtained by the conversion process, described in section A.2.1. The nano-clay utilized in this study was Cloisite 30B, which is an montmorillonite, which have been organically modified with a quaternary ammonium salt. Cloisite 30B contains methyl tallow bis-2-hydroxyethyl ammonium cations, at a loading of 90 meq/100g clay, where tallow is 65% $C_{18}H_{37}$; 30% $C_{16}H_{33}$; 5% $C_{14}H_{29}$ [Saad and Dimitry, 2012]. The chemical structure of the modifier is presented in figure A.10.

The importance of this study for this project was the addition of the nano-clay to the bio-binder. The bio-binder served as a surfactant for the nano-clay, which exfoliated the structure of the nano-clay. This result was verified by X-ray diffraction (XRD), where the basal spacing of the

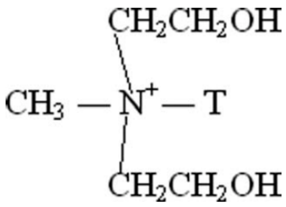

Figure A.10. The chemical modifier for Cloisite 30B, where T stands for tallow[Saad and Dimitry, 2012].

montmorillonite layer increased. In the figure A.11, no peaks are visible between 0-10 degrees, which indicates an exfoliated structure. The modified Cloisite 30B had a more reactive surface for surfactant interaction compared to an untreated montmorillonite. The addition of the nano-clay to the bio-binder had a effect on the viscosity, where the addition of the clay, in small weight fraction of 2-4 %, increased the viscosity [Walters et al., 2014].

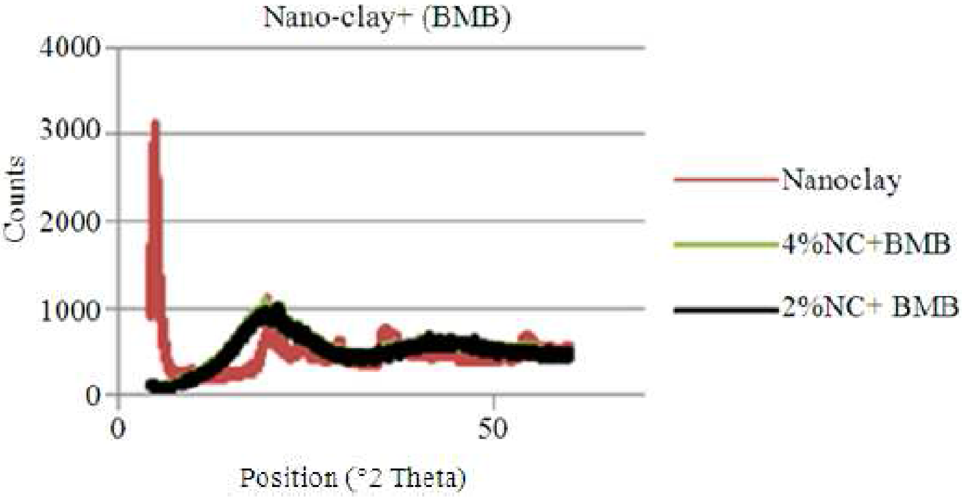

Figure A.11. XRD spectra of bio-oil samples with different weight percentage of nano-clay Hosseinnezhad et al. [2015].

Another study, conducted by Rooj et al. [2012] could indirectly support the possibility of a intercalated state between the montmorillonite and the bio-residue. The study showed that intercalation between long fatty acids and organically modified montmorillonite were possible. This is an interesting result, because as reported by Hosseinnezhad et al. [2015], the bio-oil has a high content of long fatty acids. The bio-residue could have a high content of long fatty acids, which potentially could works as intercalants in the unmodified Na-montmorillonite, utilized in this project.

A.2.4 Problem statement

In this project, it is was chosen to investigate if it is possible to improve the properties of the investigated material, bio-residue, with montmorillonite (MMT) as a possible nanofiller, or as an organoclay (organically modified clay), where the bio-residue is used as an modifier/intercalant to achieve a changed morphology and structure of the montmorillonite.

The literature studies showed that the bio-residue potentially could be used as a organic modifier to achieve intercalated or exfoliated structure of the montmorillonite. Other studies with organically modified clay have showed similar promising results.

The problem statement for this project was chosen to be:

Can the investigated bio-residue be used as an modifier for Na-montmorillonite to achieve a intercalated/exfoliated structure?

The effect of the possible intercalated structure on the clay morphology, will be investigated. The bio-residue will be characterized with the following techniques; X-ray diffraction (XRD), Attenuated Total Reflectance Fourier transform infrared spectroscopy (ATR-FTIR), Oscillatory rheometry(OR) and Simultaneous Thermal Analysis (STA) to achieve a baseline to evaluate the effects of the modification, or pre-intercalation, process of the montmorillonite.

A.3 Characterization of the materials

Several techniques were employed in order to characterize the raw and modified bio-residue with the addition of the montmorillonite(MMT).

X-ray diffraction (XRD) was used to study the degree of possible intercalation or exfoliation of montmorillonite layers of the modified silicate BR/MMT by assessment of the d-spacing and peak intensities.

Attenuated Total Reflectance Fourier transform infrared spectroscopy (ATR-FTIR) was performed to obtain an infrared spectrum of the raw material and the modified silicate to determine the possible chemical compositions and the state of intercalation/exfoliation.

Oscillatory rheometry is performed to determine the elastic, visco-elastic behavior and viscosity of the materials.

Thermogravimetric analysis (TGA) is used to asses the decomposition and thermal stability of materials to examine the physic-chemical processes occurring in the materials at different temperatures.

A.3.1 X-ray diffraction (XRD)

X-ray diffraction is a analytical technique, which is used for identifying unknown crystalline materials (e.g. minerals, inorganic compounds). The technique can identify the crystalline phases, crystal structure, orientations present in solid materials and powders. Furthermore the structural properties, such as stress, grain size, phase composition, crystal orientation, and defects of the phases can be investigated and determined. The technique is fast and non destructive, because the process uses X-rays on sample from various angles, and based on the reflective intensities, gives information about the inorganic solids materials in the investigated sample [Poppe et al., 2001]. The setup of X-ray diffraction is called a x-ray diffractometer, which consist of three basic elements; a source of monochromatic radiation, a x-ray detector to receive the altered x-ray beams after contact with sample and a sample holder, which is situated on the circumference of a graduated circle centered on the sample. Several aligning divergent slits limits scattered (non-diffracted) radiation and reduce the background noise. The mechanical setup, which couples the detector and specimen holder together, is a goniometer. The goniometer controls the rotation in a fixed 2:1 ratio, as seen in figure A.12.

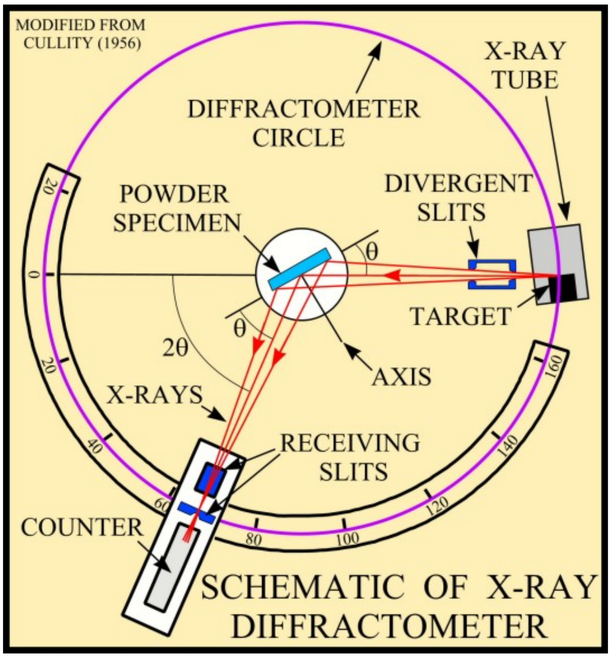

Figure A.12. Shcematic of the x-ray diffractometer Poppe et al. [2001].

The X-rays, which are generated in the source of radiation, produces electrons, that are accelerated by an applied voltage, and the accelerated electrons bombard the sample material. If the bombarded electrons have enough energy to dislodge inner shell electrons of the target material, the characteristic X-ray spectra peaks are produced. This occurs, when the incident X-ray beams encounters a crystal lattice, which alters the angle of the diffracted beams. Each crystalline material has a characteristic atomic structure, which will diffract X-rays in a unique characteristic pattern, and this can acts a fingerprint, which can be used as an identification tool.

The incident and reflected X-rays are diffracted according to Bragg's law.

$$n\lambda = 2d\sin\theta \tag{A.1}$$

Where λ is the incident X-ray wavelength, θ is the reflection angle of the X-ray beam, n is the integration constant, or reflection number (usually 1 is utilized), and d is interplanar lattice spacing, or d-spacing, of the investigated material. Sine θ is the experimental diffraction angle, which is used for the spectra. The principle of Bragg's law is illustrated in figure A.13.

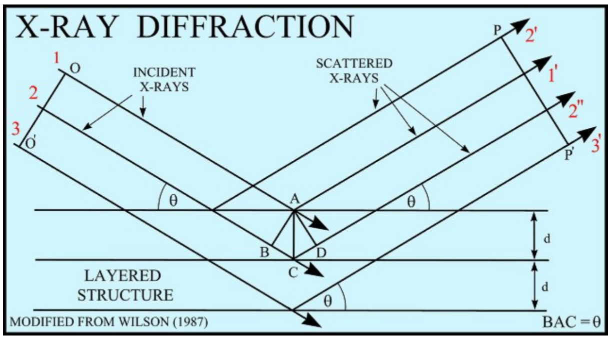

Figure A.13. Principle for Bragg's law [Poppe et al., 2001].

A.3.2 Attenuated Total Reflectance Fourier transform infrared spectroscopy (ATR-FTIR)

Fourier transform infrared (FTIR) spectroscopy is a measurement technique, that records the infrared spectra(IR) of a sample, where light is reflected first through an interferometer and then through the investigated sample. The technique is fast and non-destructive method for qualitative and quantitative measurements[Newport, 2015]. The setup allows for the alteration of the distribution of the infrared light, and the recorded signal, an interferogram, which represents the light output. The raw data is treated with a data-processing technique, called Fourier transform, which converts the raw data into the spectrum, where the light output, as a function of infrared wavelength, or wave number, of the investigated sample. The peaks of the spectrum is the vibrational movements of the molecules or the internal energy levels(e.g. stretching, rotational and bending bonds) of specific functional groups. Each internal energy level has a specific peak and this can be used to determine the functional group of the investigated peak. The peaks can be used as identification tool of the functional groups of the investigated material. The intensity of a peak also increases with increasing content of the functional group is present in the molecule[Newport, 2015].

Attenuated Total Reflectance (ATR) is a supplementary technique for FTIR, which removes the need for sample preparation steps(e.g. transmission cells and KBr pellets), when performing measurements on liquid, semi-solid and solid materials. A sample is placed on the measuring crystal, which have a high refractive index. In this project a DiCompTM crystal, from Perkin Elmer, was utilized Perkin Elmer [2004]. The crystal is composed of a diamond ATR with a zinc selenide focusing element, which is in direct contact with the diamond. An infrared beam is directed, in a angle, at the crystal, to maintain the total reflexion internally in the crystal. The contact between the crystal and the sample measures the light absorption by the sample. The drawback of this technique is the penetration depth, which is only 1.66 μm for the chosen crystal Perkin Elmer [2004]. Therefore good contact between sample and crystal is required. In figure A.15, an illustration, which explains the principle behind the technique can be seen.

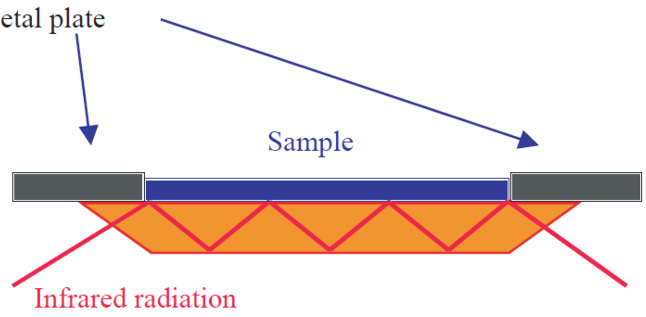

Figure A.14. Principle behind ATR [Perkin Elmer, 2004].

A.3.3 Oscillatory rheometry

Oscillatory rheometry is one of different analyses, within rheology, to asses the linear visco-elastic response of a material[Cambridge Polymer Group]. A sample is placed in a geometry(e.g. cone-plate or parallel plate-plate), where a sine-wave-shaped input of strain is applied.

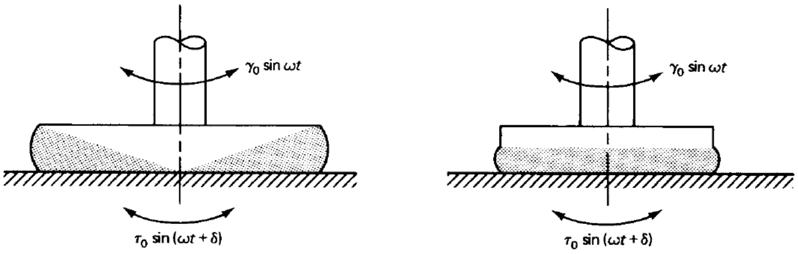

Figure A.15. Geometries(e.g. cone-plate, plate-plate) utilized for small angle oscillatory rheometry Lampman et al. [2003].

If a imposed strain wave is utilized, it can be described as

$$\gamma \;=\; \gamma_0 \, \sin(\omega \mathrm{t}) \tag{A.2}$$

and the resulting stress wave as

$$\tau \;=\; \tau_0 \, \sin(\omega \mathrm{t} + \delta) \tag{A.3}$$

where the angular velocity(ω), in rad/s, is equal to 2πf, where f(frequency), time(t) and phase angle(δ). The relationship between the imposed strain wave, which is in phase, and resulting stress wave, which is is $\pi/2$ out of phase, is illustrated in figure A.16.

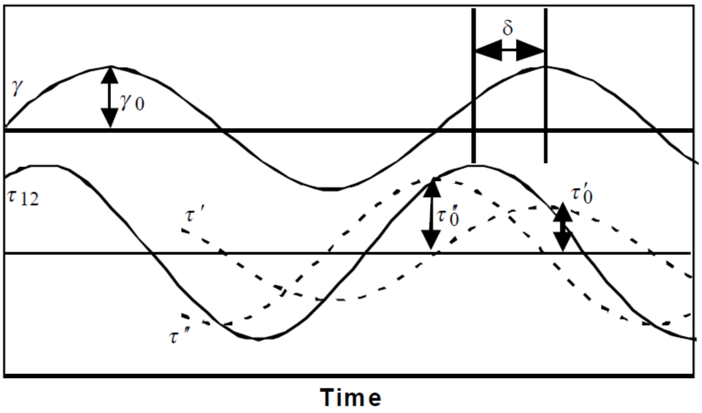

Figure A.16. Relationship between imposed strain and resulting stress wave [Cambridge Polymer Group].

The two terms for the strain and stress waves can be collected to

$$\tau = \tau' + \tau'' = \tau_0'\sin(\omega \mathrm{t}) + \tau_0''\cos(\omega \mathrm{t}) \tag{A.4}$$

The resulting stress response can be separated into two responses; solid and liquid. The solid response, or storage modulus G´, is in phase with the input and the corresponding liquid response, or loss modulus G´´, is $\pi/2$ out of phase with the input [Barnes, 2000]. The storage modulus, or elastic response, can be expressed as

$$\mathrm{G}' = \frac{\tau_0'}{\gamma_0} = \frac{\tau_0'}{\dot{\gamma}_0}\omega \tag{A.5}$$

and the loss modulus, or visco-elastic response, as

$$\mathrm{G}'' = \frac{\tau_0''}{\gamma_0} = \frac{\tau_0''}{\dot{\gamma}_0}\omega \tag{A.6}$$

The phase angle can be determined as

$$\tan\delta = \frac{\mathrm{G}''}{\mathrm{G}'} \tag{A.7}$$

The complex viscosity, or the resistance of fluid to flow, can be determined from the two dynamic moduli(storage and loss) to be

$$|\eta^*| = \sqrt{\left(\frac{\mathrm{G}'}{\omega}\right)^2 + \left(\frac{\mathrm{G}''}{\omega}\right)^2} \tag{A.8}$$

The phase angle, storage modulus, loss modulus, viscosity, which is obtained from standard oscillatory frequency sweep tests, can be utilized to determine various types of material properties. The properties are listed in table B.1 and illustrated in figure B.2.

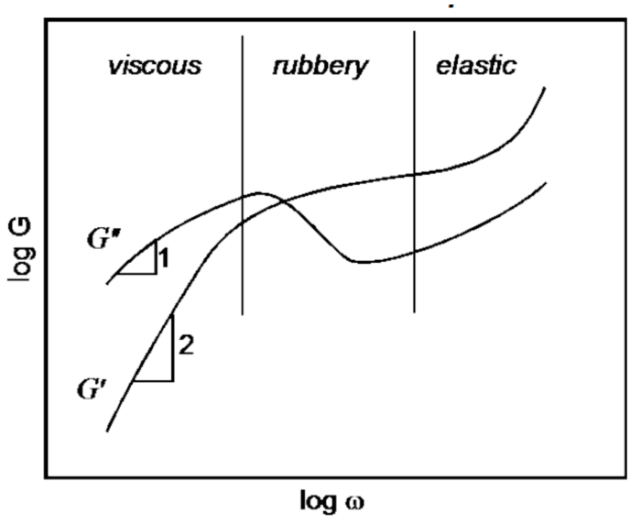

Figure A.17. A schematic of viscoelastic spectrum for a polymer solution when subjected to an oscillatory frequency sweep test [Cambridge Polymer Group].

Table A.7. Basis material values obtained from oscillatory rheometry [Cambridge Polymer Group].

Newtonian liquid	G'	$\eta' = \mu$	$\delta = \pi/2$
Hookean solid	G=G'	$\eta' = 0$	$\delta = 0$
Visco-elastic material	G'$(\omega) > 0$	G"$(\omega) > 0$	$0 < \delta(\omega) = \pi/2$

A.3.4 Simultaneous Thermal Analysis(STA)

Simultaneous Thermal Analysis(STA) constitutes two different analysis methods; Thermogravimetric analysis(TGA) and Differential scanning calorimetry(DSC). The method enables a sample to be analyzed simultaneously by both techniques. Thermogravimetric analysis (TGA) is a thermal analysis technique, that examines the mass loss or gain, due to decomposition, oxidation or loss of volatiles of a sample, as a function of temperature or time. The mass change can be used to characterize the decomposition and thermal stability of a materials under different conditions, which describes the physical and chemical processes occurring in the sample as the conditions change. The other method is Differential scanning calorimetry (DSC), which is a other thermo-analytical technique for evaluation of the thermal behavior of a material with respect to time and/or temperature; by determining any mesomorphic transitions exhibited on the material, which in turn give rise to the characterization of the material's physical properties [Lampman et al., 2003].

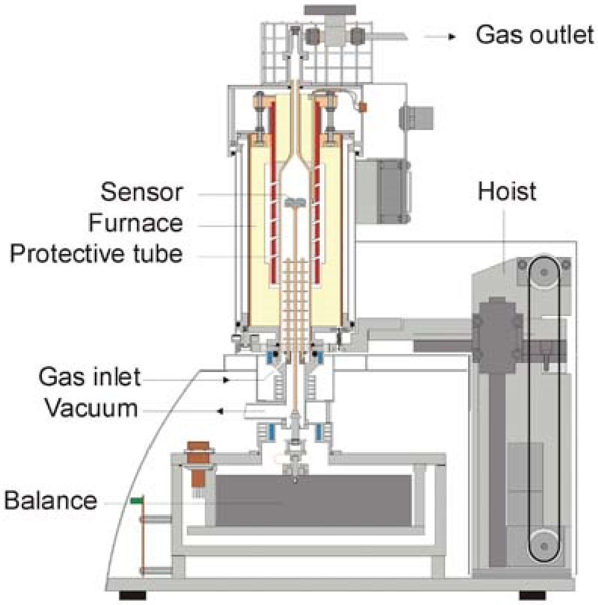

Figure A.18. Schematic of the NETZSCH STA 409 PC LuxxÂ® simultaneous thermal analyzer [Ceramicindustry, 2005].

The STA set-up consists of two parts; the measurement chamber, and the calculation and monitoring unit(e.g. computer with software), that monitors the evolution of heat flow and weight change. Two crucibles are placed in the measurement chamber, were one crucible is loaded with a few grams of the investigated sample and the other is the reference; commonly an empty crucible. The furnace is closed and the atmosphere of the furnace is purged with air or inert gas (e.g. nitrogen or argon). When the atmosphere is replaced by gas, the heater is turned on and the temperature increases with a heating rate rate until a desired end temperature. The real-time measurement of the difference between the two crucibles in heat flow and weight change are the output of the STA experiment, can be plotted as a function of time or temperature for analysis [Lampman et al., 2003].

A.4 Experimental procedure

The experimental procedure is divided in three parts; the materials, preparation and processing of the materials, and the characterizations settings and chosen procedures.

A.4.1 The materials

Bio-residue(BR)

According to the data safety sheet, which were included with the material, the material is stable at room temperatures. The material will not polymerize and it is not compatible with strong oxidizing agents. The decomposition products can include carbon monoxide, carbon dioxide and water vapor. The amount of supplied material was limited, and it was observed to have two different phases. The material was investigated with an initial TGA to determine if the clear phases was excess water content, which was not removed during the conversion process. The results of the analysis, are listed in section A.5.5, showed a mass reduction, which could be consistent with a water content. ATR-FTIR was performed on the clear phase and compared with a measurement of deionized water, where the results showed that the clear phase was primarily water with some small amount of organic matter. The results of the ATR-FTIR analysis are listed in section A.5.3. The water content is not desired for this project and have to be removed for further processing and characterization. The drying process are described in section A.4.1. The material was a black, sticky substance after the drying process, as illustrated in figure A.19.

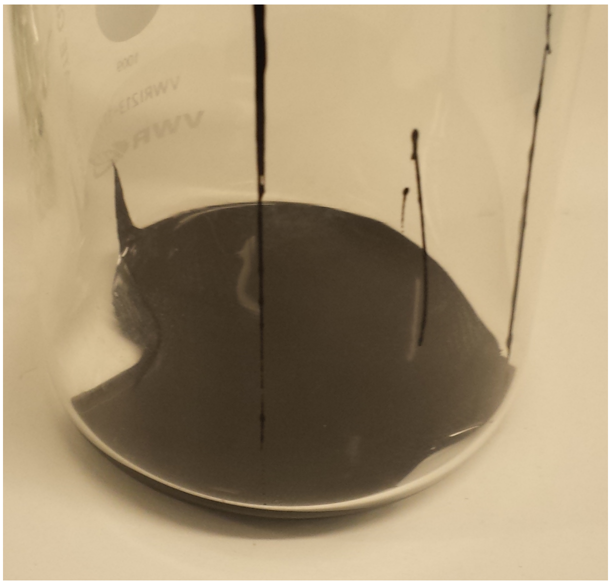

Figure A.19. Bio-residue after drying, BR_{dried}.

Montmorillonite(MMT)

The nanofiller used in this project is Cloisite NA+, a natural MMT modified for higher Na^+, from Southern Clay Products, which is now a part of BYK Additives. Cloisite Na+, which is a natural montmorillonite, has a typical dry particle size (d_{50}) of $< 25\mu$m, which contains 4-9% of moisture and a density of 2.86 g/cm^3. The color of the powder is grayish/white, see figure A.20, and the material was not individually dried in the processing process, but used as found at storage. Hereby is the moisture content unknown for the further processing. The material can be used to improve various physical properties, such as reinforcement, synergistic flame retardant and barrier properties [Additives and Instruments, 2015].

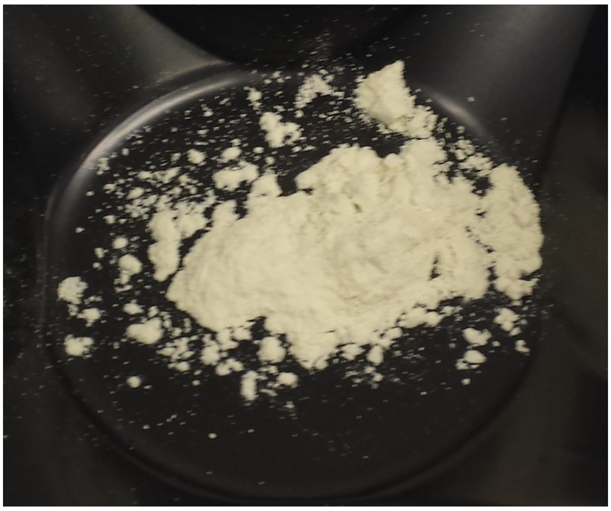

Figure A.20. Cloisite NA+ from BYK, MMT.

A.4.2 Preparation and processing of the materials

The bio-residue was prepared for the modification, and intercalation, process with montmorillonite. The first step is a drying process to remove the excess water content. The modification process is performed and completed with a secondary drying process, to remove the excess solvent, utilized to modify the silicate.

Drying process of the BR

The bio-residue, which were provided, was observed to be a two phase component material after transport. A small clear phase, which contained excess water content, and a darker phase contained the bio-residue. The clear phase was investigated with ATR-FTIR and TGA, and it was determined to be excess water content from the original processing of the bio-residue. The results are described in sections A.5.3 and A.5.5. The clear phase is removed from the material, with a drying process, using a conventional oven at 60 °C in normal atmosphere. The material was sent in a glass container with no specified weight of the container and the precise amount of material was therefore unclear. The mass is checked at selected intervals until mass stability, where the excess water content should have been removed. The dried bio-residue is before every analysis hand mixed for 15 min to ensure homogeneity of the sample.

Preparation of the BR/MMT modified silicate

The modification process chosen for this project is a solution-intercalation procedure, where a solvent capable of dissolving the bio-residue and swelling the clay is selected. The reason for swelling is to is to increases interlayer distance between the clay platelets for increased intercalation penetration. The mixture of clay, bio-residue and solvent is then mixed to a homogeneous substance, with aid of heating and mechanical stirring. The mixture is then ultrasonicated, and subsequently followed by a drying process, where the solvents are removed by evaporation from the substance.

A suspension was prepared by mixing 0.314 grams of Cloisite Na+ clay with 30 ml of deionized water and 30 ml of ethanol for a period of 15 min with a magnetic stirrer at 80 °C, see figure A.21. The two component mixture of solvents were required, because the bio-residue is not solvable in pure water and the clay do not swell in pure ethanol. The suspension was left to cool down to room temperature for 10 min.

Figure A.21. Temperature controlled bath with magnetic stirring.

Another suspension, with 3.09 grams of the bio-residue and 10 ml of ethanol, was prepared simultaneously, but mixed by hand at room temperature. The two solutions were mixed together with a ultrasonic horn for maximum of 2 min.

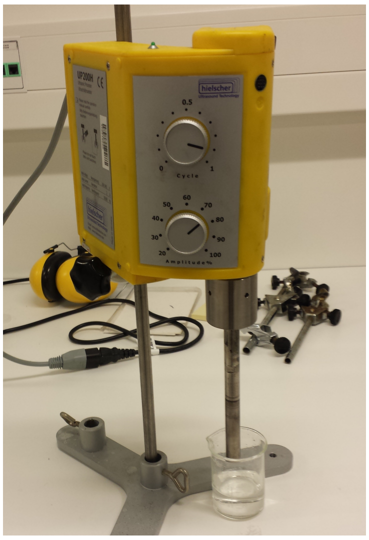

Figure A.22. Setup for ultrasonification of the mixtures.

The short mixing time was chosen to avoid heat development which could affect the properties. After wards the mixed solution is dried in a conventional oven at 60 °C until the excess water content is removed from the solution to obtain the modified BR/MMT silicate BRMMT$_{dried}$.

Preparation of the BR/MMT modified silicate for oscillatory rheometry

After the second drying process the BRMMT modified silicate had become to solid to perform oscillatory rheometry. It was chosen to mix the BRMMT$_{dried}$ with BR$_{dried}$. The mixture was performed to reduce concentration of montmorillonite in the substance.

A.4.3 Characterization of the materials

Selected samples from each of the processing steps and the raw materials were characterized to obtain enough knowledge, about the raw materials and the modified silicate. The selected tests are listed in table A.8. The settings for analysis are described in the following sections.

Table A.8. Materials characterization

Material	BR_{raw}	MMT	BR_{dried}	$BRMMT_{dried}$	$BRMMT_{liquid}$
XRD		x		x	
ATR-FTIR	x	x	x	x	
Os.Rheo.			x		x
STA	x		x	x	

X-ray diffraction (XRD)

The X-ray diffraction patterns were investigated on a PANalytical Empyrean diffractometer, see figure A.23 with CuKα radiation, running at 45 kV and 40 mA.

Figure A.23. PANalytical - Empyrean diffractometer Panalytical [2015].

The setup was operated in the 2θ interval from 3 to 40°. The samples were prepared, as illustrated in figure A.24, where the BR/MMT modified silicate were placed on a amorphous surface and the MMT were placed in a traditional sample holder.

Figure A.24. The prepared samples, $BRMMT_{dried}$ and MMT, for XRD analysis.

The reason for the amorphous surface was the limited sample size and to enhance the possibility of the obtained results, this setup was utilized. The test was performed to evaluate both intercalation and exfoliation. This was done with the evaluation of the intensity and placement of the peaks of the raw montmorillonite(Cloisite NA+), and the modified silicate BRMMT$_{dried}$ to determine the basal distance d001 between clay platelets. The spacing is determined using Bragg's law, which is described in section A.3.1. The results of the analysis are listed in section A.5.2 .

Attenuated Total Reflectance Fourier Transform Infrared Spectroscopy (ATR-FTIR)

The attenuated total reflectance Fourier transform infrared spectroscopy (ATR-FTIR) was performed on a Spectrum One spectrometer from Perkin Elmer. The tests were performed with the applied zinc selenide crystal, which penetrated the sample with a depth was 1.66 μm in absorbance mode to acquire the spectra of the raw and modified materials in wave numbers ranging from 500 cm^{-1} to 4000 cm^{-1}.

Figure A.25. Spectrum One spectrometer, with the applied a DiCompTM crystal, from Perkin Elmer

The samples were placed directly on the zinc selenide crystal and the measurements were conducted once for each sample type, due to limited material supply. The force gauge was applied for the montmorillonite powder, to ensure appropriate contact. The crystal was cleaned after, the measurement was conducted, with acetone and deionized water.

Oscillatory rheometry

The rheological properties of the BR$_{dried}$ and the modified silicate BRMMT$_{liquid}$ was investigated with the Paar Physica MCR 500(Modular Compact Rheometer). Initial amplitude sweeps were conducted to ensure that the measurements remained within the linear visco-elastic regime. The raw BR was tested with a amplitude of 10 and the modified silicate BR/MMT at 0.1. The angular frequencies ranged from 8 rad/sec to 0.0628 rad/sec (0,01Hz to 100 Hz) in a CP25 cone-plate configuration with a 25 mm diameter disc, a cone angle of 2° and a gap height of 0.105 mm. The tests were performed at 30°C with a sample size 0.2 g. The materials were applied with a make-shift teflon spatula. It was noted that the BRMMT$_{liquid}$ was prepared specifically for this measurement, because the BRMMT_{dried} was to solid for the measurement to be performed. The preparation for obtained the BR/MMT_{liquid} is described in section A.4.2. The setup was cleaned after, the measurement was conducted, with acetone to remove the substance.

Simultaneous Thermal Analysis (STA)

The STA analysis was performed on a Netzsch STA 409 PC Luxx and a Netzsch STA 449 C Jupiter, where the STA 409 PC Luxx was configured to only performing a TGA with DTA analysis and the Netzsch STA 449 C Jupiter was configured to performing simultaneous DSC and TGA analysis. The measurements were used for determining the thermal properties of the raw and dried bio-residue, the raw and modified montmorillonite. The test for the BR_{raw} was performed in crucibles in nitrogen atmosphere with a heating rate of 10°C/min, from ambient temperature around 20°C to 800 °C. The BR_{dried} and the BRMMT_{dried} were performed in crucibles in argon atmosphere with a heating rate of 10°C/min, from ambient temperature around 20°C to 1000 °C.

A.5 Results

In this chapter, the results of the performed experiments, are presented to investigate the hypothesis. The relevant results will be presented in this chapter with a discussion of the individual results. The results are based on limited sample amounts, due to limited supply of the bio-residue, and this have to be considered in the evaluation of each of the individual results.

A.5.1 Preparation and processing

The initial drying process of BR_{dried} showed no significant observation or results. The modification process with ultrasonication, showed a surprising observation. After around 90 seconds some of the mixed substance started to aggregate onto the horn, as illustrated in figure A.26.

Figure A.26. The aggregated substance.

The aggregated substance was regarded as a processing error and disregarded from the further processing of the material. However the aggregated substance was separately analyzed with ATR-FTIR and XRD, and the results showed a similar substance to that of

BRMMT$_{dried}$, with regard to chemical composition and the resulting spectra, and the state of intercalation/exfoliation. The results of this separate analysis are not included in this project. The mixed substance was observed to have a solid and liquid phase, as seen in (a) of figure A.27.

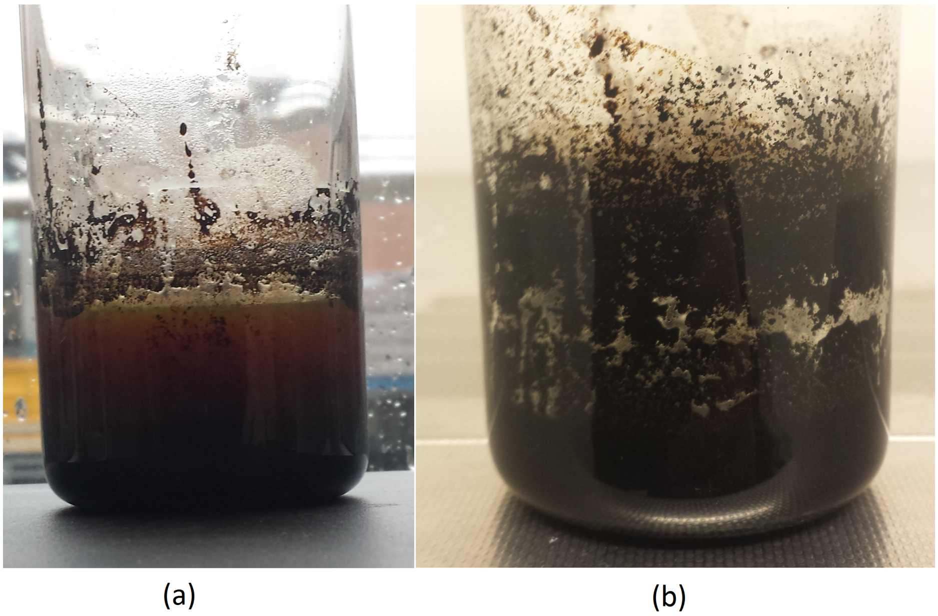

Figure A.27. The BRMMT$_{dried}$, (a) before and (b) after the second drying process.

The liquid phase is believed to be the solvents(e.g. deionized water and ethanol). After the second drying process, the liquid phase was condensed with the solid to a single phase, (b) in figure A.27. The weight of the BRMMT$_{dried}$ indicated a weight loss of 0.533 g. This weight loss is attributed to the aggregated substance, which was removed in the processing. The initial content of montmorillonite was calculated to yield a 10% solution, however due the processing error, the exact content of montmorillonite is unclear. The results of the following characterization of the material, will be affected and this have be taken into consideration in the evaluation of the obtained results. In the preparation of the BRMMT$_{liquid}$, the precise content of montmorillonite after dilution with the BR$_{dried}$ is also unclear.

A.5.2 XRD analysis

XRD was used to evaluate the d-spacing between the inorganic layers of the raw montmoriollionite(Cloisite Na+) and the organically modified BRMMT$_{dried}$, to determine the possible state of intercalation and/or exfoliation. The results of the X-ray diffraction of the MMT (Cloisite Na+), see figure A.28, showed a peak at 7.38 degrees. When applying Bragg's law for the interlayer d-spacing, the spacing is determined to be 12.00 Å. This fits with the existing results and measurements, conducted by other studies, where the peaks for Cloisite NA+ is found around 7.57 degrees with d_{001} of 11.7 Å. This indicates that the measured MMT utilized had an increase in the d-spacing, which indicates an increased moisture content, compared to the data sheet from the supplier[Additives and Instruments, 2015]. The BR$_{dried}$ showed a peak at 5.45 degrees with a d-spacing of 16.23 Å. The interlayer d-spacing increased with 4.26 Å and the peak shifted downwards with 2.11 degrees. This indicates that some of the BR$_{dried}$ had intercalated the galleries of the MMT and increased the interlayer spacing between the inorganic silicate layers of the montmorillonite. The results of the XRD analysis are listed in table A.9. The peak of BRMMT$_{dried}$is broader, compared to the narrower peak of the MMT. This could indicate a non-uniform orientation and spacing between the platelets. This could be attributed to a different amount of the modifier, which has been intercalated, and hereby a non-uniform distribution of the clay particles in the modified BRMMT$_{dried}$.

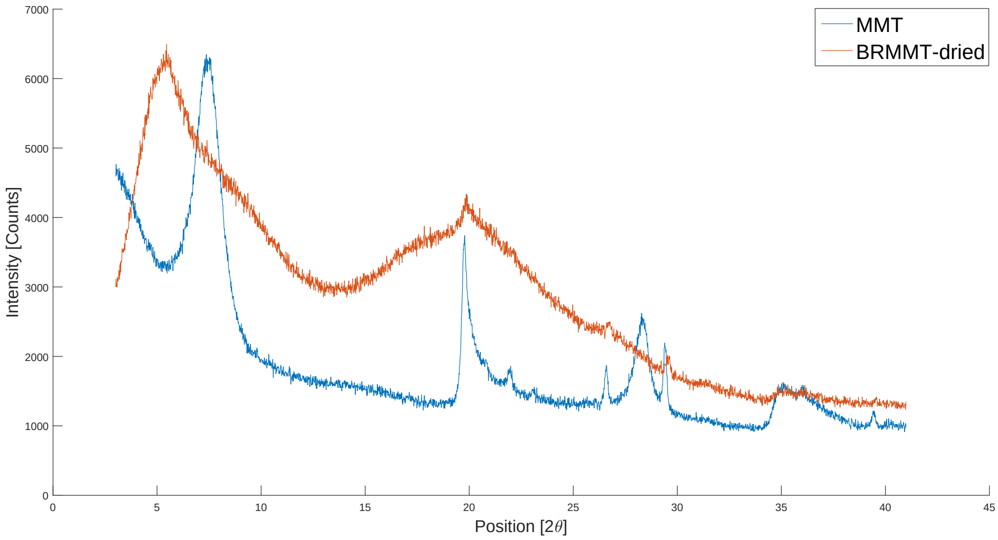

Figure A.28. XRD analysis for BRMMT$_{dried}$ and MMT.

Table A.9. XRD data of MMT and BRMMT$_{dried}$.

Sample	2θ	d-spacing (Å)	d-spacing (nm)
Cloisite Na+(supplied)	7.57	11.7	1.17
Cloisite Na+(measured)	7.38	12.00	12.20
BRMMT$_{dried}$	5.45	16.23	1.62

A.5.3 FTIR analysis

The FTIR analysis was conducted to possible determine the functional groups of the different processed bio-residue and MMT, and to investigate the state of intercalation and exfoliation of the modified BRMMT$_{dried}$. An initial analysis was conducted for the clear phase of the BR$_{r}aw$ to determine the chemical composition of this phase.

Investigation of the clear phase

The clear phase of the BR$_{raw}$ were investigated, due to the two phases, which were present in the delivered material. The clear phase was scanned and compared to deionized water in figure A.29. The two spectra are almost identical with small variations, which could be attributed some organic particles. The results of the initial TGA, in section A.5.5, supports this result with an onset of evaporation of 102.9 °C, which is consistent with the evaporation temperature of pure water.

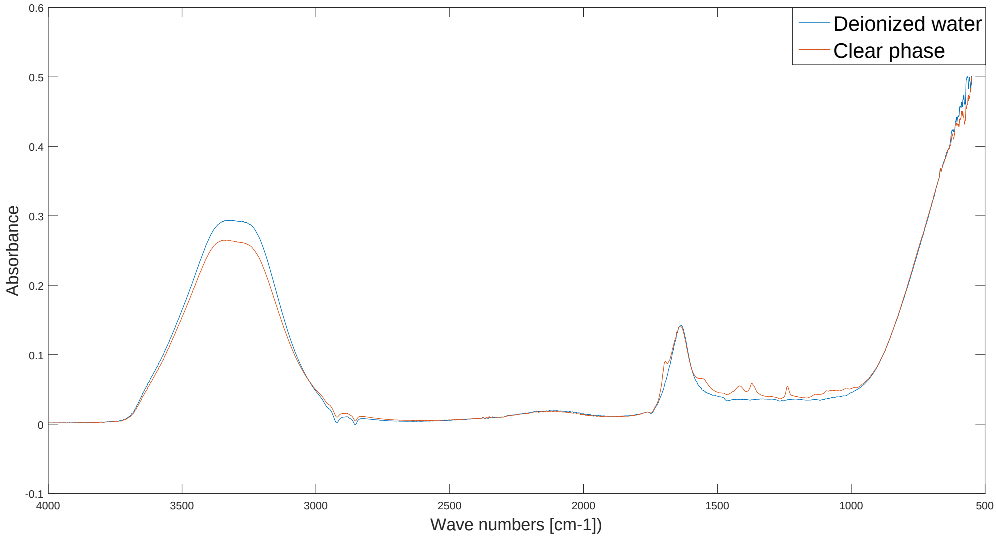

Figure A.29. ATR-FTIR analysis for clear phase and deionized water.

The excess water content were removed from the BR_{raw}, because the excess water is not desired in the further processing and modification of the bio-residue.

Investigation of the functional groups of the Bio-residue and MMT

The spectra of BR_{raw}, BR_{dried}, $BRMMT_{dried}$ and MMT are shown in figure A.30 and A.31.

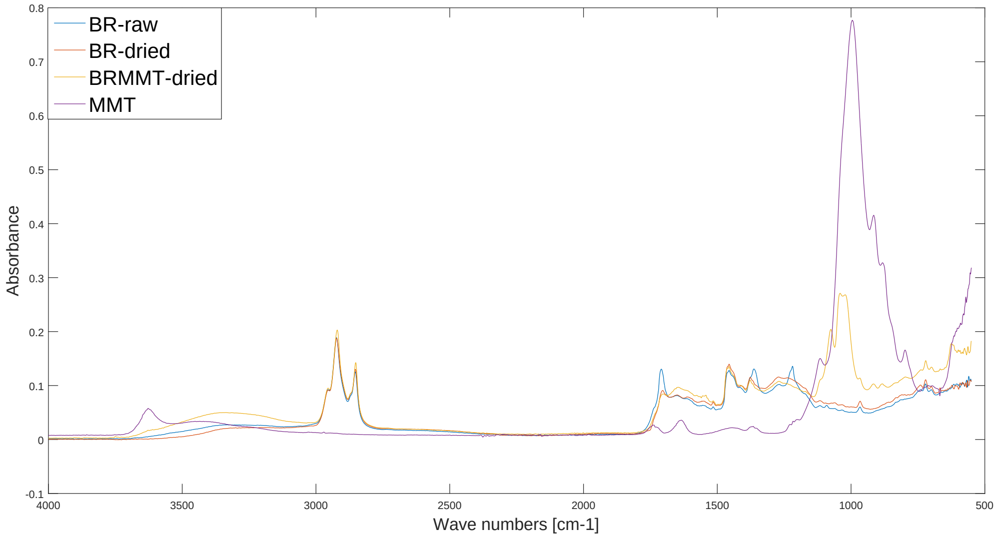

Figure A.30. Absorbance spectra for BR_{raw}, BR_{dried}, $BRMMT_{dried}$ and MMT.

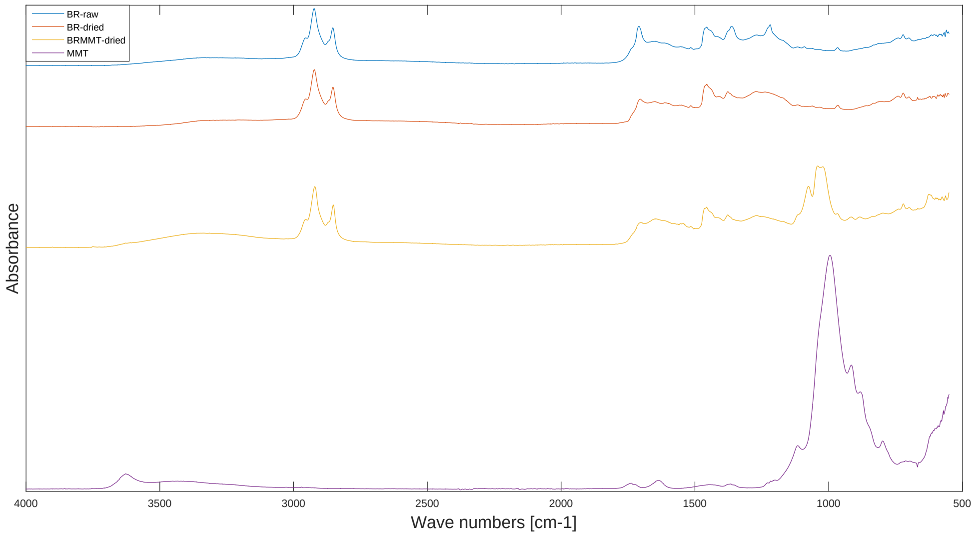

Figure A.31. Split absorbance spectra for BR_{raw}, BR_{dried}, $BRMMT_{dried}$ and MMT.

A visual comparison with the spectra, described in the literature study, indicated similar spectra of the bio-residue, compared to the bio-oil and bio-binder. The functional groups of the bio-oil and the bio-binder are compared with the measured spectra. The peaks of each individual spectra were analyzed and determined with the provided software of the Spectrum One. In table A.11, the results of the measured peaks, for BR_{raw}, BR_{dried} and $BRMMT_{dried}$, are listed and compared with the ranges of functional groups described by Hosseinnezhad et al. [2015] for bio-oil. The same procedure were conducted for MMT and $BRMMT_{dried}$, where the results are listed in table A.10.

Table A.10. Functional groups of Cloisite Na+ [Rafiei and Ghomi, 2013].

Functional groups	Range	MMT	$BRMMT_{dried}$
O-H stretching	3100-3700	3628, 3435	3338
O-H bending	1600-1700	1737, 1635	1647
Si-O stretching	1040	-	1041, 1021
Si-O and Al-O bending	400-600	571	599, 576, 563

Table A.11. Functional groups of bio-oil [Hosseinnezhad et al., 2015].

Functional group	Range	BR_{raw}	BR_{dried}	$BRMMT_{dried}$
O-H stretching	3200-3400	-	-	3337.87
O-H stretching	2800-3000	2923.27 2853.25	2922.65 2852.71	2920.60 2851.41
Aromatic carbonyl/carboxyl C=0 stretching	1700-1710	1709.05	1704.05	-
Aromatic C=C ring stretching	1514-1560	-	1515.33	1542.43
Aliphatic C-H deformation	1454	1456.08	1455.91	1456.51
Aliphatic CH3 deformation	1370	1363.05	1376.79	1377.21
Aromatic CO- and phenolic -OH stretching	1250-1270	1218.66	1271.39	1269.09

It can be seen in the results for both tables, that the functional groups of the MMT and the bio-oil are present in the different processed bio-residues and the organically modified $BRMMT_{dried}$. The analysis is however inconclusive, because the peaks of the functional groups are a not direct indication of the full chemical composition of the bio-residue. The obtained spectra can be used to asses the effects of the modification and state of intercalation/exfoliation, which is utilized in the next section.

Investigation of state of intercalation/exfoliation

The approach for this technique is to determine the presence of four distinct Si-O stretching bands in the range 1000-1150 cm^{-1} of the modified BRMMT$_{dried}$. It can be seen in figure A.30 and A.31, that the region where the four bands should be present, have peaks present in the spectra of the BRMMT$_{dried}$. In figure A.32, the four distinctive bands are determined, with a small margin for shifts in the placement. The four peaks were determined to be 1116, 1076, 1041 and 1023 cm^{-1}. The measured values fits with the values, obtained by Cole [2008], which were 1120, 1080, 1048 and 1025 cm^{-1}. The peak of 1080 cm^{-1} is clearly present and this indicates intercalation/exfoliation.

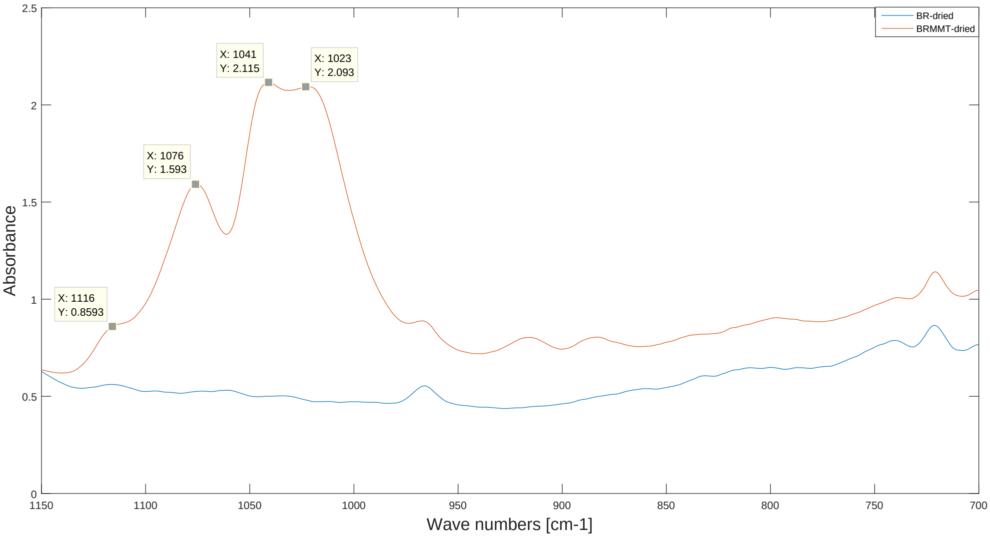

Figure A.32. Normalized, raw absorbance spectra for BR$_{dried}$ and BRMMT$_{dried}$.

It was chosen to investigate if the four peaks determined in the raw spectra is affected by the presence of the bio-residue. Therefore, the spectra of BR$_{dried}$ and BRMMT$_{dried}$ were normalized with respect to the unit peak height of 1456cm^{-1} and used as a reference. The normalized spectra of BR$_{dried}$ is subtracted from the normalized spectra of BR$_{dried}$, which is illustrated in figure A.33. The only registered shift of the four peaks, is the peak of 1023 cm^{-1}, which shifted to a lower position of 1021 cm^{-1}. However this small shift is negligible and deemed insignificant.

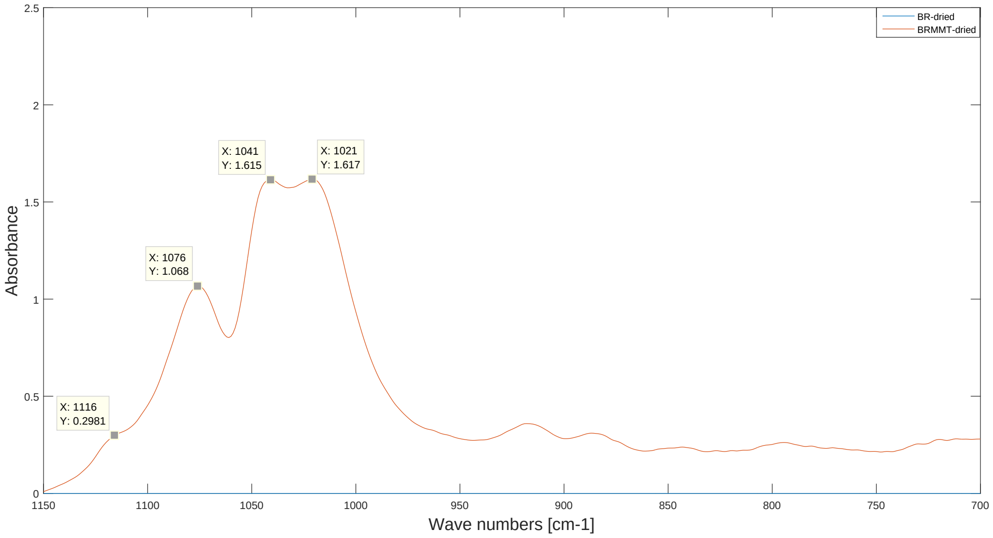

Figure A.33. Normalized, subtracted absorbance spectra for BR_{dried} and BRMMT_{dried}.

The results showed clear intercalation/exfoliation of the BRMMT_{dried}, however the results are based on single measurements of both the BR_{dried} and the modified BRMMT_{dried}. Therefore the results can only be interpreted as a qualitative interpretation of the state of intercalation/exfoliation.

A.5.4 Rheological properties

The rheological properties of the BR_{dried} were investigated and compared to the modified BRMMT_{liquid}. The initial modification with 10 % montmorillonite to BR_{dried}, the BRMMT_{dried}, produced a solid material, where the setup could not reach a appropriate gap height to conduct measurements. Therefore the BRMMT_{dried} were diluted with $\mathrm{BRMMT}_{dried}$to produce the BRMMT_{liquid} to lower the content of MMT.

Amplitude sweeps

The amplitude of the oscillatory test was selected with an amplitude sweep to ensure that the material deformations remained within the linear viscoelastic regime. The results of the amplitude sweeps showed that the loss modulus of the BR_{dried} was much larger than the storage modulus.

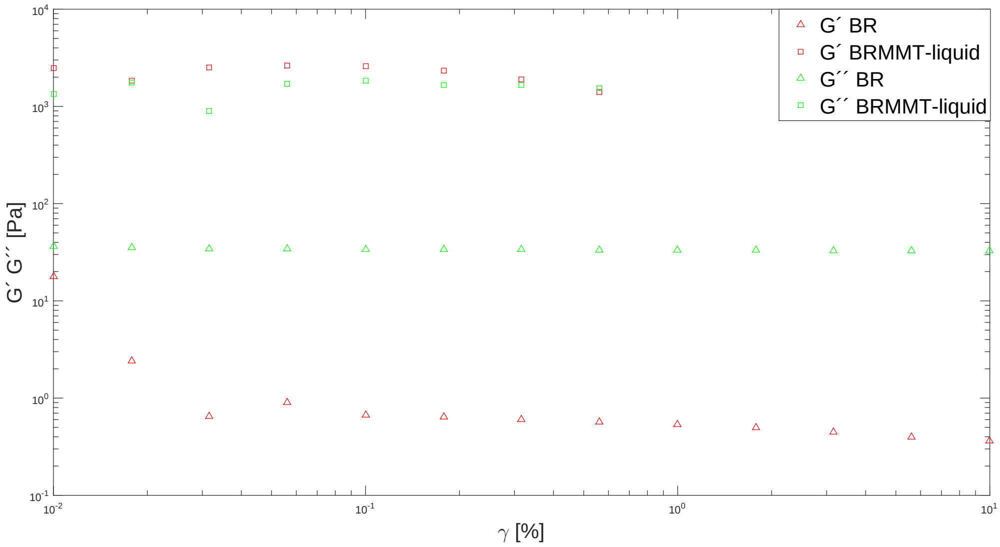

Figure A.34. Storage(G´) and loss(G´´) modulus, as a function of angular frequency ω, for BR_{dried} and BRMMT_{liquid}

This indicates, that the BR_{dried} is a visco elastic fluid, and the ratio between the G´ and G´´ modulus started to become constant, at higher impose strain levels. The large constant ratio between the two moduli, see figure A.34 at increasing strain levels, indicates a almost pure fluid.

The BRMMT_{liquid} has a higher value of G´ compared to the G´´, which indicates a more solid substance compare to the BR_{dried}. The measurement was terminated and the strains(γ) for the frequency sweeps were chosen in accordance with the theory and within the linear viscoelastic regime.

Frequency sweeps

The selected strains(γ), from the initial amplitude sweeps, were chosen to be 10 % and 0.1 % for the BR_{dried} and BRMMT_{liquid} respectively. This ensured, that the investigated materials remained within the linear visco elastic regime. The results of the frequency sweeps indicated a almost pure Newtonian fluid for BR_{dried}, where the ratio between the storage and loss modulus remained constant with decreasing angular frequencyω. The complex viscosity for BR_{dried} remained almost constant, with the decreasing angular frequency, with a small increase at lower angular frequencies, as seen in figure A.36. The phase angle for the BR_{dried} was constant at 89 degrees, which collaborates with the viscosity for a almost perfect Newtonian fluid, as seen in figure A.37.

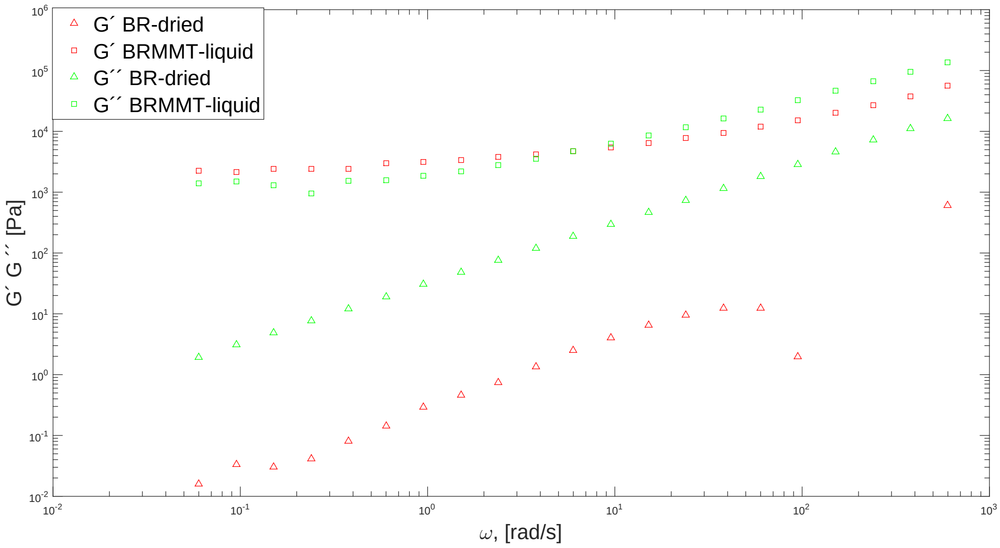

Figure A.35. Storage(G´) and loss(G´´) modulus, as a function of angular frequency ω, for BR$_{dried}$ and BRMMT$_{liquid}$.

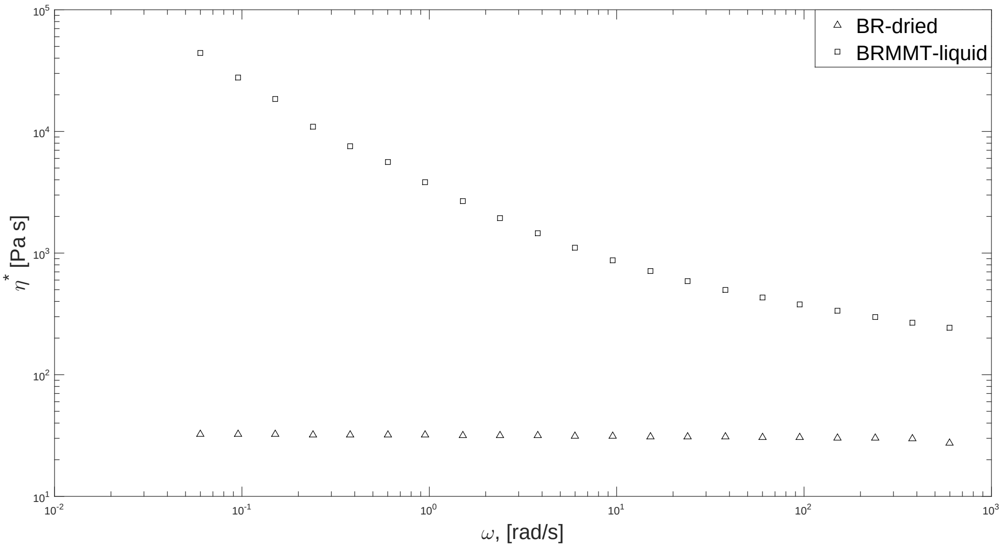

Figure A.36. Complex viscosity $\eta*$, as a function of angular frequency ω, for BR$_{dried}$ and BRMMT$_{liquid}$.

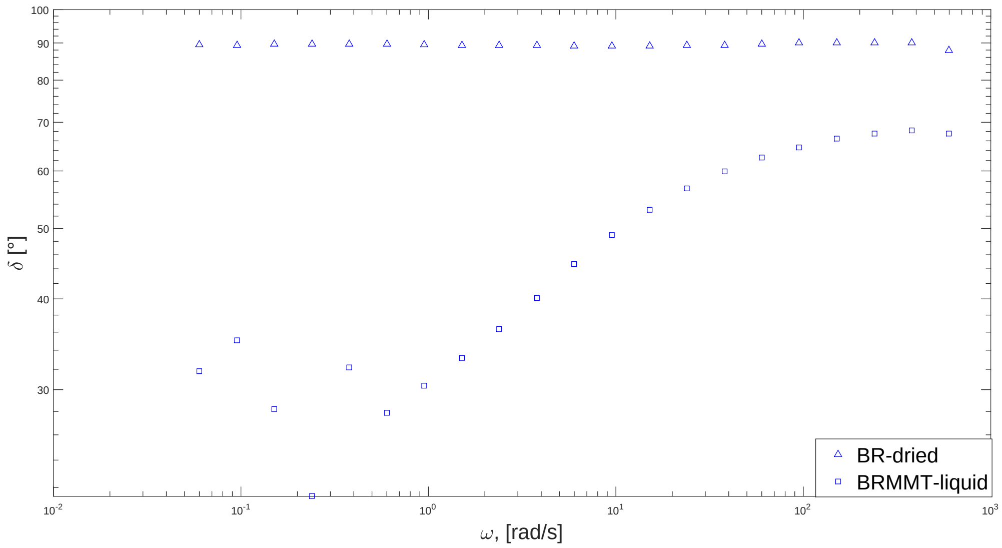

Figure A.37. Phase angle δ, as a function of angular frequency ω, for BR$_{dried}$ and BRMMT$_{liquid}$.

The results for BRMMT$_{liquid}$ showed, at low angular frequencies, a plateau in the storage modulus. The complex viscosity increased with decreasing angular frequency. The phase angle decreased with decreasing angular frequency. The three observations could indicate that the BRMMT$_{liquid}$ transitioned from a visco-elastic liquid substance to a more solid material. This observed transition from the liquid-like behavior to the so-called pseudo-solid-like behavior fits with observations by other studies[Klitkou, 2012]. In nanocomposites with polymeric matrix materials and clay fillers, the low frequency solidification behavior can be used as an indicator of the state of particle dispersion. The results of the rheological properties indicated that the organic modification process, with MMT, changed the rheological properties of BR$_{dried}$, which changed from a almost pure Newtonian fluid to pseudo-solid-like behavior. This fits with visual observations of the materials, where BR$_{dried}$ was observed to be a thick, sticky oil and the BRMMT$_{liquid}$ could rather be described as a thick paste. This could indicate an interaction between the dried bio-residue and the MMT utilized.

A.5.5 Thermogrametric analysis

The results of the weight loss of the untreated BR$_{raw}$, the dried BR$_{dried}$ and the modified silicate BR$_{dried}$ and the MMT are presented in figure A.38. It can be seen from the results of table A.12, that the BR$_{raw}$ undergoes two thermal degradations steps, where the first is determined with ATR-FTIR analysis, section A.5.3, to be a excess water content from the TCC conversion process. The mass loss was registered to be 16.48 %. The BR$_{dried}$ had a higher thermal stability and has therefore a higher decomposition temperature compared to the BR$_{raw}$. This increase in thermal stability can be attributed to the drying process, where water and some of the volitiale compounds of the the BR$_{raw}$ were removed.

Table A.12. TGA data of BR_{raw}, BR_{dried}, $BRMMT_{dried}$ and MMT.

Sample	Onset[°C]	Mass change[%]	Residual mass[%]
BR_{raw}	102.9	16.48	
	299.4	70.12	13.4
BR_{dried}	334.4	70.12	13.46
$BRMMT_{dried}$	240.0	77.68	22.32
MMT	69.9	3.21	90.25
	628.8	4.65	

The drying process increased the resistance against thermal degradation and shifted the onset temperature by 231.5 °C compared to the initial onset temperature of the BR_{raw}. The thermal stability of the $BRMMT_{dried}$ was lower than the $BRMMT_{dried}$, where the onset temperature of degradation was lowered with 114.4 °C to 240.0°C. This decrease could be interpreted as the release and evaporation of bounded water within the MMT, which were untreated. This fits with measured results of the MMT, where there was a small mass loss, which was associated with bounded water, which fits with the theory. It is observed in the results of table A.12 and figure A.38, that the decomposition of MMT occurred in two steps; the first at 69.9 °C with a mass loss of 3.21 % , the second at 6.28 °C with a mass loss of 4.65 %. The measured results fits with theoretical data and observations from other studies about the utilized MMT, Cloisite Na+. According to Mallakpour and Dinari [2012], the first step of the decomposition before 100°C, is attributed to the desorption of water from the interlayer space. The second decomposition around 600 °C is attributed to dehydroxylation of the layers and this proceeds until around 700°C.

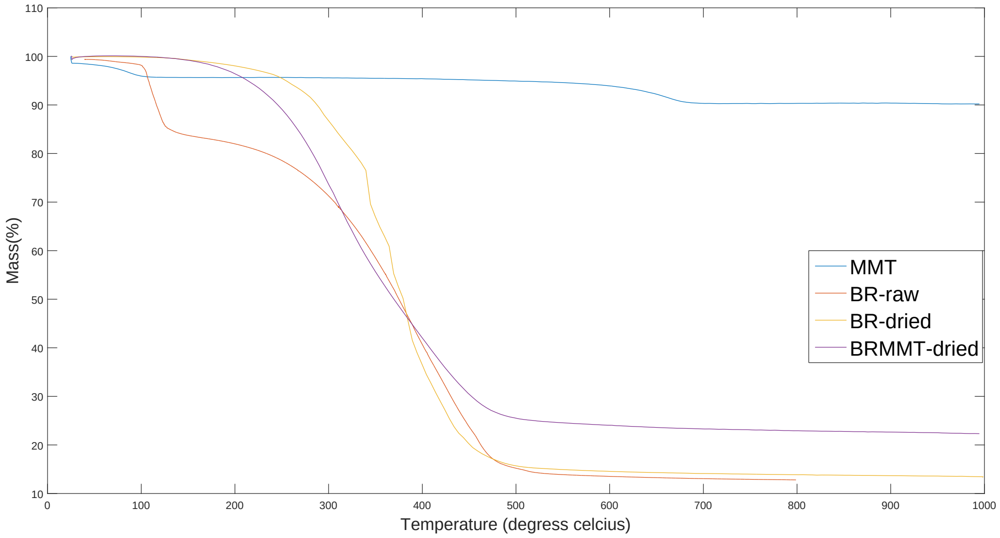

Figure A.38. TGA measurement of weight loss, as a function of temperature, for the differently processed bio-reside and the MMT.

Another possible explanation for the decrease of the decomposition temperature for the organically modified $BRMMT_{dried}$, is the possible high content of long fatty acids within the material. According to Rooj et al. [2012], clay minerals will accelerate the degradation rate of fatty acids. In his study, Rooj et al. [2012] reported that the degradation temperature of fatty acids, which were mixed with organically modified montmorillonite, increased with increasing length of the carbon chain of the long fatty acids. This fits with the measured results of the BRMMT_{dried}, because the decomposition temperatures of long fatty acids, unmodified and modified with organically modified montmorillonite, are around 200-250 °C, as seen in figure A.39

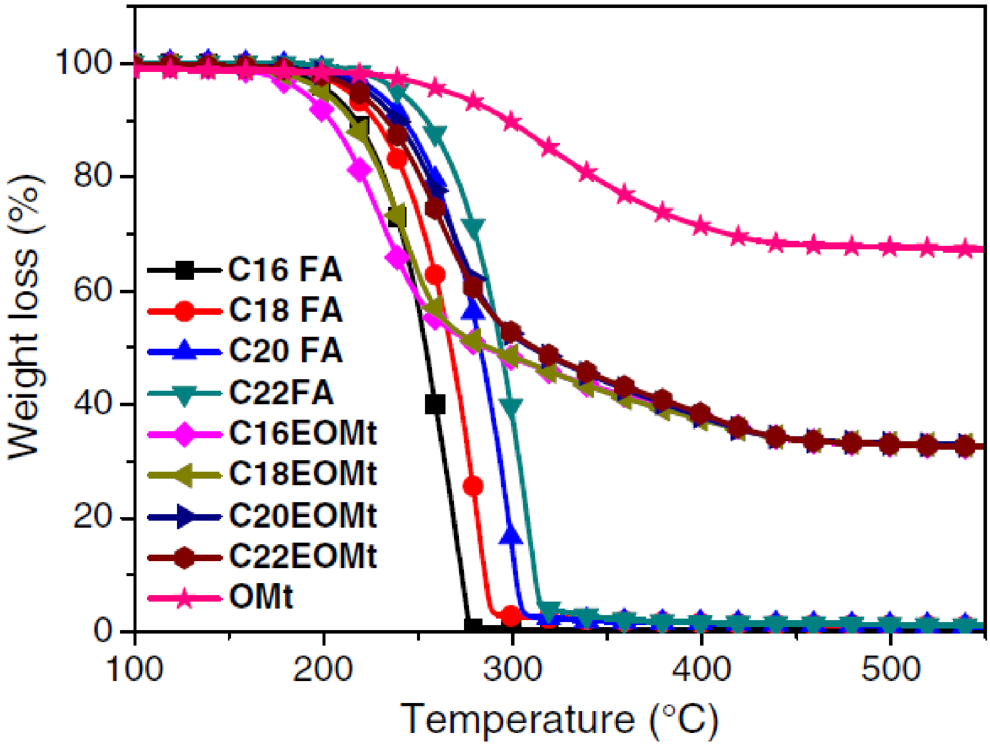

Figure A.39. TGA measurement of weight loss, as a function of temperature, for long fatty acids, unmodified and modified with MMT)[Rooj et al., 2012]

The residual mass of the investigated materials showed similar results for the BR_{raw} and BR_{dried} with a small change of 0.04 %. The modified BRMMT_{dried} had an increase in residual mass by 8.86 %, compared to BRMMT_{dried} . This increase can be explained by the addition of the 10% MMT in the modification process. There was observed a small loss of 1.14 %, which could be interpreted as the loss of bounded water from the MMT or as the processing error in the modification process, where the aggregated substance had a presence of MMT.

A.6 Discussion

This chapter focuses on the discussion of the obtained experimental results of the performed experiments, when compared to the theory described in the literature study, to investigate the chosen problem statement. The initial characterization of the bio-residue, showed that the material had a similar chemical composition to the bio-oil, described by Hosseinnezhad et al. [2015], which had a high presence of long fatty acids, a high content of nitrogen and oxygen compounds(e.g. amines, amides and olefins). The FTIR analysis for the bio-residue showed peaks in the described ranges for the bio-binder and the bio-oil. The initial characterization were performed primarily to to obtained a baseline for the effects of the modification process.

The modification process were performed with a solution-intercalation blending process with ultrasonification. The results of the experiments yielded the following results:

- **The basal d-spacing increased with the addition of MMT.**
  The increase in the interlayer d-spacing of BRMMT$_{dried}$ indicates a intercalated state. This was verified with XRD and FTIR, where the basal d-spacing were increased with approximately 35%, compared to the measured d-spacing of the MMT. This was supported by the measurement conducted in the ATR-FTIR, where the peak of 1080 cm^{-1} was clearly present.
- **The viscosity of the bio-residue increased with the addition of MMT.**
  The increased viscosity is associated with clay dispersion. The registered transition from a liquid-like to a semi-solid behavior of the treated bio-residue, which indicated an interaction between the MMT and bio-residue.
- **The thermal stability of the bio-residue decreased with the addition of MMT.**
  The decreases in thermal stability could be attributed to release of bounded water within the MMT or the degradation fatty acids of the bio-residue.

The obtained results clearly indicated that the modification process was a success, however there are some uncertainties on which organic compounds of the bio-residue, and mechanism, which facilitated the intercalation process. The results of the FTIR showed the presence of peaks from both the MMT and bio-residue, however the peaks of the bio-residue could have overwhelmed some of the peaks of the MMT. Initial trials to determine the hidden peaks with subtraction were attempted, but was deemed inconclusive. A way to determine a more precise spectra of the modified BRMMT$_{dried}$ could be to wash the substance with deionized water, to remove excess intercalant. In his study, Xi et al. [2005] showed it was possible to determine the placement of intercalant within the MMT, with respect to the degradation temperature. According to Xi et al. [2005], the placement of the intercalant of an organoclay can be placed in three positions; where the first is were the intercalant cations are intercalated into the clay interlayers through cation exchange and bound to surface sites via electrostatic interaction. The second, is where intercalant (cations and/or molecules) are physically adsorbed onto the external surface of the clay. The last environment, is where the intercalant molecules are located within the clay interlayer. The different states have different thermal degradation temperatures. This could be used to possible determine the state of intercalation for further processing. Therefore the processing of a pristine organoclay could be a way to get a more precise determination of the intercalation mechanism. The bio-residue intercalated the interlayer galleries of the MMT, and produced a intercalated state. The results of the rheological properties supported a interaction between the bio-residue and the MMT, the transition from a liquid to a semi solid state. In his study, Walters et al. [2014], showed that full exfoliation with organically modified Cloisite 30B could be achieved with the bio-binder, however there is no clear explanation for the the exfoliated state, except the XRD measurements. The difference between the Cloisite 30B and Cloisite Na+ is the replaced alkyl quaternary ammonium salt as cations of the Cloisite 30B. This could indicate that the presence of the alkyl quaternary ammonium cations facilitated a cation-exchange and this in turn produced the exfoliated state. These results could be supported by the results, observed by Rooj et al. [2012], where the quaternary amines with long alkyl chain, which were present in the interlayer space of organically modified MMT, increased the spacing between the silicate layers. This enabled the intercalation process of long chain fatty acids, as seen in figure A.40

The intercalated state of BRMMT$_{dried}$ could indicate, a different interaction mechanism between the intercalant and the MMT. The bio-reside had a high content of polar compounds, due to the high presence of oxygen and fatty acids. These polar groups could have formed a dipole-dipole force interaction, where the different charges of two polar molecules attracts each other. The requirement for this interaction, is close contact between the molecules, as

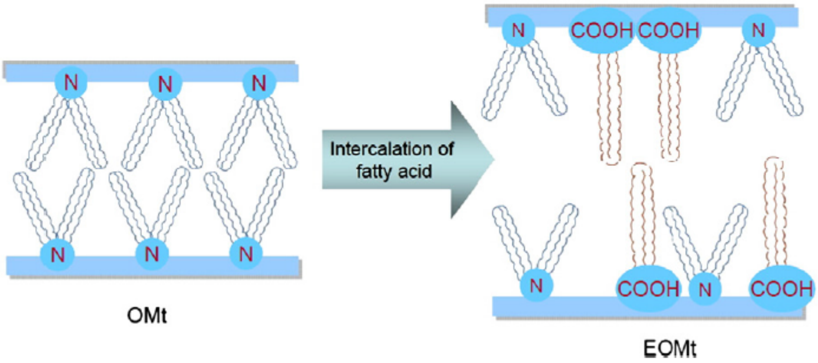

Figure A.40. Hypothetical representation of clay minerals layer expansion in presence of long fatty acids[Rooj et al., 2012].

achieved in a liquid state. However cation-exchange could be possible, due to high amount of nitrogen rich compounds in the bio-residue, especially the presence of amines and amides is promising. The amines could be altered in the modification process to quaternary ammonium cations. The precise mechanism of intercalation is not determined in this project, but TGA and FTIR analyses of washed organoclay coupled with a GC-MS analysis, could be utilized to determine the interaction. Additionally a comparison study between Cloisite Na+ and Cloisite 30B, where the the bio-residue is used as intercalant, could yield more information about the intercalation/exfoliation process. However the goal of this project was to determine if intercalation/exfoliation was possible and this was proven.

The most surprising result of the modification process was the reduction of the thermal stability, because the addition of clay particles is reported to improve thermal stability of a matrix material. The unclear moisture content, detected by XRD and TGA, could explained this reduction. However the study conducted by Rooj et al. [2012], could be just as viable an explanation. The possible degradation of the high presence of fatty acids in the bio-residue, could reduce the thermal stability of the whole substance. It is unclear if this degradation is significant for the further processing to obtaining a nanocomposite.

A.7 Conclusion

The project was to investigate the new bio-renewable material, bio-residue , which has been converted from swine manure to a bio-adhesive by a patented process from NC A&T, could be compatibility with untreated Na-montmorillonite, to achieve a intercalated/exfoliated state, as a preliminary step for further processing of nanocomposites. The modification process, solution-intercalation blending with ultrasonication, was deemed a success, despite the processing error of the removed aggregated substance. The raw bio-residue, in its supplied state, was a two phase material. Therefore additional processing(e.g. a drying process) was required before the modification process could be commenced.

The characterization of the raw bio-residue indicated a very complex organic material with a high content of long fatty acids, a high content of nitrogen and oxygen compounds(e.g. amines, amides and olefins). The intercalation was successful, however it is unclear, which functional or polar group of the bio-residue, which facilitated the intercalated state, which was produced. The intercalation mechanism could be a dipole-dipole interaction, a cation-exchange or a mixture of both. The reduction in the thermal degradation temperature, which occur with the addition of the MMT, is possible a factor, that have be taking in to consideration in the further processing to obtaining a nanocomposite.

The modification process was deemed a success, however the process have to be improved for further processing. The utilized MMT could be exchange with a organically modified version(e.g. Cloisite 30B), to possibly achieve a more exfoliated state. A washing process, to remove excess modifier, have to be determined to achieve a pristine organoclay version of BRMMT_{dried}, which enables easier processing and compatibility with a chosen polymeric material. The cleaned organoclay version can be used to assess and determine the intercalation mechanism. The results of the organoclay could be supported by a GC-MS of the bio-residue. The projects showed a great potential for converting a waste material(e.g. swine manure) to new applications and nanocomposite materials. The described economical drawbacks of the conversion procedure have to be taken in account, however this does not diminish the potential of the usages of this new type of materials.

Characterization methods B

B.1 Gas Chromatography/Mass Spectrometry (GC-MS)

Gas chromatography / mass spectrometry (GC-MS) are two different analytical methods, which can be used in conjunction for the identification of complex volatile materials. Gas chromatography (GC) effectively separates the different constituents of the sample for subsequent analysis and identification by mass spectrometry (MS). This is done with a column, where part of the compounds travel trough carried by an inert gas, like helium, for separation. The speed of the particle through the column is affected by the affinity/polarity and size of the particular compound. A more polar and heavier compound travels slower than a lighter compound, which determines the retention time(RT) of each compound. The eluting compounds, from the GC column, enters the ionization chamber of the mass spectrometer where the molecules are ionized, by electron impact. The impact of the electrons on the molecules of the compounds, produces positives ions. These ions are separated according to their mass by a mass analyzer. The first results of the test is a total-ion chromatogram (TIC), which is a plot of the total mass eluting from the GC and detected by MS as a function of time. However each peak or band in the chromatogram represents a discrete chemical compound and this is analyzed separately. Each peak correlates to a compound with some certainty and this is determined by the analyzer.

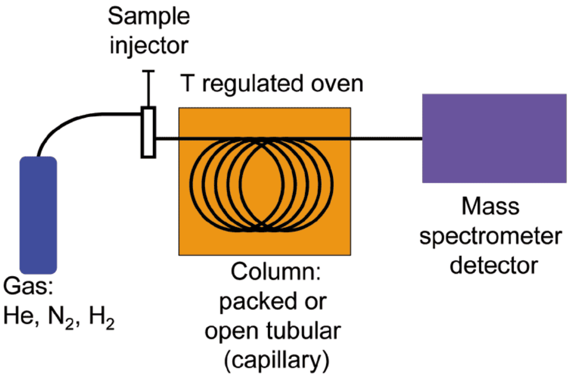

Figure B.1. Schematic of a GC-MS setup, with an sample injector, oven with a column and MS detector

B.2 X-ray diffraction (XRD)

X-ray diffraction can be utilized to identify crystalline materials(e.g. minerals, inorganic compounds, the crystalline structure of polymers) from various angles and reflective intensities, can obtain information about the inorganic solids materials in the investigated sample [Poppe et al., 2001].This technique is fast and non destructive, because the process utilizes X-rays. Results can be processed and yield information about the crystalline structure and basal distance in clay materials. Unique patterns can be used to identify the materials, if the materials are crystalline. Bragg's law can be utilized to determine the basal d-spacing of the clay types(HNT and MMT), by the placement of the angles of the investigated peaks.

$$\mathrm{n}\lambda = 2\mathrm{d}\sin\theta \tag{B.1}$$

Where λ is the incident X-ray wavelength, θ is the reflection angle of the X-ray beam, n is the integration constant, or reflection number (usually 1 is utilized), and d is interplanar lattice spacing, or d-spacing, of the investigated material. Sine θ is the experimental diffraction angle, which is used for the spectra.

B.3 Attenuated Total Reflectance Fourier transform infrared spectroscopy (ATR-FTIR)

Fourier transform infrared (FTIR) spectroscopy is a measurement technique, that records the infrared spectra(IR) of a sample, where light is reflected first through an interferometer and then through the investigated sample. The technique is a fast and non-destructive method for qualitative and quantitative measurements[Newport, 2015]. The inferferogram, the recorded light signal, can be treated and yield information of the investigated sample. The recorded peaks of the spectrum are related to or correspond to the vibrational movements of the molecules or the internal energy levels(e.g. stretching, rotational and bending bonds) of specific functional groups.[Newport, 2015]. This can be utilized to determine the changes or composition of a sample, which is being investigated. There are two versions of FTIR, transmittance, which shoots the light trough the sample, or absorbance using the ATR crystal for the reflective light. In this project, it is absorbance with an ATR crystal, which is utilized. Therefore no preparation of the samples is required, except good contact between sample and crystal is needed. This can be achieved by the force gauge, which is applied with the same pressure for all sample. The only drawback of this technique is the penetration depth, which is only 1.66 μm for the chosen crystal Perkin Elmer [2004].

B.4 Thermogravimetric analysis(TGA)

Thermogravimetric analysis (TGA) analyzes the mass loss or gain, due to decomposition, oxidation or loss of volatiles of a sample, as a function of temperature or time. Mass change can be used to characterize the decomposition and thermal stability of a materials under different conditions, which describes the physical and chemical processes occurring in the sample as the conditions change [Lampman et al., 2003]. Two different set of equipment were utilized, one is TGA and the other STA. STA stands for simultaneous thermal analysis and is comprised of two different techniques; Thermogravimetric analysis and Differential scanning calorimetry(DSC). Results of the DSC are not utilized in this project. Samples are placed in both setups in the measurement chamber in a crucible or platinum pan. Two crucibles/pans are placed in the measurement chamber, where one crucible is loaded with a few grams of the investigated sample and the other is the reference; commonly an empty crucible. The furnace is closed and the atmosphere of the furnace is purged with air or inert gas(nitrogen in one setup and argon in the other). When the atmosphere is replaced by gas, the heater is turned on and the temperature increases with a fixed heating rate until a desired temperature. The real-time measurement of the difference between the two crucibles in heat flow and weight change are the output of the experiment. The results can be plotted as a function of time or temperature for analysis [Lampman et al., 2003].

B.5 Oscillatory rheometry

Oscillatory rheometry can be used to asses the linear visco-elastic response of a material[Cambridge Polymer Group]. A sine-wave-shaped input of strain is applied to a sample and the resulting stress response can be separated into two responses; solid and liquid. The solid response, or storage modulus G', is in phase with the input and the corresponding liquid response, or loss modulus G", is $\pi/2$ out of phase with the input [Barnes, 2000]. From the storage and loss moduli, the complex viscosity or the resistance of fluid to flow, can be determined.

The material properties can be determined from the two moduli and the complex viscosity. These are listed in table B.1 and illustrated in figure B.2.

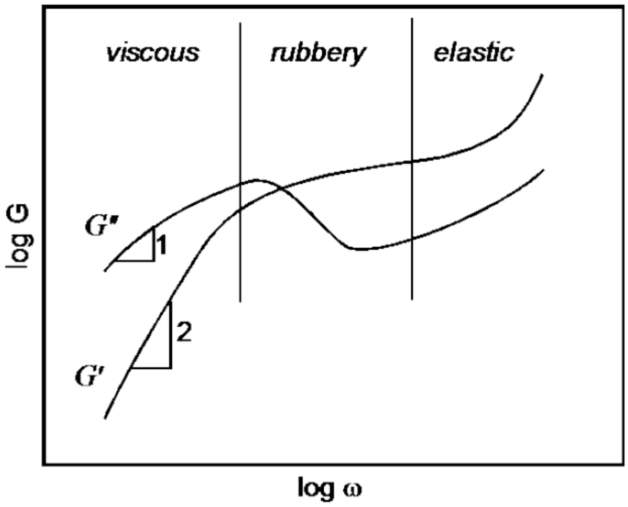

Figure B.2. A schematic of visco-elastic spectrum for a polymer solution when subjected to an oscillatory frequency sweep test [Cambridge Polymer Group].

Table B.1. Basis material values obtained from oscillatory rheometry [Cambridge Polymer Group].

Newtonian liquid	G'	$\eta' = \mu$	$\delta = \pi/2$
Hookean solid	G=G'	$\eta' = 0$	$\delta = 0$
Visco-elastic material	G'(ω) > 0	G"(ω) > 0	$0 < \delta(\omega) = \pi/2$

B.6 Uni-axial tensile testing

The evaluation of the tensile behavior of nanocomposites can be determined under axial tensile loading. A force is applied to the sample under a controlled crosshead speed. The crosshead speed can be varied to control the rate of strain of the sample. From the raw data tensile strength, yield strength, and modulus of elasticity can be determined.

Ultimate tensile strength(UTS) is the maximum tensile stress a material can sustain without fracture. It is calculated by dividing the maximum load applied during the tensile test by the original cross sectional area of the sample.

A general tensile stress-strain curve for a thermoplastic is illustrated in figure B.3.

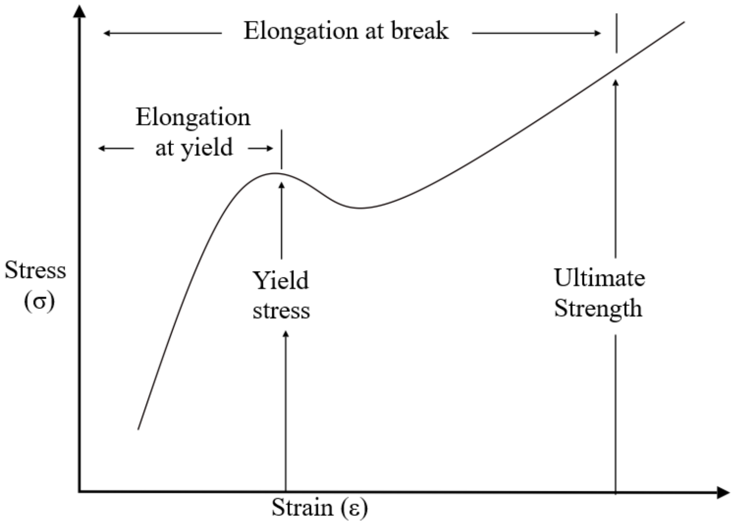

Figure B.3. General tensile stress-strain curve for a thermoplastic[Stevens, 1999].